Understanding progressive changes in cochlear supporting cells: implications for age-related hearing loss

By: Sarah Anne Hool

A thesis submitted in partial fulfilment of the requirements for the degree of Doctor of Philosophy

The University of Sheffield

Faculty of Science

School of Biosciences

September 2024

Acknowledgements:

First of all, I would like to thank my supervisor, Professor Walter Marcotti, for providing me with amazing support and guidance throughout the entirety of my time as a PhD student. I am extremely grateful for all of his valuable scientific advice and feedback which helped to shape and direct this research project. Additionally, I would like to thank my co-supervisor Professor Dan Jagger for sharing his expertise on cochlear supporting cells and giving useful critiques to improve my experiments.

An enormous thanks must also go to Dr Federico Ceriani for his endless support at every step of this project. I am very appreciative of his patience when teaching me about Ca^{2+} imaging and electrophysiology, and for the hours spent helping me with data analysis and coding. I could always rely on his advice to overcome any and all problems.

Additionally, I am very grateful to all other past and present members in the Sheffield hearing research group. The variety of skills and knowledge from everyone in this lab has been invaluable during my time working here. Especially, I would like to thank Dr Jing-Yi Jeng and Dr Adam Carlton for being there to help with any questions I had about immunolabelling or electrophysiology, and for providing me with feedback on my thesis. I am also appreciative of the kindness I have received from the members of this lab, and for their company, which made my time as a PhD student very enjoyable.

Finally, I would like to thank my family and friends for their constant encouragement during my studies. I am extremely grateful to my parents, brother, and sister for always being there for me, and to my amazing friends who could always cheer me up whenever I needed it.

Abstract:

The sensory epithelium within the mammalian auditory organ contains two groups of specialised cells: hair cells and glia-like supporting cells. The sensory hair cells detect sound-induced vibrations and transduce them into neural signals to be sent to the central auditory pathway. The supporting cells promote normal hair cell development and function which maintains our sense of hearing. Age-related hearing loss (ARHL) is thought to occur due to degeneration of the hair cells over time, the causes of which remain largely unknown. Since the supporting cells encourage hair cell longevity, this thesis aimed to investigate age-related changes in supporting cell protein expression and functioning to evaluate whether they could influence this hair cell deterioration associated with ARHL.

Supporting cells express P2Y purinergic receptors during development, which generate intracellular Ca^{2+} transients thought to modulate hair cell synaptic maturation. After the onset of hearing, P2Y receptors are largely down-regulated. Using immunolabelling and Ca^{2+} imaging experiments on C57BL/6N mouse cochleae, it was revealed that P2Y receptors are re-upregulated in the aged supporting cells, resembling the expression observed during development. In addition to P2Y receptors, the supporting cells are interconnected via a gap junction channel network allowing the diffusion of ions and small molecules between cells, to/from hair cells. Immunolabelling of these gap junction channel plaques revealed a progressive fragmentation with increasing age (older cells exhibited a higher frequency of significantly shorter plaques per cell). However, this fragmentation did not appear to affect the channel permeability as no age-related differences were found in Lucifer yellow dye diffusion experiments.

Therefore, the supporting cells appear to exhibit changes in the expression and functioning of certain membrane proteins unique to the aged cochlea. In conclusion, these age-related changes could have important implications on their ability to support hair cell function and maintain our sense of hearing with ageing.

Contents:

List of Figures:

List of Tables:

List of Abbreviations:

ABR	Auditory brainstem response
ADP	Adenosine di-phosphate
AMPA	α-amino-3-hydroxy-5-methyl-4-isoxazolepropionic acid
ANF	Auditory nerve fibre
ARHL	Age-related hearing loss
ATP	Adenosine tri-phosphate
BAAV	Bovine adeno-associated virus
BC	Border cell
BF	Background fluorescence
CC	Claudius' cell
Cx26	Connexin 26
Cx30	Connexin 30
C3H	C3H/HeJ
DC	Deiters' cell
DPOAE	Distortion product otoacoustic emission
ECS	Extracellular solution
ERRG	Oestrogen-related receptor gamma
ER	Endoplasmic reticulum
FRAP	Fluorescence recovery after photobleaching
GER	Greater epithelial ridge
GJC	Gap junction channel

GLAST	Glutamate aspartate transporter
GPCR	G-protein coupled receptor
HC	Hensen's cell
IBC	Inner border cell
ICS	Intracellular solution
IHC	Inner hair cell
IP_3	Inositol 1,4,5-trisphosphate
IPC	Inner pillar cell
IPhC	Interphalangeal cell
ISC	Inner sulcus cell
LED	Light-emitting diode
MET	Mechano-electrical transducer
NIHL	Noise-induced hearing loss
OHC	Outer hair cell
OPC	Outer pillar cell
OSC	Outer sulcus cell
PBS	Phosphate buffer saline
PFA	Paraformaldehyde
PM	Plasma membrane
ROI	Region of interest
ROS	Reactive oxygen species
SGN	Spiral ganglion neuron
TTS	Temporary threshold shift

UTP	Uridine-5’-triphosphate
6N	C57BL/6N
6N-repaired	C57BL/6N $^{Cdh23+}$

Chapter 1. General Introduction

1.1 Structure and functioning of the auditory system

Sound is directed into the ear via the pinna and travels down the ear canal towards the tympanic membrane (ear drum; Figure 1.1) (Møller, 2012). The inner surface of the tympanic membrane is connected to the first of a chain of three bones called the ossicles (malleus, incus, and stapes). Incoming sound will induce vibrations across the tympanic membrane, which are then transferred down this chain of bones across the length of the middle ear cavity. The ossicles gradually decrease in size the closer they are to the cochlea, causing the sound-induced vibrations to become significantly amplified as they progress down the chain (Mason, 2016). The last ossicular bone, the stapes, is connected to a membrane called the oval window which separates the middle ear from the inner ear (cochlea).

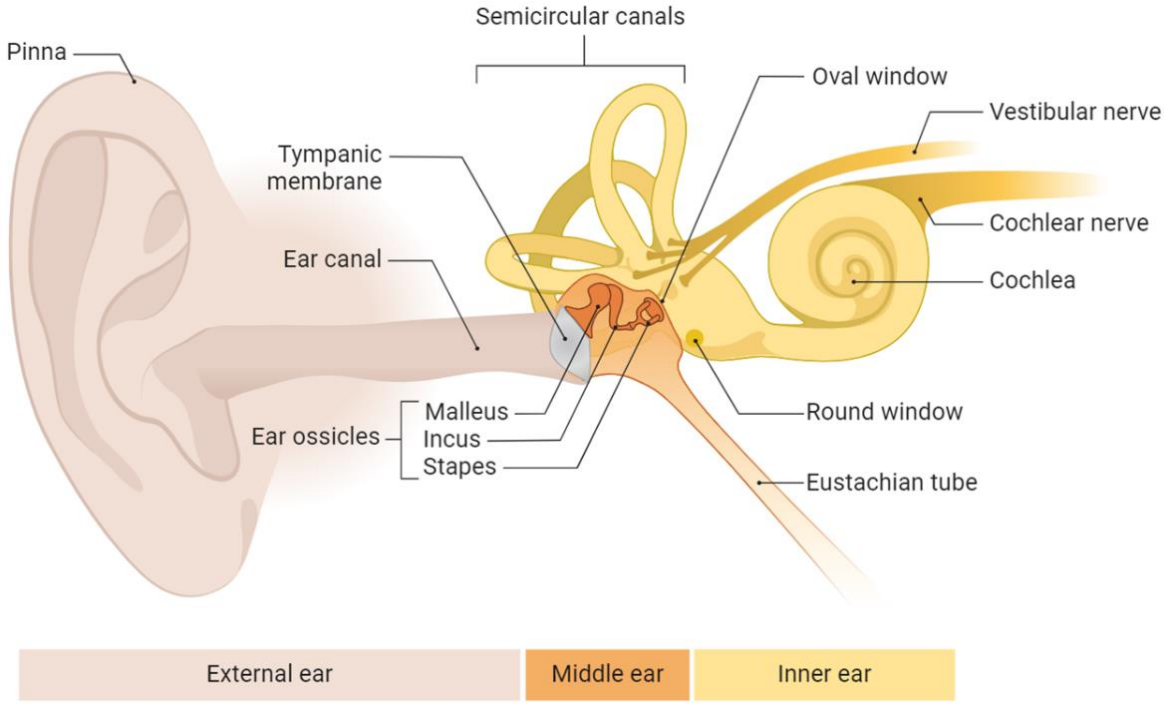

Figure 1.1: The auditory system

The pinna and ear canal (outer/external ear) lead sound towards the tympanic membrane (eardrum) (grey). The inner surface of the eardrum connects to the ossicles (malleus, incus, and stapes), which form a chain across the middle ear towards the inner ear. The cochlea is innervated by the cochlear nerve which relays sound-related neural messages to auditory processing centres in the brain. Adapted from "Middle and Inner Ear Anatomy", by BioRender.com (2024) and retrieved from https://app.biorender.com/biorender-templates.&apos.

The cochlea is responsible for transducing sound-induced vibrations from the middle ear into neural messages encoding specific acoustic information (Møller, 2012). It's spiral shape winds around a structure called the modiolus for ~2.5 turns in humans. Branches of the vestibulocochlear nerve extend outwards from within the modiolus to gather and relay sound-related neural messages to deeper parts of the central auditory pathway. The internal structure of the cochlea consists of three fluid-filled compartments: The scala vestibuli, scala media and scala tympani (Figure 1.2). These compartments span the full length of the cochlea, starting at the oval and round windows (basal end of cochlea) and ending at the tip of the spiral known as the helicotrema (apical end of cochlea).

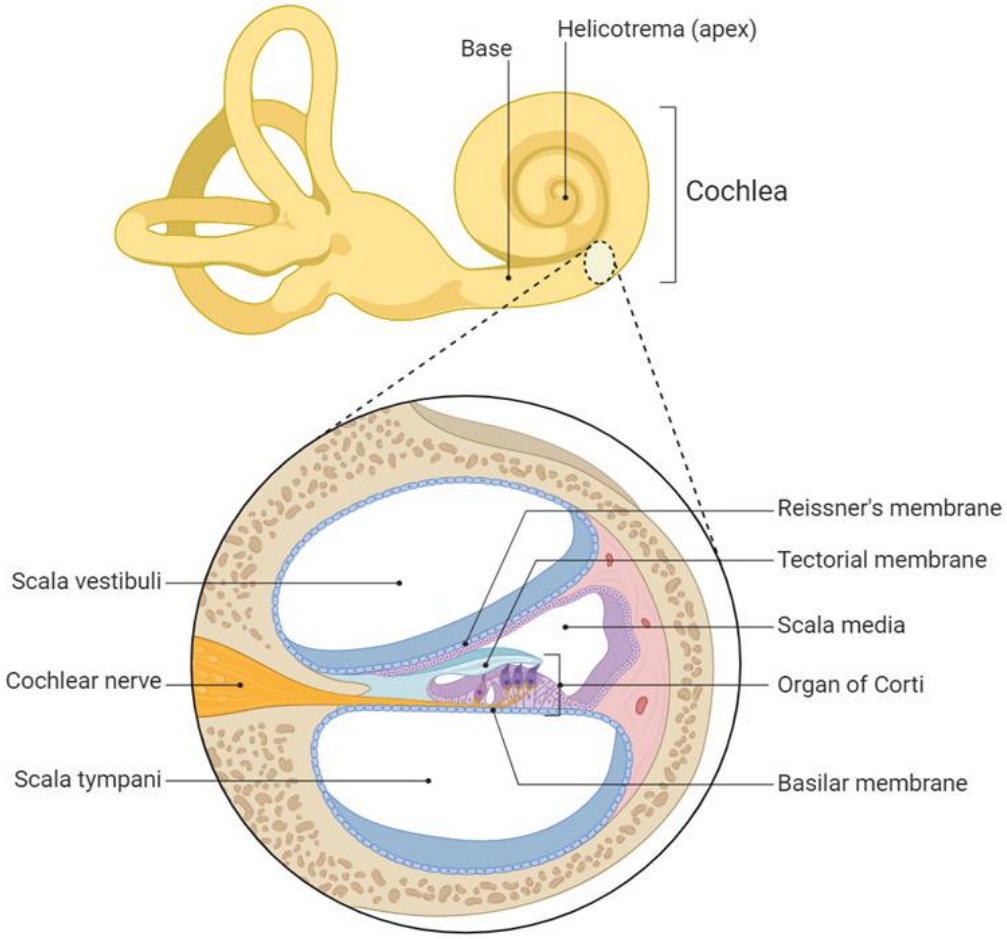

Figure 1.2: The internal structure of the cochlea

The cochlea spans from the apical end of the spiral (helicotrema) for ~2.5 turns and ends at the base. A cross section schematic image of the cochlear spiral shows the three internal compartments: scala vestibuli, scala tympani and scala media. The scala media contains the sensory epithelium (the organ of Corti) which sends sound-related information via the cochlear nerve to the brain. Adapted from "Inner Ear and Cochlear Anatomy", by BioRender.com (2024) and retrieved from https://app.biorender.com/biorender-templates.&apos.

During sound stimulation, the vibration of the stapes resembles a piston-like movement, pushing the oval window into and away from the cochlea (Figure 1.3). The inner surface of the oval window will flex against the adjacent fluid within the scala vestibuli. This will send vibrations through the fluid, down the length of the cochlea, to the helicotrema. At this apical point of the cochlea, the scala vestibuli compartment joins with the scala tympani, and so the vibrations then spread basally towards the round window. This means that altogether, the oval and round windows are flexing towards and away from the cochlea in opposing directions during sound stimulation. This produces vibrations travelling up and down the full length of the cochlear compartments (Figure 1.3) (Møller, 2012).

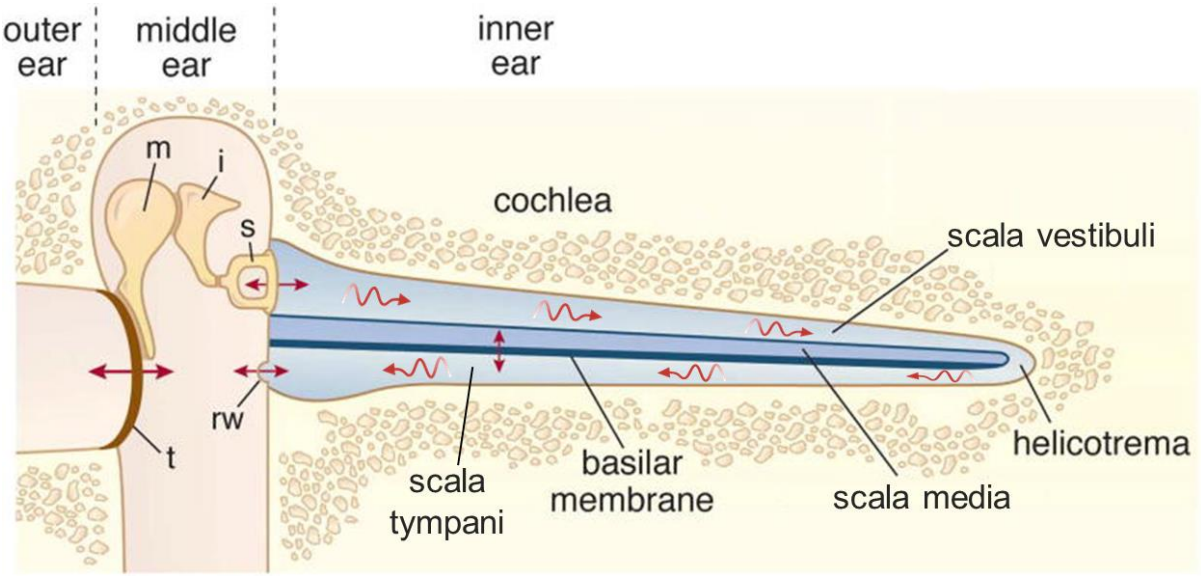

Figure 1.3: Sound transduction within the auditory system

Schematic image of the cochlea with its spiral uncoiled. Sound-induced vibrations (red arrows) vibrate the tympanic membrane (t) and the bones of the middle ear (m: malleus, i: incus, s: stapes). The stapes pushes against the oval window of the cochlea and sends vibrations throughout the fluid within the scala vestibuli. These vibrations travel to the apical end of the cochlea, pass into the scala tympani and move basally to the round window (rw). The scala media contains the organ of Corti (containing sensory hair cells) which sits on top of the basilar membrane. Figure modified from (Fettiplace, 2017).

Between the scala media and the scala tympani there is the basilar membrane, which is also displaced by these sound-induced waves (Figure 1.3, Figure 1.4). The basal end of the basilar membrane is narrow and thick, and it becomes increasingly wider and thinner towards the apex, producing a gradient in its stiffness. This means that different points along the basilar membrane will be maximally displaced by different frequencies of sound due to its gradual change in structure. Higher frequency sounds vibrate at the narrow (stiffer), basal end of the membrane, whereas low frequency sounds travel to the apical end of the membrane and cause larger vibrations there (Von Békésy, 1960). Thus, each point along the length of the cochlear spiral is maximally displaced by a different sound frequency, this is known as tonotopical organisation.

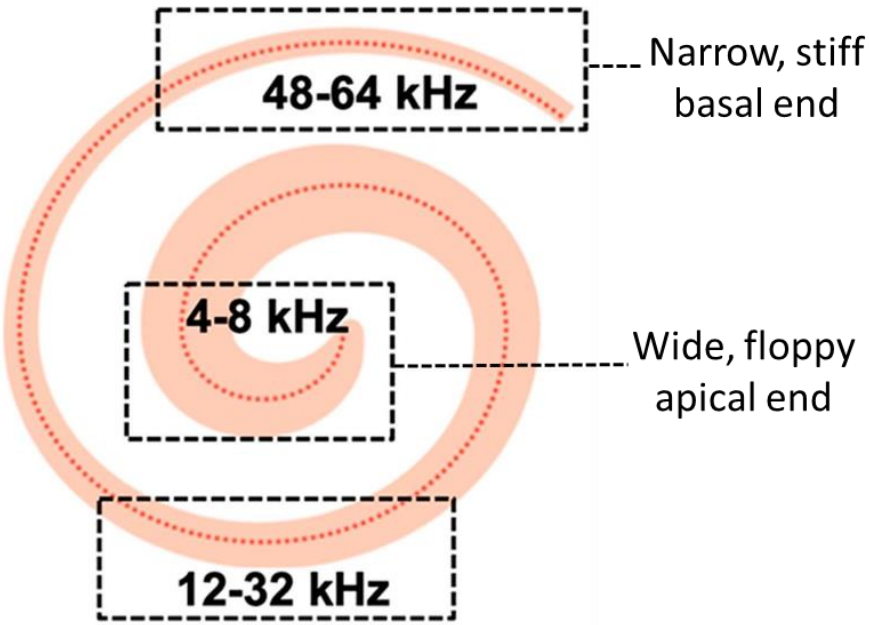

Figure 1.4: The basilar membrane

The basilar membrane spans the full length of the cochlea's spiral (pale pink). Its structure gradually changes from the basal end (narrow and stiff) towards the apical end (flexible and wide). Different frequencies of sound are able to maximally displace different areas along the basilar membrane due to its gradual change in structure. Low frequency sounds cause larger vibrations at the apical end, and high frequency sounds cause larger vibrations at the basal end. The frequencies labelled represent the tonotopic organisation of the mouse cochlea. The small red dots along the basilar membrane represent the hair cells activated by different frequencies of sound. Figure modified from (Klotz-Weigand and Enz, 2022).

1.1.1 The organ of Corti

The cochlear sensory epithelium is located within the organ of Corti (Figure 1.5). This is found above the basilar membrane, in the lining of the scala media cavity (Figure 1.2, Figure 1.3). The cells in this specialised epithelium work together to detect the sound-induced vibrations within the compartments of the cochlea and generate neural messages encoding the acoustic information (Møller, 2012). Two groups of specialised cells are found in this epithelium: sensory hair cells and glia-like supporting cells.

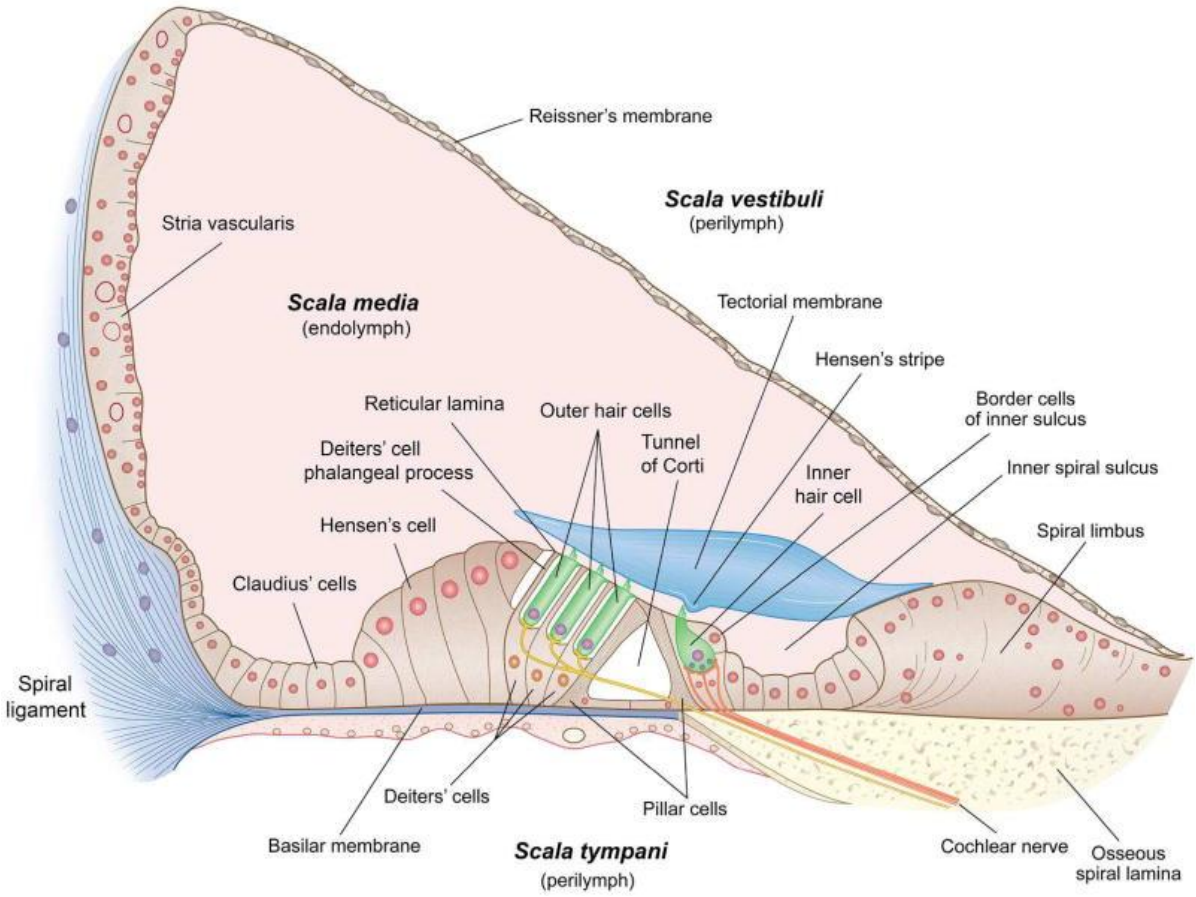

Figure 1.5: The organ of Corti

The organ of Corti is located in the boundary between the scala media and scala tympani. This sensory epithelium contains the hair cells (inner and outer) and various non-sensory cells (Deiters' cells, Hensen's cells, Claudius cells, pillar cells, inner border cells, inner phalangeal cells, and Boettcher cells). The hair cells are situated between the basilar membrane below and the tectorial membrane above; hair cells generate neural signals to be transmitted down the cochlear nerve to the brain. Figure from (Fettiplace, 2017).

1.1.1.1 The sensory hair cells

Hair cells are the auditory sensory receptors that transduce the sound-induced mechanical stimuli into electrical signals. The cochlea contains two types of hair cell, inner hair cells (IHCs) and outer hair cells (OHCs), which each perform different roles in the cochlea's response to sound stimulation. There is one row of IHCs and three rows of OHCs (Figure 1.5). OHCs contract and elongate in response to sound stimuli, which generates additional movement within the cochlear partition and amplifies the displacement of adjacent cochlear structures (Brownell *et al.*, 1985). The IHCs are the primary sensory receptors of the cochlea and as such, are innervated by ~95% of auditory afferent fibres (Spoendlin, 1972). These IHCs release the neurotransmitter glutamate onto auditory afferents in response to sound-induced cochlea vibrations.

These mechanosensitive cells have a bundle of hair-like projections on their apical surface known as stereocilia. In mice, each hair cell in the cochlea has three rows of stereocilia organised in a staircase-like formation, with the height of each row gradually increasing as you move to the back of the bundle (Figure 1.6A, B) (Lim, 1986). The shorter two rows of stereocilia express mechanically sensitive ion channels at their tips named mechano-electrical transducer (MET) channels (Beurg *et al.*, 2009). The movement of the stereocilia due to sound-induced vibrations triggers the opening/closing of these motion-sensitive MET channels (Kros, Rusch and Richardson, 1992). Sound-induced deflection of the hair bundles towards the posterior tallest row of stereocilia triggers the opening of these MET channels, while bundle deflection in the opposing direction towards the shorter stereocilia row promotes the closing of these channels (Kros, Rusch and Richardson, 1992).

All stereocilia within the bundle of one hair cell move together because of small connections between adjacent stereocilia known as tip link complexes (Figure 1.6C, D) (Pickles, Comis and Osborne, 1984). These connections join stereocilia within the same row, and also join the tips of shorter stereocilia to the middle of taller cilia in the row behind. The MET channels are located adjacent to the tip links at the top of the shorter rows, and it is believed that the tension applied to these links during bundle deflection is responsible for the opening of these mechanosensitive channels (Assad, Shepherd and Corey, 1991). The larger the deflection of the stereocilia, the greater the stretching applied to the tip links and the larger the open probability of the MET channels. Thus, these linkages are crucial for hair cell

mechanotransduction, since mutations affecting the proteins which make up the tip link (cadherin-23 and protocadherin-15) are known to cause deafness, further highlighting how critical these linkages are for hearing (Figure 1.6) (Zheng *et al.*, 2005).

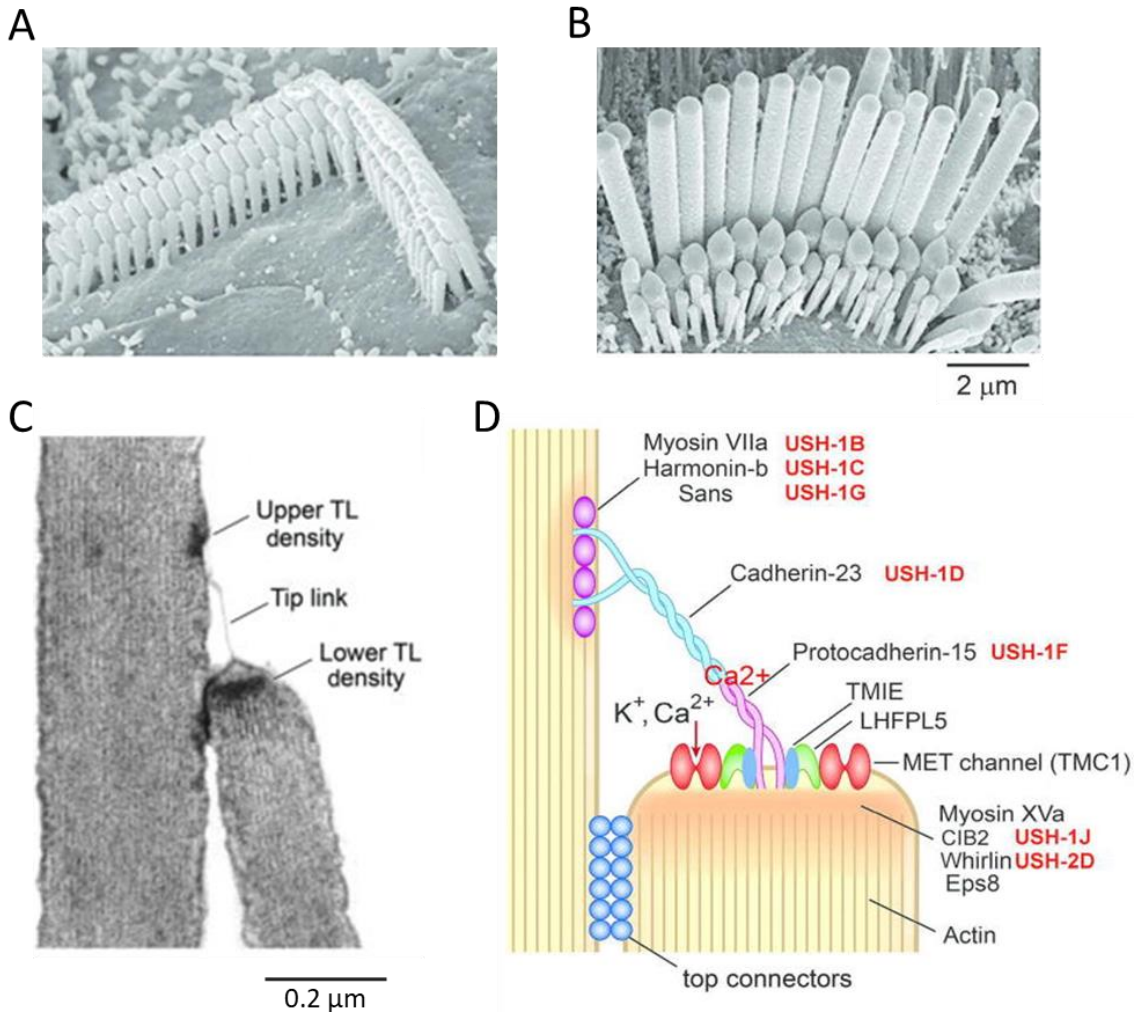

Figure 1.6: Hair cell stereocilia bundle structure and tip links

A, **B**: Scanning electron micrographs of mature outer hair cell (**A**) and inner hair cell (**B**) stereocilia bundle orientation. Three rows of stereocilia display staircase-like formation on both hair cell types. Mechano-electrical transducer (MET) channels are located on the shortest two rows within the bundle. **C**: Transmission electron micrograph of an outer hair cell tip link joining the tip of a shorter stereocilium to the middle of a taller stereocilium behind. **D**: Schematic diagram showing MET channels located adjacent to tip links on the shorter cilia (red channel), thus stretching of the tip links is believed to influence the opening of these channels. The tip link contains many components, each of which are crucial for correct functioning, these include cadherin-23 and protocadherin-15. The mutations associated with these components, known to result in different types of hearing loss (Usher syndrome), are shown in red adjacent to the relevant component. Figure from (Fettiplace, 2017).

The hair cells are situated between two very different ionic environments which creates a steep electrical gradient (v. Békésy, 1951; Casale *et al.*, 2022). The apical surface of the sensory epithelium, including the stereocilia, are bathed in endolymph fluid within the scala media compartment (Figure 1.5, Figure 1.7). This has a K^+ rich composition with low Ca^{2+} and a very positive electrical potential compared to the perilymph solution (Bosher, Warren and Hallpike, 1997). K^+ transport pumps on the stria vascularis, located on the lateral wall of the scala media, are responsible for maintaining the high K^+ concentration in the endolymph (Figure 1.5) (Wangemann, Liu and Marcus, 1995). All apical hair cell surfaces are adhered to other surrounding cells in the epithelium via tight junctions (Ben-Yosef *et al.*, 2003). This creates a barrier known as the reticular lamina, separating the endolymph fluid in the scala media from the basal part of the hair cells, which instead are surrounded by intercellular perilymph fluid (Figure 1.7). Perilymph fluid has an ionic composition like that of typical extracellular fluid (high Na^+ and Ca^{2+} and low K^+ concentrations) (Smith, Lowry and Wu, 1954; Citron, Exley and Hallpike, 1956). The difference in ionic composition between these neighbouring compartments generates a potential difference known as the endocochlear potential of about +80mV in the endolymph compared to the perilymph (v. Békésy, 1951; Hibino *et al.*, 2010).

Due to these specific ionic environments, the opening of the hair cell MET channels will drive the flow of ions down the electrical gradient. This is between the very positively charged endolymph (approximately +80mV) surrounding the stereocilia and the more negative intracellular environment of the hair cell (approximately -60mV), giving a very large driving force of ~140mV (v. Békésy, 1952). The MET channels are non-selective cation channels and so positive ions, such as K^+ and Ca^{2+}, will flood into the hair cell from the endolymph to balance out the large potential difference. Thus, sound-induced vibrations and stereocilia deflection (towards the taller posterior row) results in the depolarisation of hair cells (Figure 1.7). This transduction of mechanical stimuli into an electrical response in hair cells relies on the maintenance of this large electrical driving force within the organ of Corti.

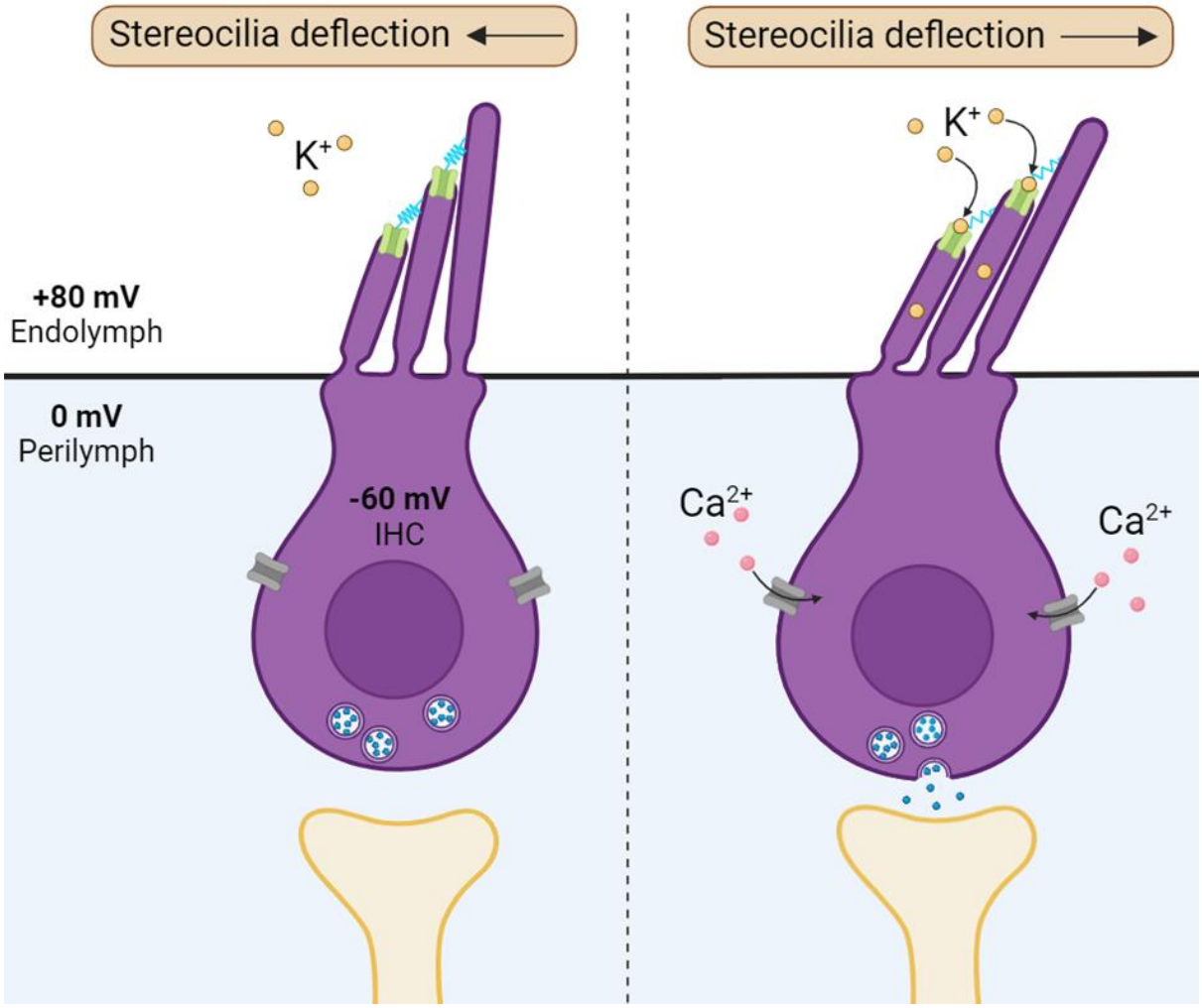

Figure 1.7: Hair cell stereocilia deflection and depolarisation

Diagram illustrating the events following hair cell stereocilia deflection. The left image shows deflection towards the front of the hair bundle which will close MET channels (green) and induce no neurotransmitter release onto auditory neurons. The right image shows hair bundle deflection towards the taller cilia, which triggers the stretching of tip linkages (cyan) and opening of MET channels (green). This leads to cation influx into the hair cell due to the electrical driving force between the endolymph (+80mV) and the hair cells intracellular environment (-60mV). The resultant hair cell depolarisation opens voltage-gated Ca^{2+} channels (grey), and the increased intracellular Ca^{2+} will promote exocytosis of synaptic vesicles, leading to neurotransmitter release onto auditory neurons. Figure created using BioRender, based on figure from (Svechtarova *et al.*, 2016).

Inner hair cell depolarisation following sound-induced stereocilia deflection triggers the opening of its voltage gated Cav1.3 Ca^{2+} channels, and Ca^{2+} influx (Lewis and Hudspeth, 1983). This high intracellular Ca^{2+} promotes the exocytosis of glutamate-containing vesicles from the hair cells presynaptic membrane (Figure 1.7) (Beutner *et al.*, 2001; Nouvian *et al.*, 2006). Large groups of these vesicles are located adjacent to the pre-synaptic membrane attached to structures called synaptic ribbons; this specialised setup allows for more temporally precise glutamate release that can be sustained throughout long periods of sound stimulation (Figure 1.8) (Smith and Sjöstrand, 1961; Vincent *et al.*, 2015). Glutamate in the synaptic cleft binds to α-amino-3-hydroxy-5-methyl-4-isoxazolepropionic acid (AMPA) receptors on postsynaptic neurons (Matsubara *et al.*, 1996). This leads to the depolarisation of the neuron via the induction of an excitatory postsynaptic current and the generation of action potentials which are relayed to central auditory centres (Glowatzki and Fuchs, 2002). These auditory afferent neurons innervating the hair cells can be split into two groups. Type 1 afferent neurons make up 95% of this neuron population and each form a synapse with a single IHCs' synaptic ribbon (Spoendlin, 1972; Berglund and Ryugo, 1987). These neurons carry sound-related information regarding frequency and intensity to deeper auditory centres. Type 2 afferent neurons make up the remaining 5% and they each innervate multiple OHCs; these neurons are believed to relay information regarding noxious stimuli to auditory centres in the brain, but their exact function is still unclear (Liu, Glowatzki and Fuchs, 2015).

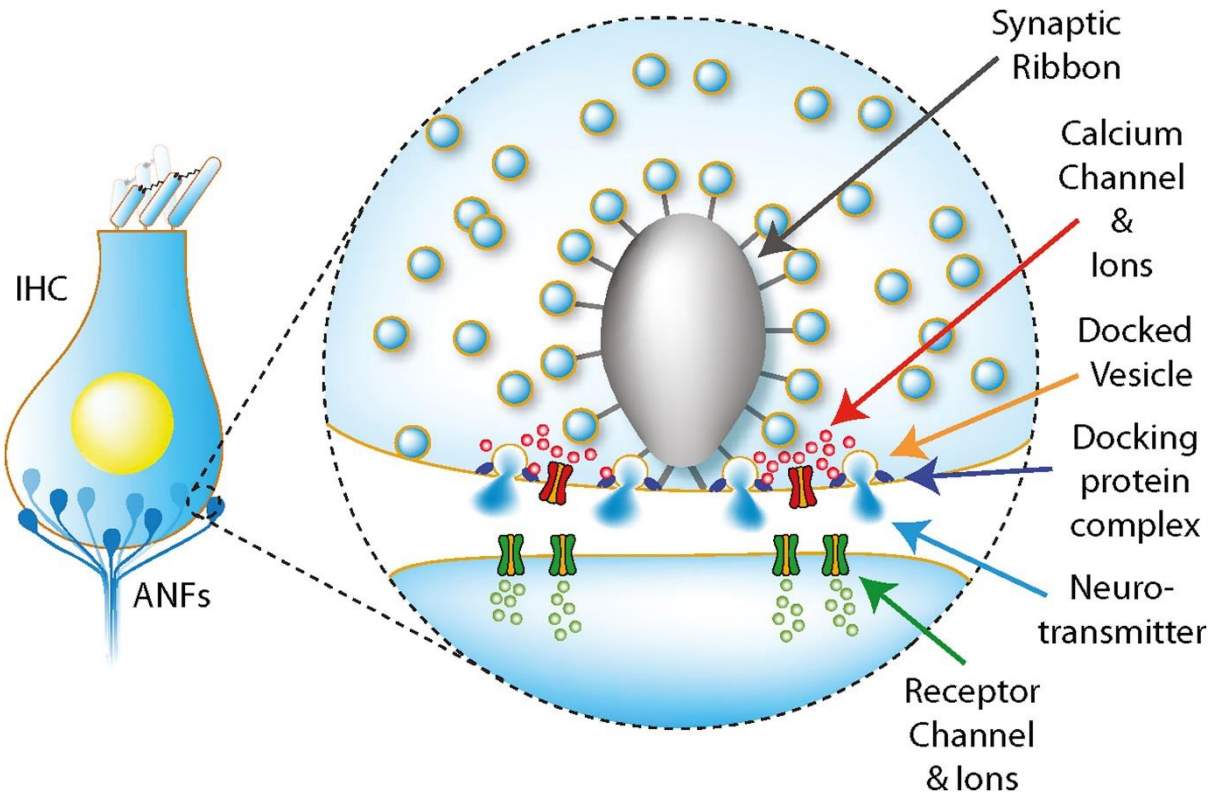

Figure 1.8: Inner hair cell ribbon synapse

Diagram of an inner hair cell (IHC) forming synapses with auditory nerve fibres (ANFs). Each synapse contains one hair cell synaptic ribbon at the pre-synapse and one auditory nerve post-synapse. One synapse is expanded to show the structures within. Each synapse contains an IHC synaptic ribbon with many glutamate containing vesicles attached. High intracellular Ca^{2+} promotes the movement of these vesicles to the cell membrane where they dock and release glutamate into the synaptic cleft. Glutamate binds to AMPA receptors on the auditory neurons and triggers post-synaptic excitatory currents. Figure from (Bruce, Erfani and Zilany, 2018).

1.1.1.2 Sensory hair cell firing during development

As discussed in the previous section, sound stimulation deflects hair cell stereocilia triggering the opening of their MET channels, K^+ influx, and hair cell depolarisation (Figure 1.7). This produces a graded receptor potential which depends on the size of the stimulus (Palmer and Russell, 1986). Louder sounds will cause greater stereocilia deflection and MET channel opening, which will lead to greater IHC depolarisation and the release of more glutamate-containing vesicles at the synapse. Hair cells in the mature cochlea don't fire action potentials and instead exhibit this graded voltage response due to the presence of a fast-activating outward K^+ current ($I_{K,f}$) and a negatively activated outward K^+ current ($I_{K,n}$) (Figure 1.9) (Kros, Ruppersberg and Rüsch, 1998; Marcotti *et al.*, 2003a). These potassium currents enhance IHC hyperpolarisation and lower the resting membrane potential to stop spiking activity.

However, during cochlear development, the difference in potassium currents allows for immature IHCs to fire action potentials. Specifically, the $I_{K,f}$ is absent and the $I_{K,n}$ is instead known as I_{K1} and only activates at very hyperpolarised membrane potentials (Marcotti *et al.*, 2003a). This produces a higher resting membrane potential and allows for spiking activity up until the onset of hearing at P12 (postnatal day 12) in neonatal mice (Figure 1.9). Furthermore, these immature IHC action potentials occur spontaneously (without sound stimulation) and so are believed to be generated intrinsically by the IHCs (Kros, Ruppersberg and Rüsch, 1998; Marcotti *et al.*, 2003b; Johnson *et al.*, 2011). The pattern of this IHC firing can be modulated by ATP-mediated Ca^{2+} waves originating in nearby supporting cells (Tritsch and Bergles, 2010; Babola *et al.*, 2018). This pattern differs between more apical and more basal IHCs and so it is thought to be important for the refinement of synapses into the correct tonotopic organisation along the cochlea (Johnson *et al.*, 2011; Johnson *et al.*, 2008).

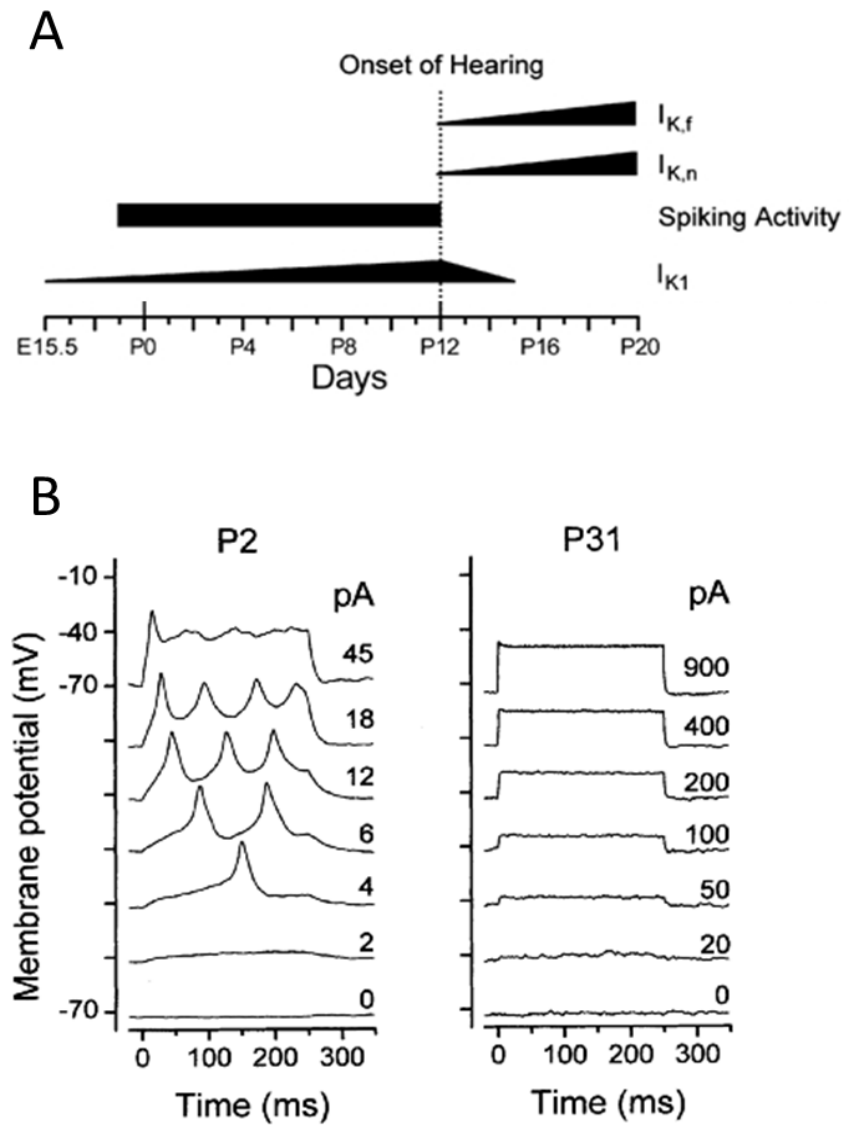

Figure 1.9: Electrophysiological properties in the developing inner hair cell

A: The diagram shows the timing of the appearance and disappearance of K^+ currents and spike activity during maturation. The change in width of the horizontal bars gives an approximate indication of developmental changes in the size of the currents. The timing is valid for the apical coil (changes in basal coil IHCs were usually shifted forward by 1–2 days). Figure and legend modified from (Marcotti *et al.*, 2003a).

B: Voltage responses of inner hair cells to current steps (duration 250 ms, step size labelled next to voltage records). On the left are the voltage responses from a P2, immature cell. Currents as small as 4 pA elicited slow depolarisations, triggering spikes. On the right are the voltage responses from a P31 adult IHC, showing rapid, graded voltage responses without regenerative depolarisations or spiking. For the largest current steps, progressively more $I_{K,f}$ is activated in the P31 cell, hence the divergence in the voltage responses. For clarity, successive voltage records were shifted by 30 mV, so that unlabelled tick marks represent −70 mV, close to the resting potential. Both cells from apical coil. Figure and legend modified from (Kros, Ruppersberg and Rüsch, 1998).

1.1.1.3 The supporting cells

Surrounding the hair cells in the cochlear sensory epithelium are non-sensory supporting cells (Figure 1.10). These include the Deiters' cells, Hensen's cells, pillar cells, inner phalangeal cells, Claudius' cells, Border cells and the cells of the inner and outer sulcus (Møller, 2012). These supporting cells display a diverse range of physiological properties which allow them to contribute to a plethora of cellular processes crucial for the development and functioning of the cochlea.

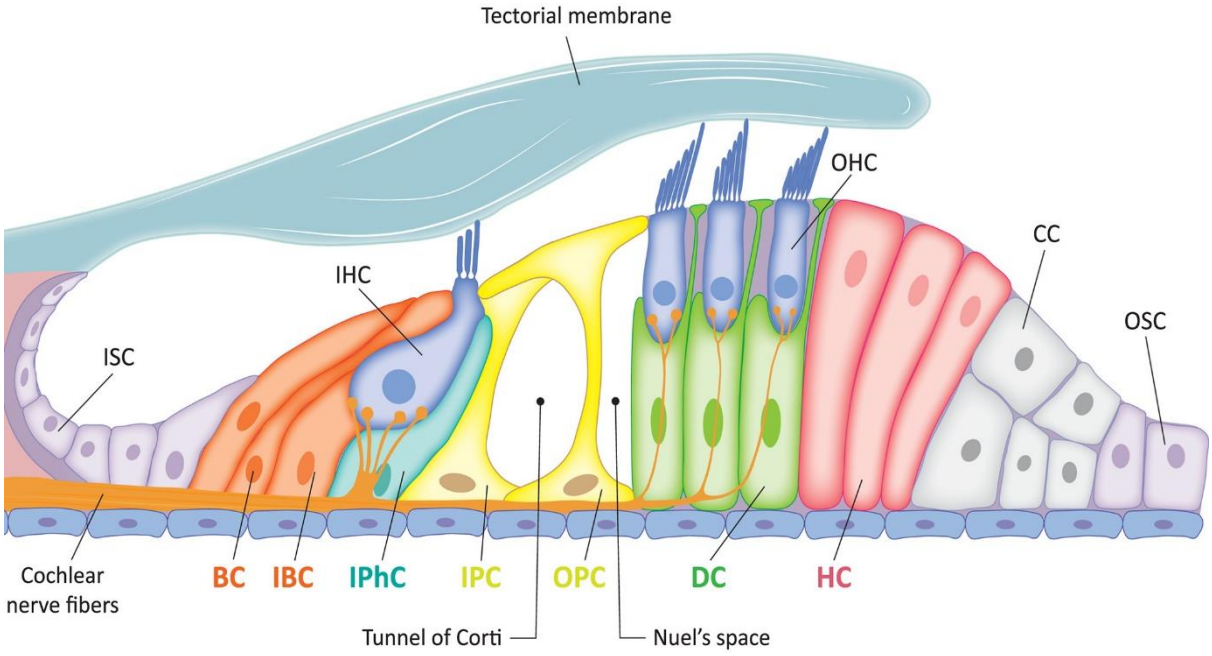

Figure 1.10: The supporting cells in the organ of Corti

Inner and outer hair cells are shown in blue (labelled IHC, OHC). The tunnel of Corti lies between these two subtypes of hair cell and is formed by inner and outer pillar cells shown in yellow (IPC, OPC). The IHC is adjacent to an inner phalangeal cell shown on the right in teal (IPhC) and an inner border cell on the left in orange (IBC). To the left of the IBC are additional border cells (BC) followed by the inner sulcus cells (ISC). The OHCs sit upon the Deiters' cells shown in green (DC). To the right of the OHCs and DCs are the Hensen's cells in red (HC), Claudius' cells in grey (CC) and finally the outer sulcus cells (OSC). Figure from (Jang *et al.*, 2022).

For instance, the Deiters' cells and pillar cells contain bundles of microtubules and actin filaments giving them a firm, but flexible cytoskeleton (Angelborg and Engström, 1972; Zetes, Tolomeo and Holley, 2012). This provides structural integrity to the sensory epithelium when sound stimulation sends vibrations throughout the cochlea. Also, adjacent to the IHCs, the inner phalangeal cells and border cells express glutamate transporters (glutamate aspartate transporter: GLAST) which clear excess neurotransmitter from the IHC synapses (Furness and Lehre, 1997; Glowatzki *et al.*, 2006). This clearance is crucial to prevent excitotoxicity, where the accumulation of glutamate can cause swelling of spiral ganglion neuron afferent terminals, synaptopathy and hearing loss (Hakuba *et al.*, 2000). Furthermore, all supporting cells are connected by gap junction channels which create passageways between the cytosol of neighbouring cells (Santos-Sacchi and Dallos, 1983; Kikuchi *et al.*, 1995; Jagger and Forge, 2006). This creates a functional syncytium allowing the transport of a variety of molecules across the epithelium. Secondary messengers such as ATP utilise this gap junction network to propagate intracellular signalling cascades into neighbouring supporting cells (Anselmi *et al.*, 2008). One example of this being the purinergic receptor signalling cascade which generates intercellular Ca^{2+} waves across the supporting cells thought to influence IHC spiking during development (Tritsch *et al.*, 2007; Babola *et al.*, 2020). Additionally, following IHC depolarisation, K^+ ions must be recycled back to the endolymph to replenish the endocochlear potential (v. Békésy, 1952; Hibino *et al.*, 2010). It is hypothesised that this is facilitated by the diffusion of K^+ ions back to the stria vascularis via the supporting cell gap junction channels (Kikuchi *et al.*, 2000; Wangemann, 2006). This is followed by the K^+ ions being pumped back out into the endolymph to maintain the steep electrical gradient for cation movement into the IHC with the opening of the MET channels.

Within this thesis, only two types of the many membrane proteins expressed by the supporting cells will be discussed in detail: purinergic receptors and gap junction channels.

1.1.1.3.1 Purinergic receptors

Purinergic receptors are a group of transmembrane proteins which respond to the extracellular binding of purines such as ATP, ADP and adenosine (Burnstock, 1972; Burnstock, 1980). These receptors are split into two subfamilies based on their agonist selectivity: P1 receptors bind adenosine and the P2 receptors bind ATP, UTP and ADP (Burnstock, 1978). The P2 family is further separated into two more subgroups: the ionotropic P2X subtype and the metabotropic P2Y subtype (Figure 1.11) (Burnstock and Kennedy, 1985). P2X receptors are ATP-gated cation channels and have seven members within their subgroup ($P2X_1$ - $P2X_7$) (North, 2002). The metabotropic P2Y receptor family has eight members ($P2Y_1$, $P2Y_2$, $P2Y_4$, $P2Y_6$, $P2Y_{11}$, $P2Y_{12}$, $P2Y_{13}$, $P2Y_{14}$) and can initiate intracellular G-protein coupled signalling pathways following agonist binding (Fredholm *et al.*, 1994; Abbracchio *et al.*, 2009). The diversity between these different purinergic receptors can explain the wide variety of cellular functions they perform across the majority of tissues in the body (Burnstock, 2018).

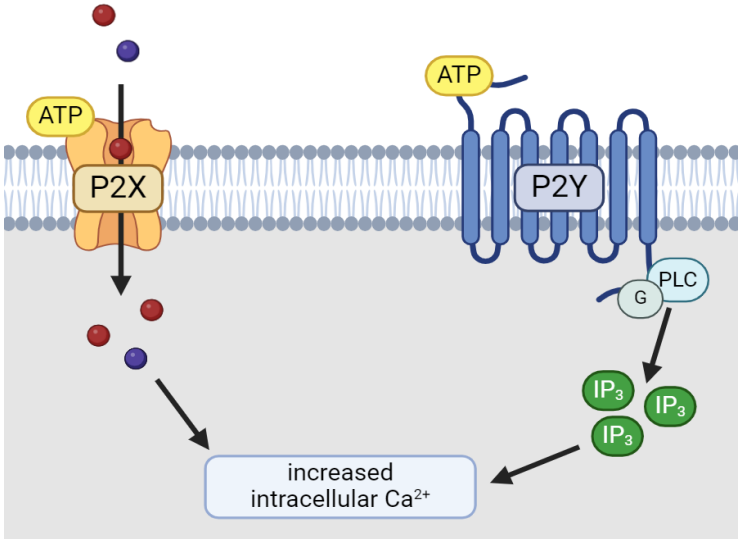

Figure 1.11: P2 purinergic receptors

Diagram illustrating the two subtypes of P2 purinergic receptors. Extracellular binding of ATP to P2X receptors triggers the opening of their cation channel. Cations such as K^+, Na^+ and Ca^{2+} then can diffuse into the cell and go on to have a range of effects on cellular function. P2Y receptors trigger intracellular G-protein coupled responses following the extracellular binding of ATP. This will lead to the production of downstream signalling molecules such as IP_3 which promotes Ca^{2+} release into the cytoplasm from intracellular stores. Figure created using BioRender.

Within the organ of Corti, members of the P2 purinergic receptor family are expressed in both hair cells and supporting cells (Housley *et al.*, 1999; Xiang, Bo and Burnstock, 1999; Huang *et al.*, 2010). ATP, or other agonists, released into the endolymph and perilymph will bind and activate these P2 receptors triggering a range of different cellular processes. In this thesis, the functioning of P2Y receptors in cochlear supporting cells will be discussed in detail.

Before hearing onset, inner hair cells and their spiral ganglion neurons fire spontaneous action potentials (Marcotti *et al.*, 2003b; Johnson *et al.*, 2011) which are crucial for the maturation of their synaptic connections and refinement of the tonotopic map (Clause *et al.*, 2014; Müller *et al.*, 2019). This spontaneous activity within the hair cells is believed to be modulated by a P2Y signalling cascade originating in nearby supporting cells (Tritsch *et al.*, 2007; Babola *et al.*, 2020). The cells of the immature inner sulcus [Kölliker's organ: (Hinojosa, 1977)] (Figure 1.12) express $P2Y_{1, 2+4}$ receptors (Huang *et al.*, 2010; Babola *et al.*, 2020). At this neonatal age, ATP is spontaneously released into the endolymph which can bind and activate these metabotropic P2Y receptors (Anselmi *et al.*, 2008). The resultant intracellular G-protein coupled signalling cascade generates the intracellular secondary messenger inositol 1, 4, 5-triphosphate (IP_3), which is known to induce Ca^{2+} release from the endoplasmic reticulum into the cytosol (Figure 1.13) (Beltramello *et al.*, 2005; Piazza *et al.*, 2007). This IP_3 can also travel to neighbouring cells, via gap junction channels, and trigger further Ca^{2+} release across other Kölliker's cells in the epithelium (Mammano, 2013). This rise in intracellular Ca^{2+} will also trigger the opening of connexin hemichannels on the Kölliker's cells, allowing ATP efflux to the extracellular space, and further autocrine activation of P2Y receptors (Anselmi *et al.*, 2008). This mechanism is termed 'ATP-induced ATP release' and facilitates these waves of intracellular Ca^{2+} transients travelling across the supporting cells in the epithelium (Tritsch *et al.*, 2007). The increased intracellular Ca^{2+} will also trigger the opening of TMEM16A chloride channels and Cl^- efflux from these supporting cells (Wang *et al.*, 2015). This is followed by K^+ and water efflux to counteract this change in the cell's potential. The loss of water causes the cells to shrink and increases the concentration of K^+, and volume of water, extracellularly. This is hypothesised to influence IHC depolarisation as the increased extracellular K^+ concentration in the perilymph will delay K^+ efflux from basolateral IHCs, and so this would influence the firing of spontaneous action potentials in immature hair cells (Babola *et al.*, 2020; Ceriani *et al.*, 2019a).

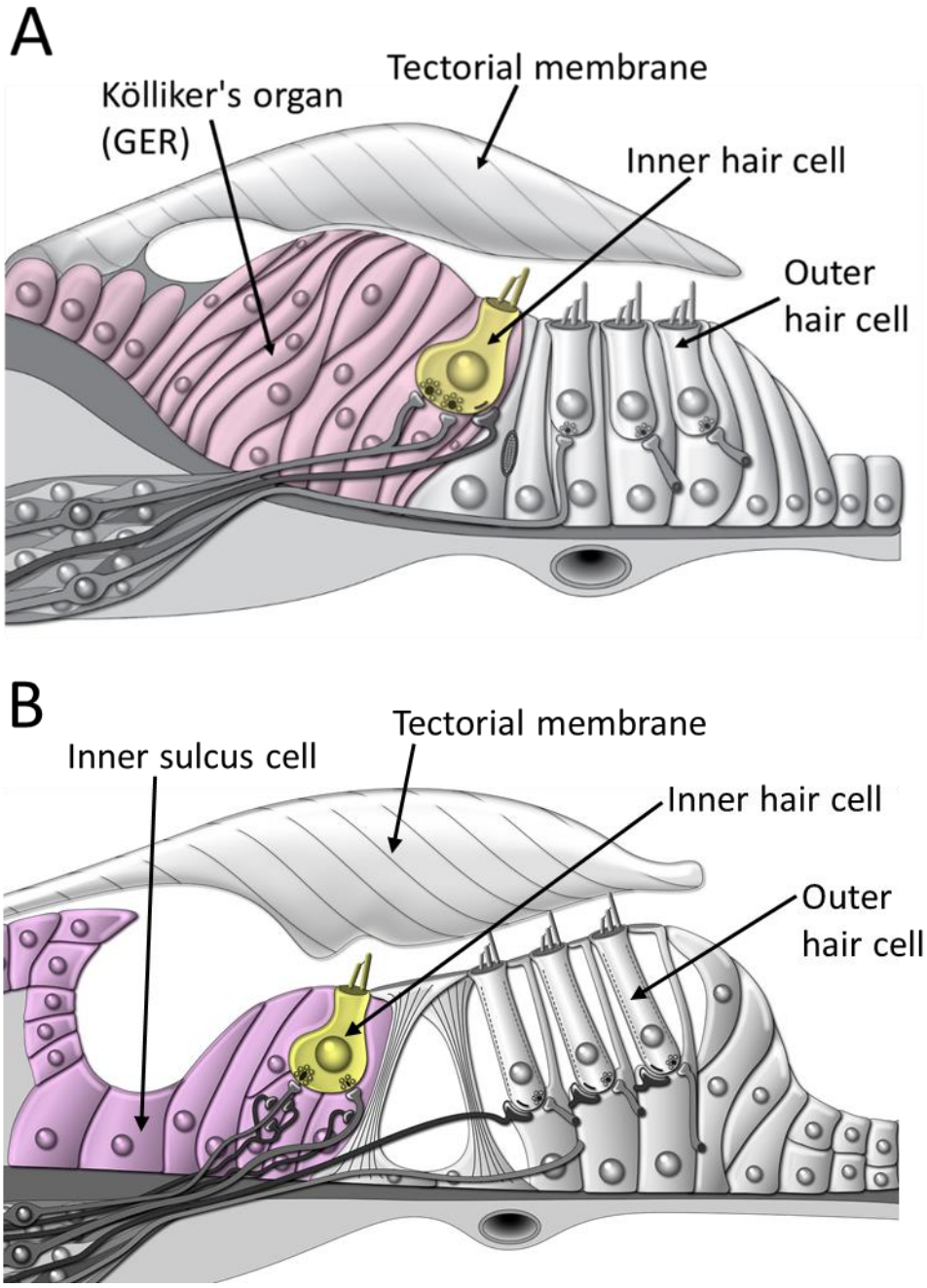

Figure 1.12: Maturation of the organ of Corti

A: Schematic image of the immature organ of Corti. An inner hair cell is shown in yellow. Next to the inner hair cell there are the cells of Kölliker's organ (pink) also known as the greater epithelial ridge (GER). **B**: Schematic image of the mature organ of Corti. After the onset of hearing, the Kölliker's organ is lost and replaced by the inner sulcus cells (pink). Figure modified from (Hool *et al.*, 2023).

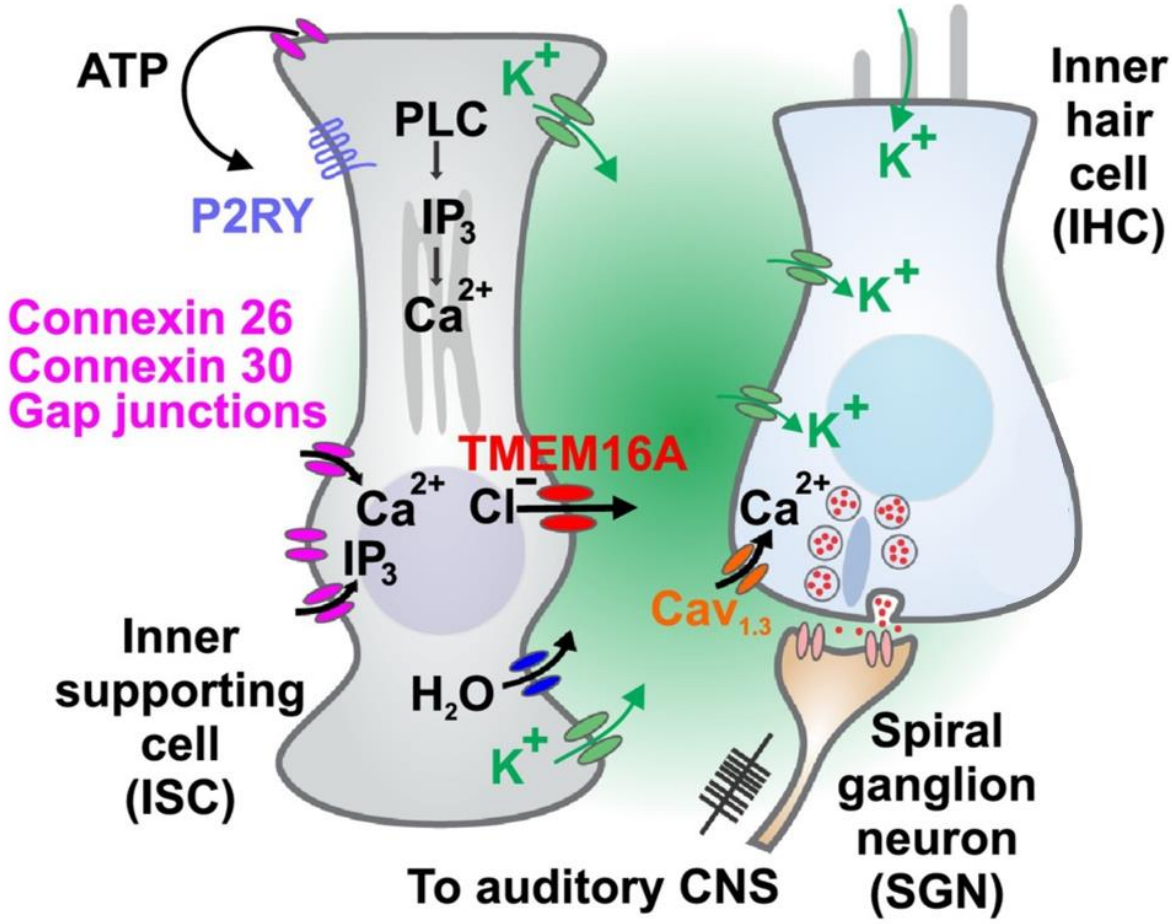

Figure 1.13: P2Y receptor signalling cascades initiated in supporting cells affect the depolarisation of immature inner hair cells

P2Y receptors are expressed by the supporting cells in Kölliker's organ prior to hearing onset (grey cell). The extracellular binding of ATP to these receptors triggers an intracellular G-protein coupled signalling cascade resulting in the production of inositol 1, 4, 5-triphosphate (IP_3). This molecule binds to IP_3 receptors on the endoplasmic reticulum and stimulates the release of Ca^{2+} into the cytoplasm. The TMEM16A Cl^- channels (red) will be activated by high intracellular Ca^{2+} and so Cl^- will leave the cell into the extracellular space. This will be followed by water and K^+ and so the electrical potential of the extracellular fluid surrounding the hair cells will become more positive. This will mean there is a smaller driving force for K^+ to leave the hair cells which will influence hair cell depolarisation and the firing of action potentials. Therefore, the activation of P2Y receptors on the supporting cells can influence the ionic composition of the intercellular fluid and impact the firing of inner hair cell action potentials. Additionally, the supporting cells are connected by gap junction channels and so Ca^{2+} and IP_3 can diffuse into neighbouring cells and trigger the same signalling cascade again. Figure modified from (Kersbergen and Bergles, 2024).

These action potentials within the inner hair cells will cause glutamate release into the synaptic cleft and elicit action potential firing in spiral ganglion neurons (SGNs) (Zhang-Hooks *et al.*, 2016). This event is reliant upon the P2Y purinergic signalling cascade within nearby supporting cells as the use of P2Y receptor antagonists abolished action potentials in IHCs and SGNs (Babola *et al.*, 2020; Babola *et al.*, 2021).

Though the mechanism is well established, there is some disagreement within the literature as to which P2Y receptors are involved in modulating these spontaneous hair cell action potentials. In the developing rat cochlea, $P2Y_2$ and $P2Y_4$ receptors have been shown to be expressed in Kölliker's organ cells (Huang *et al.*, 2010). Furthermore, UTP (a potent agonist for $P2Y_2$ and $P2Y_4$, but not for $P2Y_1$) was reported to trigger large Ca^{2+} oscillations across the Kölliker's cells of the rat cochlea (Piazza *et al.*, 2007). In addition to this, a significantly larger Ca^{2+} response was observed in the Kölliker's cells following ATP administration compared to ADP administration. ATP is known to be the principal agonist for $P2Y_2$ and $P2Y_4$ receptors, whereas $P2Y_1$ receptors have a weak response to ATP and respond most strongly to ADP (von Kügelgen and Hoffmann, 2016). Therefore, these papers suggest $P2Y_2$ and $P2Y_4$ receptors are responsible for the Ca^{2+} transients observed within Kölliker's organ before hearing onset. However, it has also been reported that $P2Y_1$ is the main receptor responsible for modulating the hair cells' immature Ca^{2+} action potentials as spontaneous activity in ISCs, IHCs and SGNs was shown to be absent when $P2Y_1$ receptor activity was blocked via an antagonist (MRS2500) (Babola *et al.*, 2020). Even though Huang et al., 2010 show no $P2Y_1$ expression in Kölliker's organ. Thus, further investigation would be beneficial to confirm which receptors drive this important process in the immature cochlea.

Following the onset of hearing, spontaneous hair cell action potentials cease, and sound stimulation is now required to trigger large enough hair cell depolarisations to elicit action potentials in SGNs (Tritsch and Bergles, 2010). In addition to this, there is limited data regarding the role of P2Y receptors in the adult inner sulcus and so their function in the mature cochlea remains unknown. For example, some data suggest a complete lack of P2Y receptor expression, and activity, in the cells of the inner sulcus after cochlear development. Rat Kölliker's organ cells have been reported to completely lose P2Y receptor expression following hearing onset at ~P12 (Huang *et al.*, 2010). Furthermore, Ca^{2+} responses were compared between neonatal and 2-month-old gerbil inner sulcus cells following ATP

application; it was shown that the 2-month-old cells elicited no response at the inner sulcus whereas the neonatal Kölliker's cells displayed propagating intracellular Ca^{2+} waves (Chan and Rouse, 2016). Therefore, this implies the P2Y receptors expressed in the neonatal Kölliker's organ cells, which drive intracellular Ca^{2+} transients, are no longer expressed in the mature inner sulcus cells.

However, other papers have presented evidence to suggest P2Y purinergic signalling may be maintained in the post-hearing inner sulcus. For example, it was reported that P16 murine inner sulcus cells displayed waves of intracellular Ca^{2+} transients, and inward currents, in response to ATP or UTP (P2Y specific agonist) application (Tritsch and Bergles, 2010). This suggests P2Y receptor expression is maintained at P16 in the inner sulcus, even though the spontaneous Ca^{2+} oscillations they are believed to mediate cease before hearing onset at ~P12. Therefore, these receptors potentially serve another function in the mature cochlea involving the propagation of intracellular Ca^{2+} transients. In support of this, ATP-induced intracellular Ca^{2+} transients, and associated inward currents, have been reported across the inner sulcus of the adult mouse cochlea (Sirko, Gale and Ashmore, 2019). However, it was concluded that it was likely a combination of both P2X and P2Y receptors driving the observed Ca^{2+} responses to ATP. This is because the Ca^{2+} response observed following UTP application was significantly smaller compared to the ATP response, suggesting P2Y receptor activation alone isn't sufficient to produce the same magnitude of activity. Nevertheless, it was proposed that these P2Y-associated Ca^{2+} transients in the mature inner sulcus may contribute to regulation of gene expression, as similar Ca^{2+} oscillations have been shown to influence gene expression and transcription factor activity in numerous other tissues (Dolmetsch, Xu and Lewis, 1998; Hu *et al.*, 1999). Thus overall, it is apparent that further investigation of P2Y purinergic receptor expression and activity is required within the mature cochlea inner sulcus to confirm whether these receptors are expressed, and if they are, what is their function following development.

1.1.1.3.2 Gap junction channels

Gap junction membrane channels form a passageway between the cytosol of two neighbouring cells allowing the transport of ions and small molecules (Bennett and Goodenough, 1978). Six connexin proteins arrange to form a hexametric ring with a central pore at the cell membrane, this is known as a connexon (Bruzzone, White and Paul, 1996; Beyer, Paul and Goodenough, 1990). The alignment of two connexon complexes on neighbouring cells creates a passageway between their intracellular environments, also known as a 'gap junction' (Figure 1.14). Additionally, a single, unpaired connexon complex is known as a 'hemichannel', and these can facilitate transport of molecules between a cell's cytosol and the extracellular space under certain circumstances (Li *et al.*, 1996).

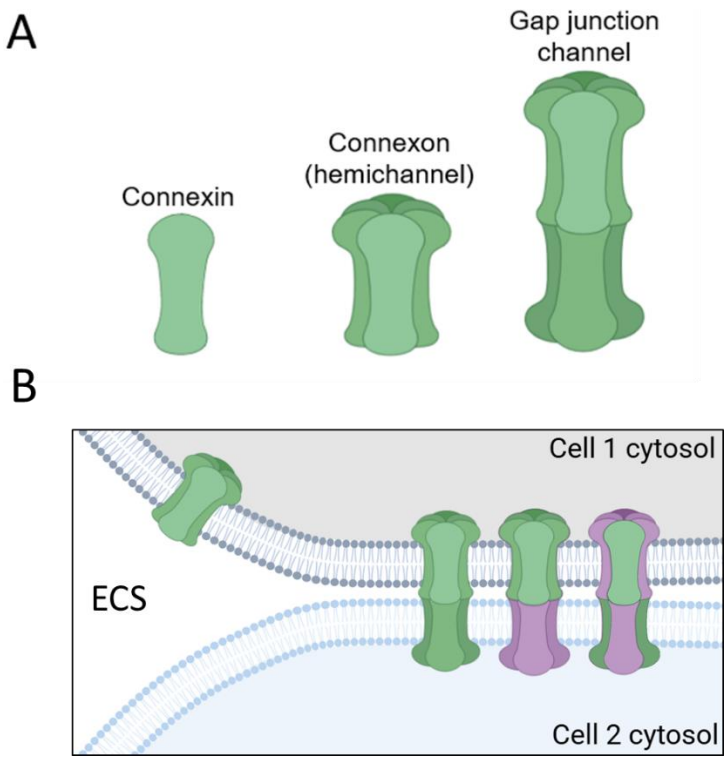

Figure 1.14: Gap junction channel structure

A: A single connexin subunit is shown on the left. In the centre, six connexin subunits are arranged in a hexametric ring with a central pore to form a connexon complex or hemichannel. On the right, two connexon complexes have aligned their pores to create a gap junction channel. **B**: An image showing how the gap junction channels arrange at the cell membrane to connect the cytosols of neighbouring cells. These channels can contain only one subtype of connexin subunit (green) or can contain different connexin subunits (green and purple). Lone connexons on the cell membrane (hemichannels) create a channel between the intracellular and extracellular space (ECS). Figure created with BioRender.

At cell-cell junctions, thousands of gap junction channels (GJCs) congregate together to form ‘plaques’. Within the mature organ of Corti, the majority of supporting cells express gap junction plaques composed of connexin 26 (Cx26) and connexin 30 (Cx30) (Figure 1.15) (Kikuchi *et al.*, 1995; Lautermann *et al.*, 1998). The only exception to this are Deiters’ cell GJCs which have been reported to express mainly Cx30 (Jagger and Forge, 2015; Jagger and Forge, 2006). Therefore in the cochlea, there are likely to be homomeric Cx26 and Cx30 gap junction channels which consist of just one type of connexin subunit, as well as heteromeric Cx26/Cx30 gap junction channels where both connexin subunits combine within one channel (Ahmad *et al.*, 2003; Defourny and Thiry, 2023). The sensory hair cells do not express GJCs.

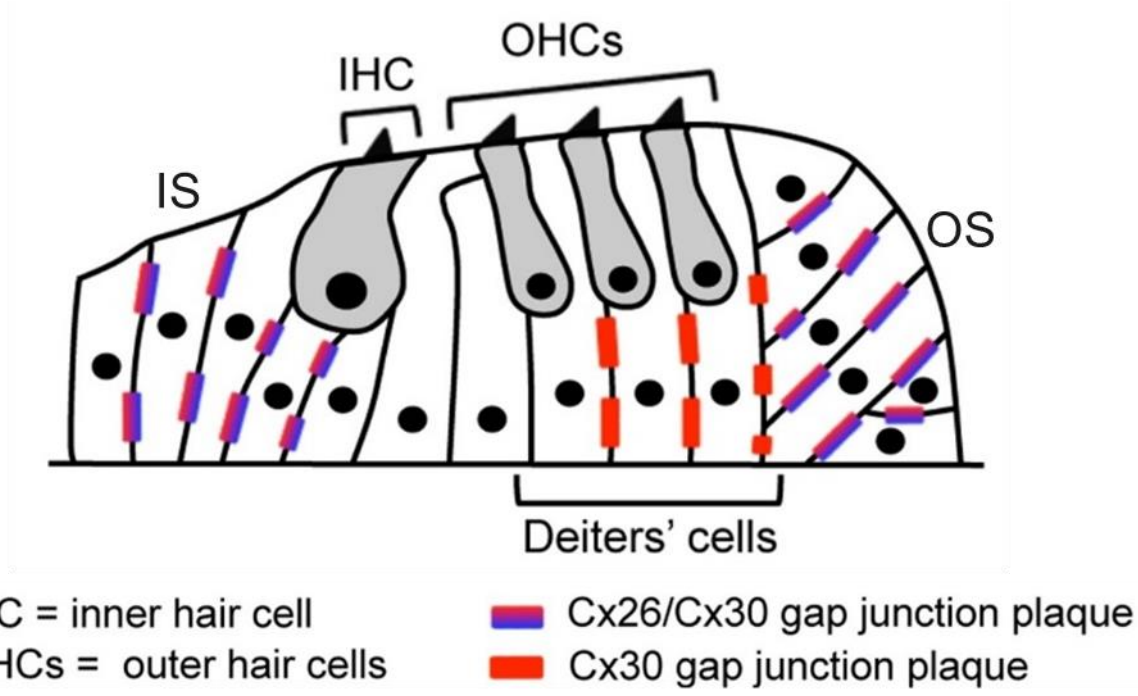

Figure 1.15: Gap junction channel expression in the organ of Corti

Schematic diagram of the organ of Corti illustrating the location and type of gap junction plaques. The inner and outer sulcus cells contain GJC plaques containing both connexin 26 and connexin 30. Whereas the Deiters’ cell plaques contain connexin 30 only. Hair cells do not express any gap junction channels. Figure taken from (Defourny *et al.*, 2021).

This widespread expression of gap junction channels throughout the organ of Corti forms a transport network across the epithelium in which molecules can travel between cells for large distances (Kikuchi *et al.*, 1995; Forge *et al.*, 2003). The size of the GJC pore allows the passage of a wide variety of molecules ranging from secondary messengers (e.g. IP_3 and ATP) (Hernandez *et al.*, 2007), ions (e.g. Ca^{2+} and K^+) (Kikuchi *et al.*, 2000; Zhang *et al.*, 2005) and metabolites (e.g. glucose) (Chang *et al.*, 2008). Therefore, the GJC network is likely to be involved in numerous aspects of cochlear function. This could explain why mutations affecting the Cx26 protein (*GJB2* gene) and the Cx30 protein (*GJB6* gene) are the most common causes of non-syndromic genetic hearing loss (del Castillo and del Castillo, 2017; Chan and Chang, 2014; Chen *et al.*, 2022). However, even though this confirms the supporting cell GJC network is crucial for hearing, the specific mechanisms by which it contributes to cochlear function remain uncertain. Furthermore, numerous connexin-related mutations have been identified which can present as a wide variety of hearing loss phenotypes, ranging from deafness at birth to progressive hearing loss later in life (Chan and Chang, 2014). This heterogeneity suggests the presence of numerous pathological mechanisms associated with GJC dysfunction which can affect both cochlear development and maintenance of hearing function. The limited understanding of the pathological mechanisms leading to GJC-related hearing loss prevents the generation of effective treatments.

It is hypothesised that GJCs contribute to the ionic homeostasis within the cochlea by promoting the recycling of K^+ ions back to the endolymph following hair cell repolarisation (Figure 1.16). Specifically, K^+ leaves the hair cell basolaterally and is taken up by nearby supporting cells (Santos-Sacchi and Dallos, 1983; Kikuchi *et al.*, 2000). The GJC network connecting the supporting cells then facilitates the diffusion of the K^+ ions across the epithelium to the stria vascularis, where they are pumped back into the endolymph (Wangemann, 2006). This replenishment of endolymphatic K^+ is crucial for hearing function as it restores the steep electrical driving force for hair cell depolarisation when the MET channels open. However, this proposed route for K^+ recycling via the supporting cell GJCs is still a hypothesis as there is yet to be any direct confirmation of this mechanism. Nevertheless, there is evidence which suggests an association between GJC function and the maintenance of the endocochlear potential. For example, both homozygous mutant Cx26 and Cx30 mice were shown to have significantly smaller endocochlear potentials and lower endolymphatic

K^+ concentrations than wild-type mice (Cohen-Salmon *et al.*, 2002; Teubner *et al.*, 2003; Crispino *et al.*, 2011). In addition to this, adult homozygous Cx26 loxP mice displayed decreased Cx26 expression, lowered endocochlear potential and hearing loss following the injection of BAAV containing cre recombinase (Crispino *et al.*, 2017). Therefore, these data suggest that defective GJCs somehow negatively influence the maintenance of a highly positive endolymph with a high K^+ concentration, and this has a damaging effect on cochlear function resulting in hearing loss.

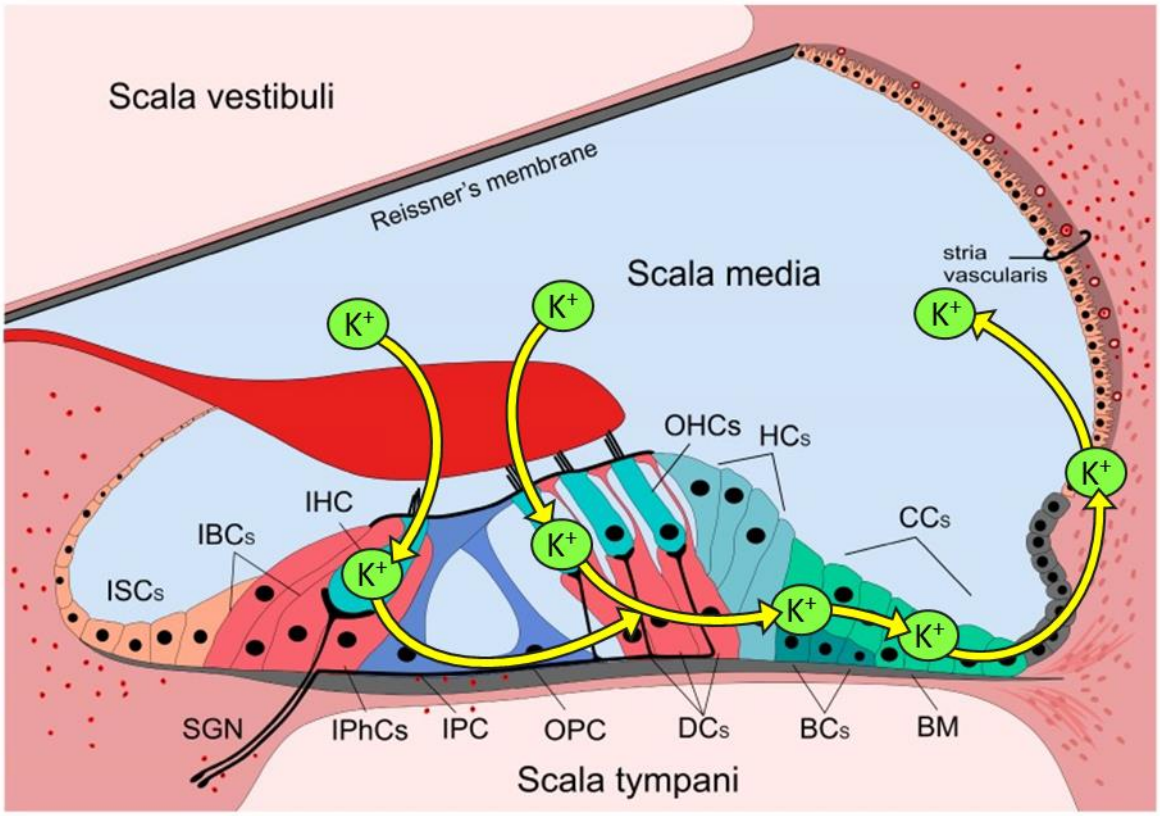

Figure 1.16: K^+ recycling via gap junction channels in the organ of Corti

The opening of mechano-electrical transducer channels on hair cells drives K^+ influx. This is followed by hair cell depolarisation and subsequent neurotransmitter release onto auditory neurons. This process relies on the maintenance of the electrical driving force promoting K^+ influx into hair cells. Therefore, after hair cell depolarisation the K^+ is believed to leave the hair cells basolaterally and be taken up by nearby supporting cells. The gap junction network connecting the supporting cells will then allow the K^+ to diffuse across the epithelium and be pumped back out into the endolymph at the stria vascularis. (ISCs: inner sulcus cells, IBCs: inner border cells, IHC: inner hair cell, IPhCs: inner phalangeal cells, IPC: inner pillar cell, OPC: outer pillar cell, DCs: Deiters' cells, OHCs: outer hair cells, HCs: Hensen's cells, BCs: Boettchers cells, BM: basilar membrane, SGN: spiral ganglion neuron). Figure modified from (Köles *et al.*, 2019).

However, this data still does not directly confirm a route for K^+ recycling via the GJC network. Furthermore, dominant negative R75W Cx26 mutant mice were reported to have hearing loss with no significant difference in endocochlear potential when compared to wild-type mice (Kudo *et al.*, 2003). In addition to this, when Cx26 was conditionally knocked out in the Dieters and pillar cells it had no effect on endocochlear potential (Zhu *et al.*, 2013). This suggests that even if GJCs do contribute to the maintenance of the endocochlear potential, it cannot be the only aspect of cochlear function they influence.

The GJC network is also believed to assist in the delivery of metabolites (such as glucose) to the cochlear epithelium as this tissue receives limited blood supply (Santos-Sacchi and Dallos, 1983). Glucose from peripheral blood vessels is hypothesised to diffuse from cell to cell via the GJC network and supply the organ of Corti. Fluorescently tagged 2-NBDG (a glucose analogue) was able to diffuse across ~100 cells following injection into one outer sulcus cell, and octanol (GJC blocker) inhibited this diffusion (Chang *et al.*, 2008). Additionally, this was repeated on Cx30 mutant mice who displayed a significant reduction in 2-NBDG diffusion, further suggesting glucose delivery to the organ of Corti utilises the GJC network. Therefore, hearing loss associated with connexin-related mutations could also be a result of glucose deprivation to the organ of Corti. It is well established that glucose deficiency prompts an increase in the production of reactive oxygen species (ROS) which are known to induce cell damage and death (Lee *et al.*, 1998). So, another potential mechanism involved in connexin-mutation-related hearing loss could be hair cell deterioration due to pathology associated with glucose deprivation and reactive oxygen species.

A further function of the GJC network is to facilitate the spread of intercellular signalling cascades across the organ of Corti. For example, during cochlear development, immature hair cells and their associated neurons fire spontaneous action potentials (Marcotti *et al.*, 2003b; Johnson *et al.*, 2011) which drive synaptic maturation (Clause *et al.*, 2014; Müller *et al.*, 2019). A purinergic signalling cascade, originating in the supporting cells, modulates this spontaneous hair cell activity (Section 1.1.1.2.1). This cascade utilises the GJC network to propagate downstream molecules across the epithelium. Specifically, purinergic receptor activation on the supporting cells stimulates the production of IP_3 (inositol triphosphate) and Ca^{2+} release from intracellular stores, both of which utilise the GJC network to induce the same response in neighbouring cells (Figure 1.17) (Ceriani, Pozzan and Mammano, 2016).

Therefore, these intracellular Ca^{2+} oscillations can spread in waves across the Kölliker's organ and trigger widespread K^{+} efflux which will influence IHC depolarisation and action potential firing (Tritsch *et al.*, 2007; Babola *et al.*, 2020). However, it seems that this mechanism is not completely reliant on the GJC network as even though Cx30 knock out mice (which also only have ~10% Cx26 expression) had a reduction in Ca^{2+} waves across the Kölliker's organ, spontaneous action potentials were still detected in IHCs similar to those seen in wild-type IHCs (Johnson *et al.*, 2017). Therefore, it was concluded that the Ca^{2+} waves in supporting cells must only modulate the IHC action potentials. This was supported by the observation that Cx30 knock out IHCs displayed increased action potential firing rarely when Ca^{2+} waves were seen in Kölliker's organ (Johnson *et al.*, 2017). However, it was also shown that the adult Cx30 knock out IHCs retained an immature phenotype, suggesting that the modulation of IHC action potentials during development may promote the correct maturation of inner hair cells. Therefore, another possible pathological mechanism contributing to the hearing loss associated with connexin-related mutations is dysfunction of intercellular Ca^{2+} wave propagation and incomplete hair cell maturation.

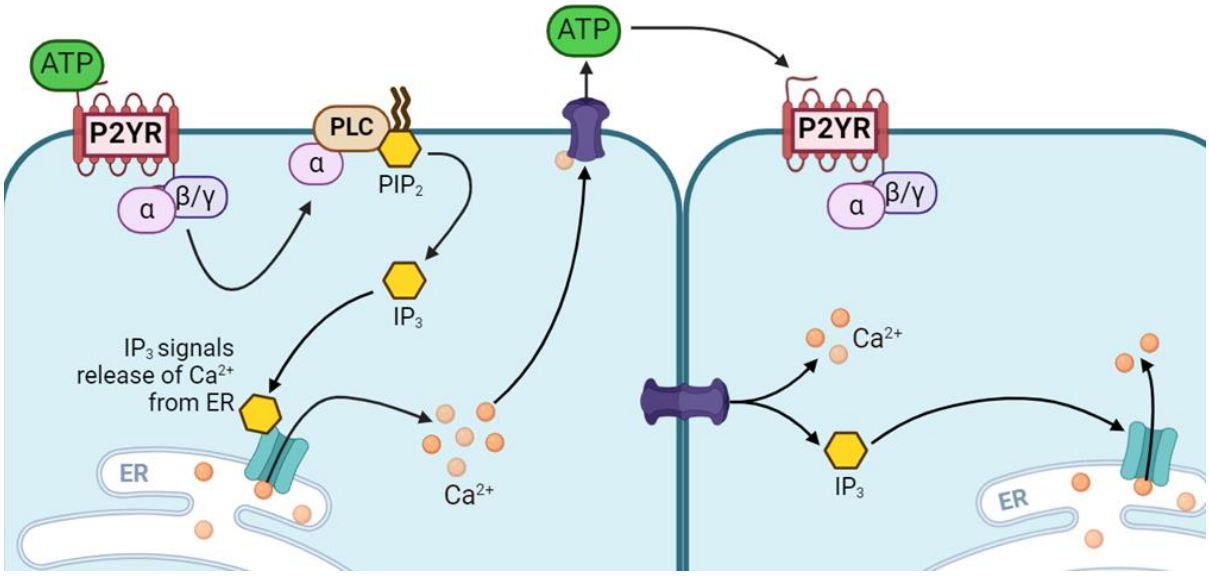

Figure 1.17: Intracellular Ca^{2+} signalling cascades can spread across the supporting cells via gap junction channels

The supporting cells in the organ of Corti express purinergic G-protein coupled receptors (P2YR) which activate in response to the extracellular binding of ATP. This triggers the production of the signalling molecule IP_3 (inositol triphosphate) which promotes the release of Ca^{2+} from the endoplasmic reticulum (ER). This will increase the cells concentration of cytosolic Ca^{2+}. The downstream signalling molecules (Ca^{2+} and IP_3) can travel to neighbouring cells via the gap junction channels (purple) and induce the release of more Ca^{2+}. This is the mechanism by which intracellular Ca^{2+} waves can propagate across the cochlear sensory epithelium. Additionally, high intracellular Ca^{2+} will promote the opening of the connexon hemichannels (purple) which can allow the release of ATP from the cell. This ATP can go onto activate other P2Y receptors on other cells. Adapted from “Activation of Protein Kinase C (PKC)”, by BioRender.com (2024) and retrieved from https://app.biorender.com/biorender-templates.&apos.

1.2 Age-related hearing loss

The remainder of this chapter will introduce age-related hearing loss as this thesis is exploring whether changes in the cochlear supporting cells (Section 1.1.1.3) could influence the progression of this condition.

Age-related hearing loss (ARHL) is defined as the progressive decline in hearing ability following the senescence of cells of the auditory system. Approximately two thirds of individuals aged 70 or above experience bilateral hearing loss, making ARHL the most prevalent sensory condition among the aged population (Goman and Lin, 2016). Typically, it presents as difficulties with speech perception (especially in a noisy environment), sound localisation and a decrease in the processing speed of auditory stimuli (Gates and Mills, 2005). ARHL initially affects the detection of high frequency sounds, followed by progressive loss of hearing of lower frequency sounds. These primary symptoms predispose numerous other related ailments, such as an increased incidence of mental health conditions, as hearing can affect many aspects of an individual's life (Brewster *et al.*, 2018). Treatments for ARHL are limited to symptomatic solutions, such as hearing aids and cochlear implants, as currently there's no cure for the underlying cause (Sprinzl and Riechelmann, 2010). The main reason for this is the limited understanding of the multiple cellular mechanisms contributing to ARHL, and how these processes are affected by the many environmental and genetic risk factors (Gates and Mills, 2005). Therefore, ARHL is described as a complex, multifactorial disorder due to the diverse set of symptoms it can lead to, but also because of the plethora of factors which have been proposed to contribute to its development.

1.2.1 ARHL pathology

ARHL is a heterogeneous condition which has been categorised into sub-types based on the presence of four main forms of pathology: sensory, neural, strial/metabolic and conductive (Schuknecht, 1955; Gacek and Schuknecht, 1969). The sensory type of ARHL pathology involves the loss of the inner and outer hair cells as the organ of Corti degenerates. The neural type involves the loss of the spiral ganglion neurons which innervate the hair cells. The strial type involves a decline in the endocochlear potential as the stria vascularis degenerates and

can no longer maintain the positive electrical potential of the endolymph (Salt, Melichar and Thalmann, 1987). Finally, the conductive type is typically associated with problems in the outer and middle ear which influence how well sound can reach the inner ear. It is also believed to involve the thickening of the basilar membrane causing it to be less efficient as carrying sound-induced vibrations (Bhatt, Liberman and Nadol Jr, 2001). It is thought that many individuals with ARHL experience pathology across several of these subgroups. This can explain why both the onset, and rate of disease progression, for ARHL is so variable between patients (Brant and Fozard, 1990; Gopinath *et al.*, 2009). Each individual is likely experiencing a differing combination of the four main ARHL pathologies, alongside various other genetic and environmental influences. Nevertheless, it is agreed within the literature that the sensory type of ARHL pathology is expected to have the largest contribution to ARHL progression and has been studied in more detail.

1.2.2 ARHL risk factors

The progression of ARHL is known to be influenced by a wide range of factors involving the dysfunction of numerous cells along the auditory pathway and molecular mechanisms over time (Keithley, 2020). A combination of the natural ageing of auditory cells, genetic contributions (Van Laer *et al.*, 2010) and multiple environmental factors (Agrawal, Platz and Niparko, 2008) have all been shown to influence ARHL development.

It has been estimated that there are ~150 genetic mutations associated with influencing the development of ARHL (Wells, Newman and Williams, 2020). These genes appear to be involved in a variety of different cellular processes suggesting ARHL pathophysiology involves the interaction of multiple different dysfunctional mechanisms in a variety of cells. One example of this being polymorphisms in genes involved in protection against oxidative damage such as GSTT1 and GSTM1 (Van Eyken *et al.*, 2007). It is expected that these mutations would disrupt the clearance of toxic reactive oxygen species and predispose mitochondrial damage and cell death (Orrenius, 2007). Additionally, mutations in estrogen related receptor gamma (ERRG) in women and female mice have also been linked to ARHL progression (Nolan *et al.*, 2013). This receptor is expressed within inner hair cells and supporting cells but its function in the cochlea remains unclear. In other tissues, ERRG is

known to regulate the expression of genes important for ionic homeostasis such as KCNE1 (Alaynick *et al.*, 2010). The maintenance of specific ionic environments is crucial for cochlear function, and so any mutations affecting ionic homeostasis would be expected to be linked to progressive hearing loss. Therefore, it is clear that ARHL pathophysiology involves the interaction of different dysfunctional mechanisms in a variety of cells.

Furthermore, numerous environmental factors are known to promote the same dysfunctional mechanisms involved in age-related cochlear pathophysiology. For instance, it is hypothesised that damage following multiple events of loud noise exposure throughout life accelerates the progression of ARHL (Fransen *et al.*, 2003). The pathophysiology involved in noise-induced hearing loss (NIHL) and ARHL occur in a similar manner; the more immediate effects include the loss of hair cell synapses, followed eventually by hair cell and neuron death (Sergeyenko *et al.*, 2013; Kujawa and Liberman, 2015). Additionally, mice exposed to sound known to cause temporary threshold shift (TTS) displayed accelerated age-related synaptopathy (Fernandez *et al.*, 2015). Therefore, this makes the distinction of damage resulting from NIHL and ARHL within one individual very challenging.

1.2.3 ARHL and supporting cells

The four categories of ARHL pathology highlight the wide range of structures in the auditory system which are affected by this disorder. Additionally, the numerous associated genetic mutations and environmental factors further suggest that ARHL pathophysiology involves multiple dysfunctional mechanisms in a variety of cells. However, most research into this condition has focused on age-related changes in the sensory hair cells of the organ of Corti. The cochlear non-sensory supporting cells are crucial for the health and functioning of the sensory hair cells, and thus, maintenance of hearing. Therefore, it is likely that any age-related changes in these supporting cells will impact hair cell function and potentially contribute to the changes in hearing ability we observe in the ageing cochlea. However, hardly any research has been conducted to investigate how these supporting cells change with age. This thesis will focus on investigating any age-related changes within the supporting cells to provide a better understanding of the senescence of the auditory system and ARHL.

1.2.3.1 Gap junction channels and ARHL

As mentioned previously, the cochlear supporting cells form a functional syncytium across the sensory epithelium composed of gap junction channels connecting the intracellular spaces of neighbouring cells (Kikuchi *et al.*, 1995; Jagger and Forge, 2015). This transport network is hypothesised to be crucial for hair cell longevity and hearing function as mutations affecting the connexin proteins which form these gap junction channels are the most common causes of non-syndromic hearing loss (del Castillo and del Castillo, 2017; Chan and Chang, 2014; Chen *et al.*, 2022). It has been reported that these cochlear GJCs exhibit changes in their structure and organisation with age. Eight-month-old C57BL/6J mouse inner sulcus cells displayed a significant decrease in GJ plaque length and abundance, alongside a more scattered structure, when compared to the typical linear organisation and length in young adult mouse cells (Figure 1.18) (Tajima *et al.*, 2020). Although it's unclear what effect these structural changes have on the GJCs ability to function, the mice were reported to have minimal hair cell damage and hearing loss at eight months, but exhibited severe hearing loss by nine months. This led to the hypothesis that the age-related changes in GJC structure reduce their functional efficiency, and thus negatively impact the transport of necessary molecules to/from the hair cells. This overall would be expected to contribute to hair cell dysfunction with age and the development of ARHL. This hypothesis seems feasible as reductions in GJC plaque size in other tissues have been associated with dysfunction in cell-cell comunication and disease. For example, reductions in the size of GJC plaques across the cardiac epithelium are strongly linked to aryhthmias due to a reduced efficiency in the GJC-mediated spread of electrical signals promoting synchronised contraction (Luke and Saffitz, 1991; Kaprielian *et al.*, 1998).

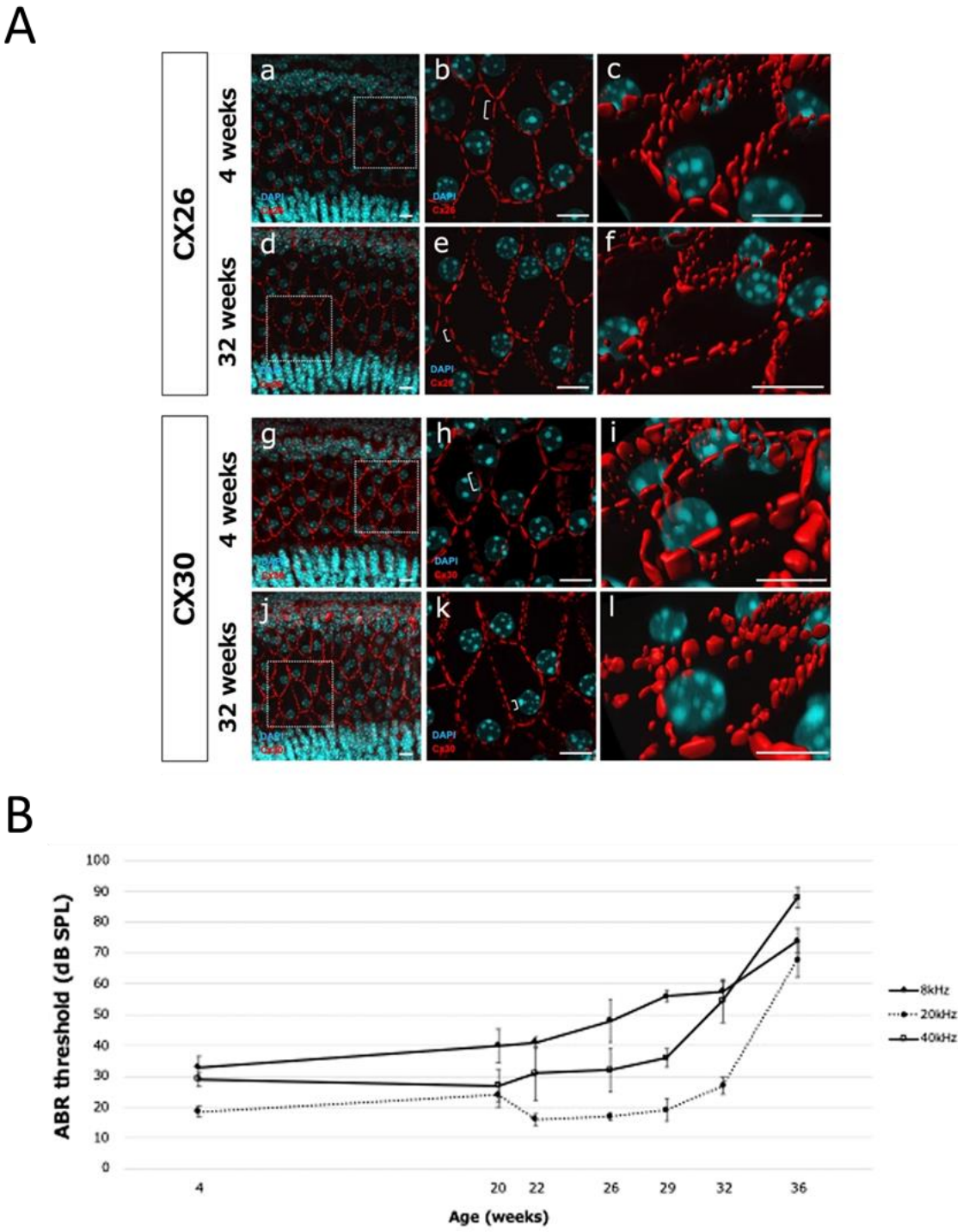

Figure 1.18: Cochlear supporting cell gap junction structure and age

A: Immunolabelling of gap junction proteins Cx26 (top two panels) and Cx30 (bottom two panels) in C57BL/6J mice aged 4 weeks old (a-c, g-i) and 32 weeks old (d-f, j-l). The older mice show a different organisation of gap junction plaques which appear more scattered and smaller in length. Scale bars 10μm. **B**: ABR thresholds of C57BL/6J mice aged 4-36 weeks old at 8, 20 and 40kHz. ARHL appears to start at 36 weeks of age, after the changes in plaque organisation. Figure from (Tajima *et al.*, 2020).

Further support for this claim comes from looking at mutations in Cx26 and Cx30 (the two main components of cochlear GJCs). *Cx26*$^{+/-}$ mutant mice were reported to have accelerated hearing decline with age (deterioration in ABRs and DPOAEs) compared to wild type mice (Fetoni *et al.*, 2018). It was hypothesised that the reduction in Cx26 made hair cells and their neurons more susceptible to damage resulting from lack of nutrient/glucose delivery, such as increased oxidative stress (a known contributor to ARHL). This was feasible as the lack of Cx26 caused dysregulation in the expression of multiple genes associated with antioxidant defence mechanisms (Fetoni *et al.*, 2018). It has also been reported that mice with total deletion of Cx30 displayed accelerated levels of age-related hearing loss compared to wild type mice (Paciello *et al.*, 2022). These knock-out mice also exhibited increases in cochlear damage associated with ARHL, such as inflammation and oxidative stress. Therefore, it is also possible that mutations in Cx26 and Cx30 predispose pathological mechanisms associated with senescence.

1.3 Aims and hypotheses of the study

The overall aim of this research is to investigate how the supporting cells in the mammalian organ of Corti change with age. It is anticipated that any senescence-related alterations in the functioning of these cells will influence their ability to support the sensory hair cells, and so may contribute to the development of ARHL. This work should lead to a better understanding of the complete pathophysiology behind ARHL, as currently it is unknown whether the supporting cells are involved in the progression of this disease.

Aim 1. Define progressive changes in the expression and functioning of P2Y receptors in the supporting cells of the organ of Corti.

During development, P2Y purinergic receptors are known to be expressed in the supporting cells of the organ of Corti and are important for modulating inner hair cell action potentials and synaptic refinement. After cochlear maturation, it is believed that P2Y receptors are lost from the adult supporting cells. Here, it was hypothesised that the senescent cochlea will display alterations in P2Y receptor expression and function because other tissues have reported similar senescence-specific changes in their P2Y receptors.

To investigate whether any age-related changes in P2Y receptors are associated with ARHL, P2Y receptor expression and functioning was compared in two mouse lines known to exhibit different phenotypes of ARHL. It was hypothesised that the C57BL/6N (early onset ARHL) will display more pronounced alterations in their P2Y receptors that C3H/HeJ (late onset ARHL) because it is anticipated that any changes in P2Y receptors specific to the aged cochlea will be associated with ARHL.

Aim 2. Define progressive changes in the expression and functioning of gap junction channels in the supporting cells of the organ of Corti.

The supporting cells of the organ of Corti are coupled together by a gap junction channel network. It is well established that these gap junction channels are crucial for cochlear function as any mutations in the connexin proteins within these membrane channels cause

hearing loss. Here, it was hypothesised that any changes in the structure or function of these gap junction channels with age in the organ of Corti may influence hearing function and could influence the progression of age-related hearing loss.

To investigate progressive changes in the gap junction channel network in the organ of Corti, the structure of the gap junction channel plaques was visualised via immunolabelling for connexin 26 and connexin 30. Furthermore, the permeability of the gap junction channel network was investigated using dye diffusion experiments.

Chapter 2. General Methods

2.1 Ethics statement

All experiments were completed in accordance with the Animals Scientific Procedures Act of 1986 under a UK Home Office project licence (PCC8E5E93 and PP1481074). The Sheffield University Ethical Review Committee has endorsed all procedures described in this thesis.

2.2 Animals

All mice were housed at the animal facility at the University of Sheffield. The care of the mice was in line with Home Office guidelines such that they were kept in a 12-hour light-dark cycle and had unlimited supply to food and water. Animals were sacrificed via the Schedule 1 procedure of cervical dislocation followed by decapitation.

Three strains of mice were used in these experiments which are known to exhibit differing severities of age-related hearing loss (ARHL) phenotype. The C57BL/6N (6N) strain displays early onset hearing loss at ~3 months of age due to a hypomorphic allele in the *Cadherin23* gene (*Cdh23*^{ahl}), which encodes for a protein required for the gating of the mechano-electrical transducer channel (Noben-Trauth, Zheng and Johnson, 2003; Mock *et al.*, 2016). The 6N strain is co-isogenic to the C57BL/6N^{Cdh23+} (6N-repaired) strain, except 6N-repaired mice have their *Cadherin23* mutation corrected via CRISPR/Cas9-mediated homology directed repair (Mianné *et al.*, 2016). This correction gives the 6N-repaired strain lower auditory brainstem response (ABR) thresholds at older ages, especially at higher sound frequencies (Figure 2.1). Finally, the C3H/HeJ (C3H) strain are known to be a good-hearing mouse model which exhibit a very late onset of ARHL (Trune, Kempton and Mitchell, 1996; Jeng *et al.*, 2021). Thus, it will be possible to compare how certain pathophysiological mechanisms associated with ARHL present in mice known to display differing onsets of this disorder.

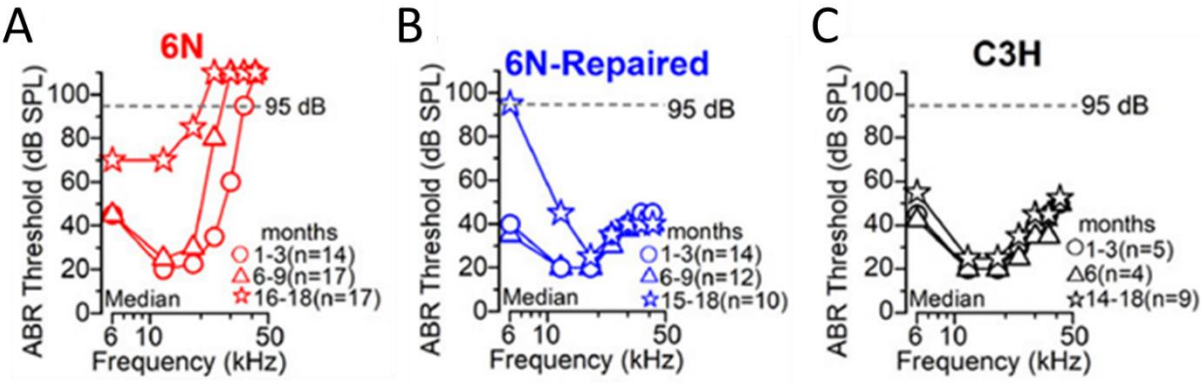

Figure 2.1: Auditory brainstem responses from C57BL/6N (6N), C57BL/6N^{Cdh23+} (6N-repaired) and C3H/HeJ (C3H) mice

ABR thresholds for frequency-specific pure tone stimulation from 6 to 42 kHz recorded from 6N (**A**, red), 6N-repaired (**B**, blue) and C3H (**C**, black) mice at different ages. ABR data are grouped into three age ranges: 1–3 months (open circle data points), 6–9 months (triangle data points) and 14–18 months (star data points). The median value for each age group is plotted. Figure and legend modified from (Jeng *et al.*, 2020a).

2.3 Immunolabelling

2.3.1 Tissue preparation

Following the decapitation of the mice, the skin was removed from the skull and the whole head was cut in half along the sagittal plane. The brain was carefully removed from each half to reveal the inner ear. Forceps were used to separate the whole inner ear (cochlea and vestibule) from the rest of the skull. If a mouse was older than P7, a small opening was made with forceps in the bony membrane surrounding the cochlea at the tip of the bulla. The whole inner ears were then perfused with 4% paraformaldehyde (PFA) solution in phosphate-buffered saline (PBS), entering via the round and oval windows and leaving through the new opening at the apex. The inner ears were then placed in an Eppendorf tube with about 1ml of the 4% PFA solution to fix for 20 minutes on a shaker at room temperature.

Following fixation, the inner ears underwent three, 10-minute-long washes in PBS. After the PBS washes, the apical turn of the organ of Corti was dissected out from the rest of the inner ear using forceps, under a microscope (Leica, Germany). These were then left in a blocking solution containing 0.5% Triton X-100 and 5% normal horse serum (H0146, Sigma-Aldrich) in PBS.

2.3.2 Antibodies

All antibodies were diluted in blocking solution containing 0.5% Triton X-100 and 1% normal horse serum (H0146, Sigma-Aldrich) in PBS. The organs of Corti were incubated at 4°C overnight in primary antibody solution. All primary antibodies used in this thesis are summarised in Table 2.1. The samples were washed three times in PBS following incubation in primary antibody solution. The secondary antibody solutions were then applied for one hour at 35°C. Secondary antibodies used included goat anti-rabbit IgG 490 (Alexa fluor 488, A11034, Thermo Fisher) and goat anti-mouse IgG_{2a} 650 (Alexa fluor 647, A21241, Thermo Fisher). DAPI nuclear staining (1:1000, 10 236 276 001, Merck Sigma) and Texas Red-X Phalloidin staining of F-actin (1:1000, T7471, Thermo Fisher) were used alongside the secondary antibodies.

Antibody	Species Isotype	Company	Reference	Concentration
Anti-$P2Y_1$	Rabbit-IgG	Alomone Labs	#APR-009	1:800
Anti-$P2Y_2$	Rabbit-IgG	Alomone Labs	#APR-010	1:800
Anti-$P2Y_4$	Rabbit-IgG	Alomone Labs	#APR-006	1:800
Anti-Connexin26	Mouse-IgG_{2a}	Thermo Fisher	33-5800	1:500
Anti-Connexin30	Rabbit-IgG	Thermo Fisher	71-2200	1:200

Table 2.1: List of primary antibodies

2.3.3 Mounting and imaging

After incubation in secondary antibody solutions, the organs of Corti underwent three PBS washes before being transferred onto a microscope slide, mounted in Vectashield (H-100, VECTOR labs) and cover-slipped. All images of the organ of Corti were taken using a Zeiss LSM880 Airyscan Confocal microscope in the Wolfson Light Microscopy Facility at the University of Sheffield. A Zeiss Plan-Apochromat 63x/1.4 oil objective was used and z-stack images were taken of the samples with 0.5 µm increments between slices. Additionally, all images are of the 9-12 kHz region of the cochlear spiral. The images were processed using Fiji ImageJ software (https://imagej.net/Fiji).

2.4 Fluorescent Ca^{2+} imaging

2.4.1 Fura-2

The fluorescent Ca^{2+} dye Fura-2 AM was used to visualise intracellular Ca^{2+} responses in inner sulcus cells. Fura-2 is readily taken up into the cells as it is used with a lipophilic acetoxymethyl ester. Then, esterases within the cells cytoplasm induce de-esterification of the molecule (Tsien, 1981). This stops Fura-2 being able to leave the cell, but also frees its Ca^{2+} binding site, ensuring only the dye within cells will fluoresce. This setup allowed the real-time visualisation of changes in intracellular Ca^{2+} concentration by observing changes in fluorescence. Therefore, the functioning of purinergic receptors within the inner sulcus cells could be investigated by applying various purinergic receptor agonists and antagonists extracellularly and monitoring the intracellular Ca^{2+} responses.

Fura-2 is a ratiometric Ca^{2+} dye which undergoes alterations in its light absorption and emission properties depending on the Ca^{2+} concentration (Grynkiewicz, Poenie and Tsien, 1985). The isosbestic point (i.e. the excitation wavelength at which the fluorescence emission intensity is equal no matter the Ca^{2+} concentration) for Fura-2 is 360 nm. The binding of Ca^{2+} ions to Fura-2 causes an increase in absorption and a shift of the absorption peak towards lower wavelengths (Figure 2.2). This results in an increase or decrease of the fluorescence emission when excited with wavelengths lower or higher than the isosbestic point, respectively. Therefore, it can be demonstrated that the ratio between the fluorescence intensities produced following excitation at two different wavelengths is a monotonic function of the Ca^{2+} concentration within the cell (Grynkiewicz, Poenie and Tsien, 1985). The use of a ratiometric dye removes the potential for tissue specific differences, such as dye loading and cell size.

All data was presented in the format of these fluorescence ratios (and not converted to Ca^{2+} concentration). This was because the conversion requires in-situ calibration of the dye for every cell investigated and this involves pharmacological alteration of the preparation. Therefore, to better preserve the explants, and because we were only interested in comparing relative sizes of the Ca^{2+} responses, we decided to not calculate the conversion and use the ratiometric values only.

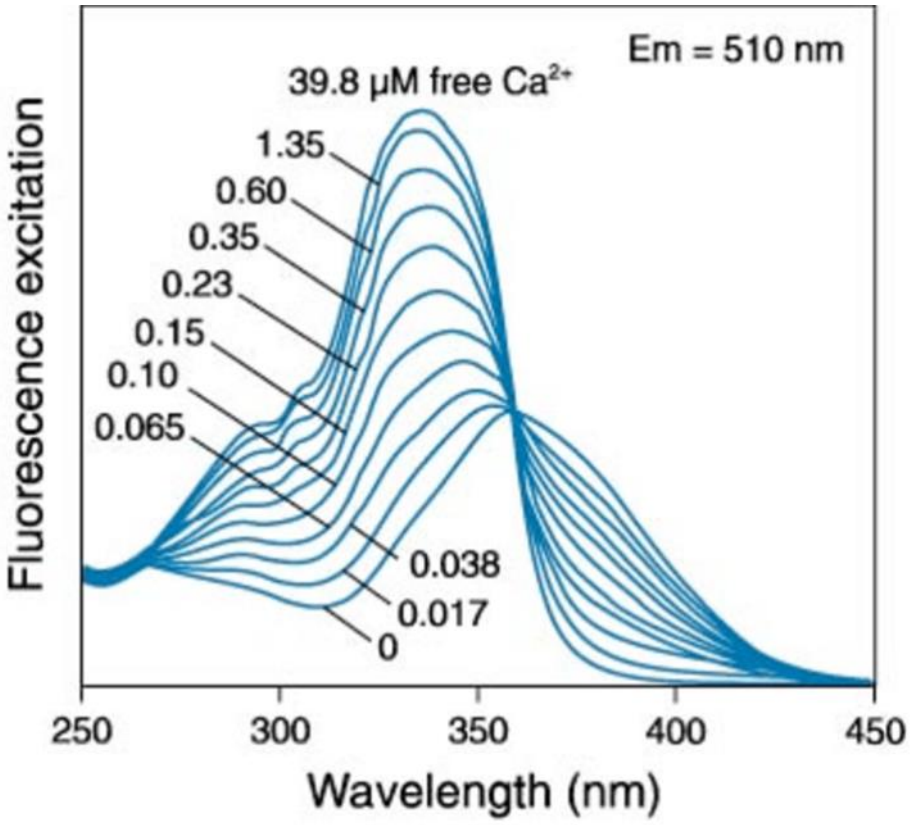

Figure 2.2: The light absorption and emission properties of Fura-2

The light absorption and emission properties of Fura-2 are dependent on the concentration of free Ca^{2+}. Each blue trace represents the excitation spectrum of Fura-2 for light emitted at 510 nm (green) for different Ca^{2+} concentrations. At the largest free Ca^{2+} concentration (39.8 µM), Fura-2 has the greatest difference between the fluorescence intensity recorded for excitation at 340nm and 380nm. (Fura-2 product information, Molecular Probes, 2006).

2.4.2 Tissue preparation

The apical cochlear turn was dissected out from the inner ear (as previously described in Section 2.3.1) in extracellular solution (ECS) (composition found in table 2.2 along with amino acids and vitamins from Thermo Fisher Scientific, UK). The pH of this solution was raised to 7.48 with 4M NaOH and had an osmolality of ~304 mmol kg^{-1}.

Chemical	Final concentration (mM)
NaCl	135
$CaCl_2$	1.3
KCl	5.8
$MgCl_2$	0.9
HEPES	10
Glucose	5.6
NaH_2PO_4	0.7
Na-Pyruvate	2

Table 2.2: Concentrations of chemicals in extracellular solution

2.4.3 Dye loading and setup

The dissected organ of Corti was incubated in dye loading solution at 35°C for 40 minutes. The loading solution contained DMEM/F12, 0.1% pluronic F-127 (Thermo Fisher Scientific, UK), 250 µM sulfinpyrazone to avoid dye sequestration (Sigma-Aldrich) and 10 µM of the fluorescent Ca^{2+} indicator Fura-2 AM (Thermo Fisher Scientific, UK). Following incubation, the organ of Corti was transferred into a microscope chamber containing ECS, and held in place with a nylon mesh grid (Figure 2.3C). The tectorial membrane was then removed from above the epithelium. The chamber was placed under custom-made epifluorescence microscope (Ceriani *et al.*, 2016) based on an Olympus BX51WI upright microscope (Japan) fitted with a 15x eyepiece and 60x water immersion objective (0.1 NA, Olympus LUMPlanFl) (Figure 2.3A).

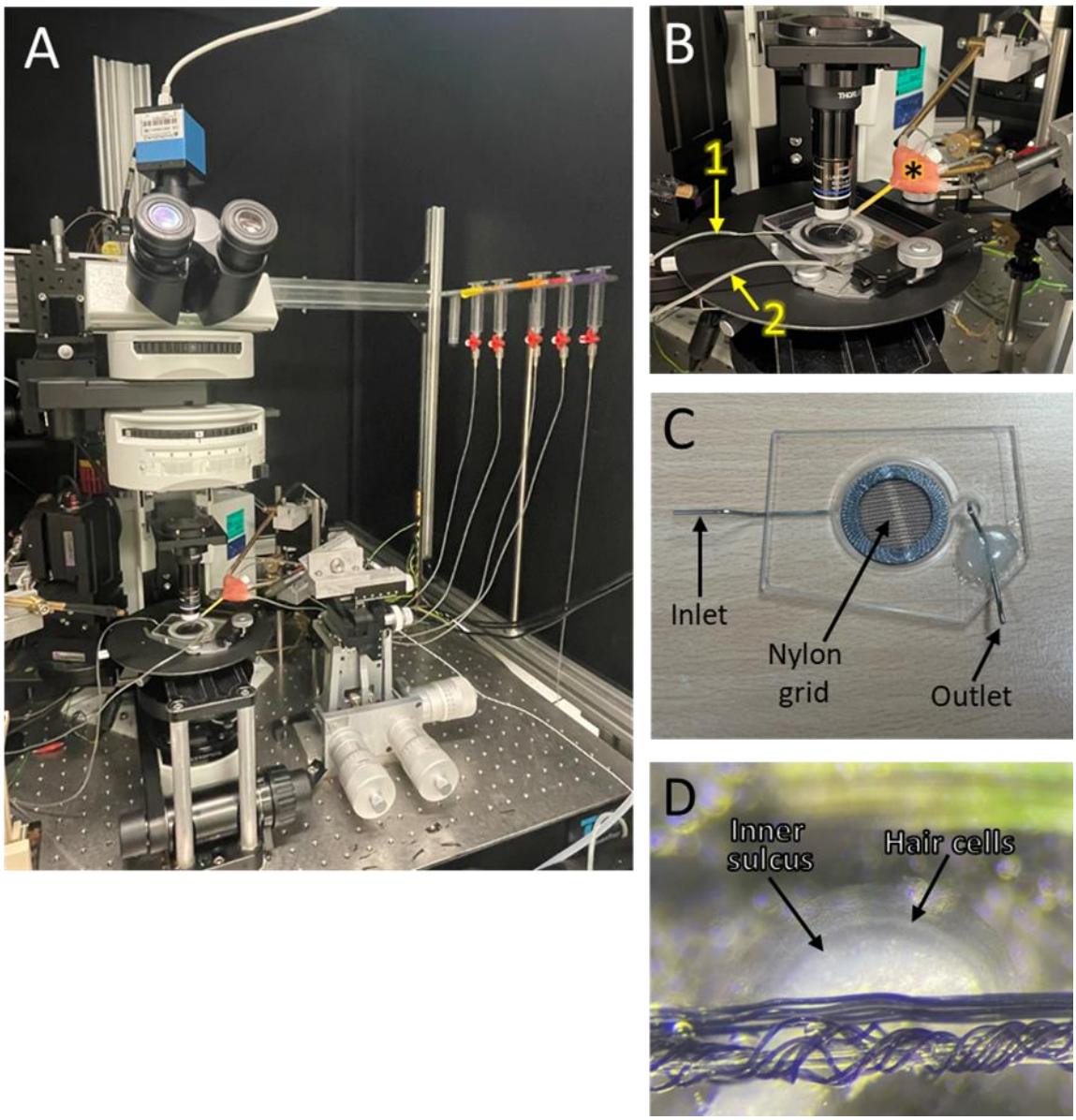

Figure 2.3: Ca^{2+} imaging experimental setup

A: Image of the equipment setup for Ca^{2+} imaging experiments. The Olympus BX51 upright microscope is shown with the ORCA Flash 4.0 V2 CMOS camera attached behind. The five tubes on the right are the gravity fed perfusion system for agonist/antagonist application. **B:** Magnified image of the microscope stage showing the perfusion pipette (asterisk) where the gravity fed perfusion system leads. The microscope chamber is continually being perfused with ECS via the inlet (1) and outlet (2) tubes connected. **C:** The microscope chamber with nylon mesh grid. **D:** A magnified image of the nylon grid within the chamber where the organ of Corti is secured for imaging. It is oriented so that there is a flat section of epithelium free containing both the hair cells and the inner sulcus.

2.4.4 Perfusion

The sample was continually perfused with fresh ECS throughout the experiment using a Peristaltic pump (Figure 2.3B) (Cole-Palmer, UK). A complete list of agonists/antagonists used in these experiments, along with the concentrations used, can be found in Table 2.3. The chemicals were diluted in ECS and applied to the preparation via a gravity-dependant perfusion system.

Name	Pharmacology	Concentration (µM)	Supplier	Reference
ATP	P2 receptor agonist	0.1	Thermo Fisher	R0441
UTP	$P2Y_2$ and $P2Y_4$ agonist	0.3	Sigma-Aldrich	U1006
ADP	$P2Y_1$ agonist	1	Sigma-Aldrich	01897
Thapsigargin	SERCA pump blocker	2	TOCRIS	1138
MRS4062	$P2Y_4$ specific agonist	10	TOCRIS	4261
AR-C 118925XX	$P2Y_2$ antagonist	15	TOCRIS	4890
MRS2500	$P2Y_1$ antagonist	1	TOCRIS	2159

Table 2.3: List of chemicals used as P2Y receptor agonists and antagonists

2.4.5 Imaging

During each recording, the tissue was exposed to alternating pulses of light via two light-emitting diodes (Thorlabs, USA) with peak emission at 365 nm and 385 nm, respectively. Light from the LEDs was passed through FF360/23 (365 nm LED) and FF392/23 (385 nm LED) narrow bandpass filters (Semrock, USA). The exposure time for 365 nm and 385 nm excitation was set at 65ms and 25ms respectively, with 100ms between these two separate pulses. The sequence of dual-wavelength light exposures was repeated every 1s (1Hz acquisition rate for the ratio signal) and controlled via Python software created in our lab (Python 3.10, Python Software Foundation). To minimise photo bleaching and phototoxic effects due to the use of UV light, the LED illumination was synchronised with camera exposure using an Arduino Microcontroller (*Arduino* Mega, Italy).

The emitted light from Fura-2 was separated from the excitation light using a T495lpxr long pass dichromatic mirror and filtered through a ET525/50M bandpass interference filter (Chroma, USA). Images of the emitted light were captured with an ORCA Flash 4.0 V2 CMOS camera (Hamamatsu, Japan) using Micro-Manager software (Edelstein *et al.*, 2014). Before a sample was disposed of when all recordings were complete, a brightfield image was sometimes taken to better illustrate the location of individual cells for later analysis (Figure 2.4A).

2.4.6 Analysis of recordings

The recordings were viewed and analysed using ImageJ (NIH) and custom-made Python scripts. From each recording, approximately 15 regions of interest (ROI) were manually chosen (Figure 2.4B). These ROIs were 3.5 µm × 3.5 µm in size and were placed over a single inner sulcus cell. This meant the changes in fluorescence over time could be analysed for around 15 individual cells per recording. The brightfield images collected following imaging experiments could be used as reference for the location of cells.

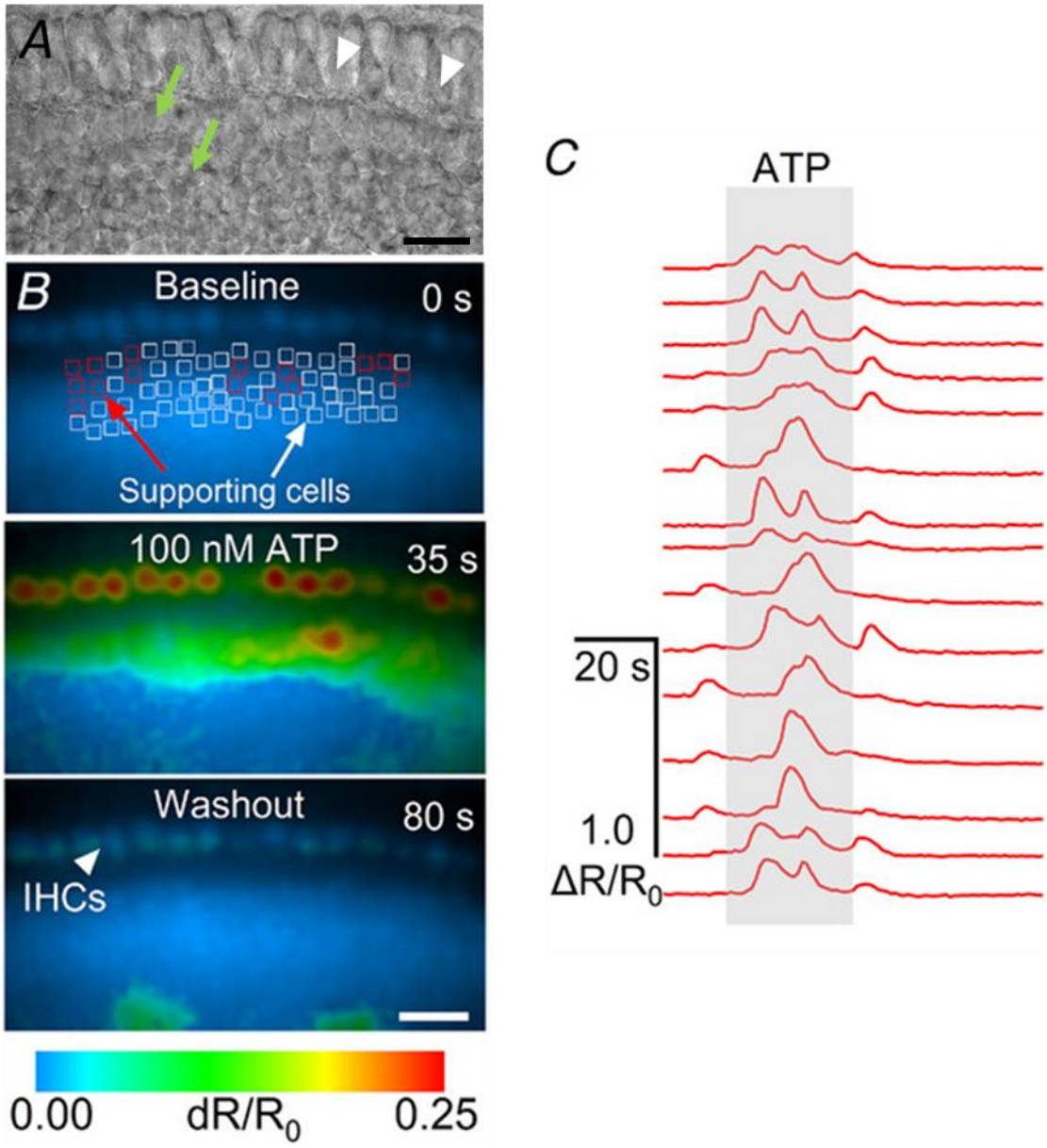

Figure 2.4: Analysis of Ca^{2+} imaging recordings from mouse organs of Corti

A: Brightfield image taken of the cochlear explant after completion of imaging to help identify individual cells on the fluorescent images. The location of inner hair cells is indicated by the white arrow heads. The location of inner sulcus cells is indicated by the green arrows. Scale bar is 20 µm. **B:** False-colour images before (top), during (middle) and after (bottom) the application of 100 nM ATP. Square regions of interest (ROIs, red and white) were manually drawn on supporting cells in the proximity of the IHCs. The arrowhead in the bottom panel shows the location of the IHCs. Scale bar is 20 µm. **C:** Ca^{2+} traces, calculated as fractional change of the ratio between the fluorescence emission for excitation at 365 nm and 385 nm ($\Delta R/R_0$), respectively, for a subset of ROIs (red ROIs shown in panel **B**). ATP (100 nM) was applied during the time-window highlighted in grey. Figure taken from (Hool *et al.*, 2023).

2.4.6.1 Calculation of fluorescence intensity ratio

To determine background fluorescence (BF) emission (e.g. due to tissue autofluorescence), an organ of Corti was imaged using the same recording conditions as in the Ca^{2+} imaging experiments (see above) but without incubation in Fura-2. An average of the pixel fluorescence following both the 365 nm and the 385 nm light were calculated and subtracted from each recording to remove any fluorescence not resulting from the excitation of Fura-2 dye.

To estimate the concentration of intracellular Ca^{2+}, the ratio between the fluorescence emission intensity following the 365 nm and 385 nm light exposures was calculated using the following equation (Eq. 1):

Eq. 1: $$R = \frac{F(365) - BF(365)}{F(385) - BF(385)}$$

The change in intracellular Ca^{2+} concentration evoked by purinergic receptor activation following agonist application could then be estimated using the following equation (Eq. 2):

Eq. 2: $$\frac{\Delta R}{R_0} = \frac{R(t) - R_0}{R_0}$$

Where *R(0)* is the baseline emission ratio before application of any chemicals and *R(t)* is the emission ratio recorded following chemical application. The baseline value was calculated for each recording by taking an average of the fluorescence ratios from the 3 seconds just before chemical application. The equation also normalises the ΔR to the specific baseline fluorescence ratio value calculated for each recording (divide whole equation by *R(0)*).

2.4.6.2 Quantification of intracellular Ca^{2+} responses

To quantify the intracellular Ca^{2+} responses to the various agonists and antagonists, both a maximum and average fluorescence intensity ratio was calculated for each ROI. The first 30 seconds of chemical application was used for these calculations. Ca^{2+} oscillations were first identified automatically using custom Python scripts (function *find_peaks* of the scipy.signal

Python module) and then reviewed manually to determine the validity of the peaks. The frequency of intracellular Ca^{2+} oscillations was determined by dividing the number of oscillations by the duration of chemical application.

2.4.6.3 Statistical analysis

The sample sizes used in the statistical tests were chosen to be similar to those used in previous work from this lab which also analysed age-related changes in cochlear cell physiology (Ceriani *et al.*, 2019b; Jeng *et al.*, 2020a; Jeng *et al.*, 2021). Mice of both sexes were used in these experiments and randomly distributed over the different experimental groups.

The statistical analysis was completed on R software (R Core Team 2022). All data analysed were non-parametric and $P < 0.05$ was the criterion for statistical significance. The Wilcoxon signed-rank test was used to compare paired data groups (analysis of Ca^{2+} responses from the same animal before and after antagonist application). The aligned ranks transformation (ART) two-way ANOVA was used to compare between unpaired data groups (analysis of Ca^{2+} responses between different animals of different ages and strains). The ART two-way ANOVA was followed by a Wilcoxon rank sum test with Bonferroni correction (for potential error from multiple comparisons) to determine which of the data groups were statistically different.

2.5 Whole-cell dye injections

2.5.1 Tissue preparation and setup

The fluorescent dye Lucifer yellow (charge -2, molecular mass 443 Da) was used to evaluate gap junction channel permeability between the supporting cells of the cochlear epithelium. The apical cochlear turn was dissected out from the inner ear as described above in extracellular solution (ECS) (Table 2.2). The cochlear epithelium was maintained intact to preserve the cell-cell connections across the inner sulcus. Once dissected, the organ of Corti was transferred into a microscope chamber containing ECS, and held in place with a nylon mesh grid (shown previously in Figure 2.3). This chamber was placed under an Olympus BX51 upright microscope (Japan) fitted with a 15x eyepiece and 60x water immersion objective (Olympus LUMPlanFl) (Figure 2.5). The sample was continually perfused with fresh ECS throughout the experiment (Peristaltic pump, Cole-Palmer, UK). The microscope was placed on an anti-vibration table (TMC, UK).

A target cell was chosen and then a patch pipette was lowered into the chamber. Patch pipettes were pulled from soda capillary glass (1413027, Hilgenberg, Germany) and were filled with intracellular solution (ICS) (Table 2.4). The pH of the ICS was raised to 7.28 with 1M KOH and had an osmolality of ~294 mOsm/kg. Additionally, 137µM Lucifer Yellow dye was also added to the intracellular solution (Thermo Fisher, Scientific). The pipettes had a resistance between 3-3.5 MΩ when lowered into the chamber containing ECS.

Chemical	Final concentration (mM)
KCl	141
$MgCl_2$	3
HEPES	5
Na_2Phosphocreatine	10
EGTA-KOH	1

Table 2.4: Chemical composition of intracellular solution

The patch pipette could be positioned adjacent to the target cell using a micromanipulator (PatchStar, Scientifica, UK). This pipette was connected to a mouthpiece so that positive/negative pressure could be applied manually. To avoid the pipette becoming blocked, positive pressure was applied continually whilst approaching the target cell. To form a seal between the cell membrane and the patch pipette tip, the pipette was pushed against the cell membrane and gentle negative pressure was applied until a seal was formed with a resistance of ~1GΩ. The voltage was stepped to -55mV and then an inward suction was applied to break the cell membrane and create a direct connection between the ICS in the pipette and the cells cytosol. After this, the resistance would largely decrease and gradually the dye would enter the cell from the pipette, this would indicate whole-cell patch-clamp configuration had been achieved.

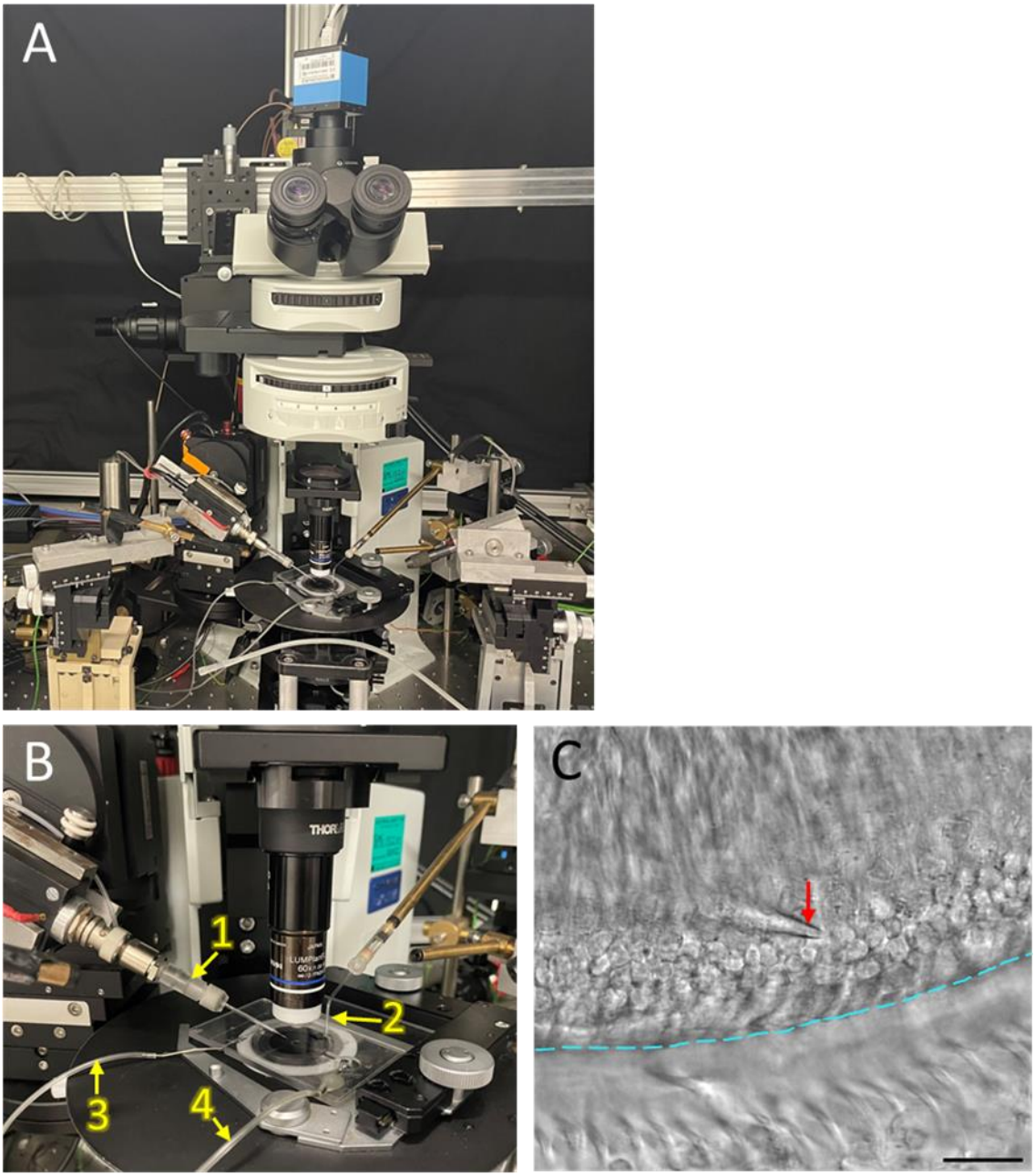

Figure 2.5: Whole-cell dye injection experiment setup

A: Image of the equipment setup for whole-cell dye injection experiments. The Olympus BX51 upright microscope is shown with the ORCA Flash 4.0 V2 CMOS camera attached behind. **B:** Zoomed in view of the microscope stage. The patch pipette holder (with the patch pipette) (1) and the ground electrode (2) are positioned into the microscope chamber. The organ of Corti is located in the chamber under the mesh grid. The chamber is continually perfused with fresh ECS via the inlet (3) and outlet (4) tubes. **C:** Brightfield image of the organ of Corti. The inner sulcus cells are in focus located above the cyan line. The hair cells are out of focus and are located below the cyan line. The patch pipette (red arrow) is positioned adjacent to a target inner sulcus cell. Scale bar: 20 µm.

2.5.2 Imaging

During each recording, the epithelium was repeatedly exposed to pulses of 470 nm light from a light-emitting diode (Thorlabs, USA) which was passed through an ET470/40X narrow bandpass filter (Chroma, USA). Each pulse of light lasted for 100ms and these were given every 300ms throughout the recording. The light exposure was controlled via Python software created in our lab (Python 3.10, Python Software Foundation).

The emitted light was isolated using a T495lpxr long pass dichromatic mirror and a ET525/50M bandpass interference filter (Chroma, USA). Recordings were taken with an ORCA Flash 4.0 V2 CMOS camera (Hamamatsu, Japan). Each recording was always started when the pipette formed a giga seal with the cell membrane, just before any suction was applied to break through into whole-cell mode. This ensured the first moment of dye entry into the cell was always included in the recording. Each recording was left to run for around 25 minutes after whole-cell mode was achieved. The recordings were viewed using Micro-Manager software (Edelstein *et al.*, 2014). After each experiment, a brightfield image was taken of the epithelium to better illustrate the location of individual cells for later analysis (Figure 2.5C).

2.5.3 Analysis of recordings

The recordings were analysed with custom-made Python scripts. A single frame at the end of the recording was used as a reference image to position ROIs (regions of interest). Each ROI measured 3.5 µm x 3.5 µm and was manually placed in the centre of every inner sulcus cell which showed fluorescence due to dye entry (Figure 2.6). An additional ROI was placed over the pipette to measure the decrease in fluorescence intensity due to photobleaching in later analysis. The pixel-average of each ROI was then used to calculate the relative fluorescence intensity (ΔF/F0). Where F is the fluorescence intensity and F0 is an average of the fluorescence in the first five frames of each recording. This was calculated for every ROI including the pipette ROI. Then, the ΔF/F0 for the pipette was subtracted from the ΔF/F0 of each cell.

A mask was generated on top of the reference image using the "label" layer of the Napari imaging software (https://napari.org) where the outline of each cell was manually highlighted

(Figure 2.6C). This then allowed for automatic determination of the location of each cell (in relation to the patched cell) using custom python routines. Specifically, cells were categorised into one of four groups based on their position: the patched cell, first order cells (cells directly adjacent to the patched cell), second order cells (cells directly adjacent to first order cells) and third order cells (cells directly adjacent to second order cells) (Figure 2.6D).

2.5.3.1 Statistical analysis

The sample sizes used in the statistical tests were chosen to be similar to those used in previous work from this lab which also analysed age-related changes in cochlear cell physiology (Ceriani *et al.*, 2019b; Jeng *et al.*, 2020a; Jeng *et al.*, 2021). Mice of both sexes were used in these experiments and randomly distributed over the different experimental groups.

The statistical analysis was completed on OriginPro 2023 (OriginLab, USA). $P < 0.05$ was the criterion for statistical significance. Two-sample t tests were used to compare the means of cells from two mouse age-groups.

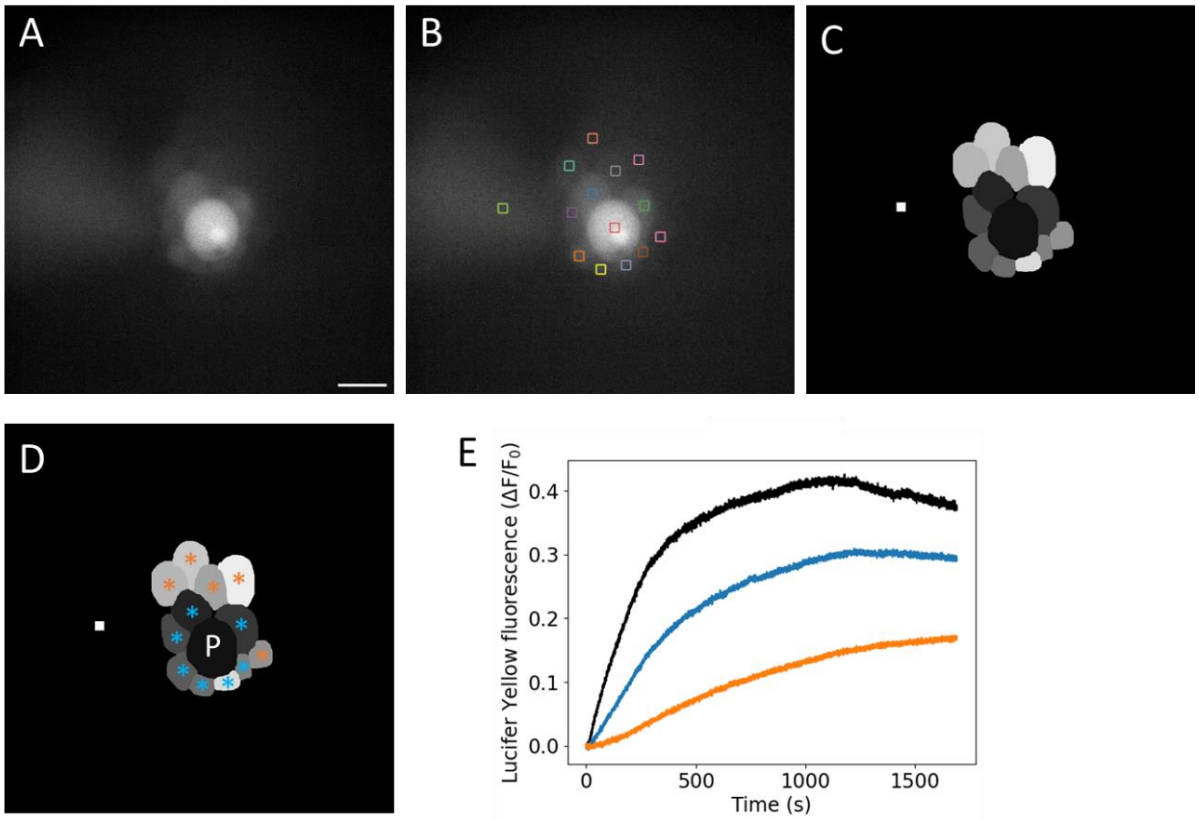

Figure 2.6: Analysis of dye injection recordings

A: Reference image from the last frame of a recording which was used to determine the location of cells for analysis. Scale bar: 20 µm (also applies to **B**, **C** and **D**). **B:** Square ROIs measuring 3.5 µm × 3.5 µm have been placed in the centre of each cell with visible dye diffusion. The ROI on the far left of the image (green) has been placed over the pipette as a reference for fluorescence decrease due to photobleaching. **C:** The ROIs in **B** have been manually extended in Napari imaging software to create this mask showing the entire visible surface of each cell. **D:** The cells were grouped depending on their distance from the patched cell (labelled 'P'). First order cells (blue asterisk) are directly adjacent to the patched cell. Second order cells (orange asterisk) are directly adjacent to first order cells. **E:** Fluorescence intensity traces normalised as ΔF/F0 where the signal from the pipette ROI is subtracted from each cell. The black line shows the fluorescence of the patched cell. The blue line shows an average trace of the individual fluorescence's of each first order cell. The orange line shows an average trace of the individual fluorescence's of each second order cell.

2.6 Electrophysiological recordings

The experimental setup and equipment for performing whole-cell electrophysiological recordings on cells of the cochlear inner sulcus were exactly the same as described in Section 2.5.1. The only difference being no Lucifer yellow was added to the intracellular solution within the patch pipette.

After breaking through the cell membrane and establishing whole-cell mode, the input resistance of the electrodes was compared between 1-month-old and 19-20-month-old inner sulcus cells. This parameter gives an indirect measurement of how coupled the patched cell is to the rest of the epithelium. As mentioned in Section 1.1.1.2.2, all cells of the inner sulcus are connected by a gap junction network. Therefore, the membrane resistance of the patched cell will be influenced by the leak of current from neighbouring cells via the gap junctions. It was hypothesised that any changes in the gap junction-mediated connectivity of the inner sulcus cells with age might be revealed as differences in the input resistances.

This data was acquired using an Optopatch patch clamp amplifier (Cairn Research LTD, UK) with pClamp software on DigiData 1440A low noise board (Molecular Devices, USA). Recordings were filtered using an 8-pole Bessel filter at 2.5 kHz and then sampled at 5 kHz. The input resistance of the electrodes was calculated by Clampex software (Molecular Devices, USA) using a 10 mV test pulse.

Chapter 3. Age-related changes in P2Y receptor signalling in mouse cochlear supporting cells

3.1 Introduction

The extracellular binding of purines to metabotropic purinergic (P2Y) receptors induces an intracellular G-protein coupled signalling cascade leading to efflux of Ca^{2+} from the endoplasmic reticulum into the cytoplasm (Housley, 2000). These resultant Ca^{2+} transients are known to regulate several cellular processes including gene expression and cell proliferation (Berridge, Bootman and Roderick, 2003).

Within the organ of Corti, P2Y receptors are expressed by various supporting cells (Gu Hur *et al.*, 2007; Horváth *et al.*, 2016). This chapter will focus on the role of P2Y receptors within the inner sulcus cells (or 'Kölliker's cells' in the neonate) (Figure 3.1A). During cochlear development, $P2Y_1$, $P2Y_2$ and $P2Y_4$ are all believed to be expressed by the cells within Kölliker's organ (Huang *et al.*, 2010; Babola *et al.*, 2020). These cells readily release ATP and activate P2Y autoreceptors, triggering intracellular Ca^{2+} transients (Piazza *et al.*, 2007; Tritsch *et al.*, 2007). The gap junction network connecting these supporting cells facilitates the spread of the Ca^{2+} transients across the cochlear epithelium (Forge *et al.*, 2003; Ceriani, Pozzan and Mammano, 2016), and the downstream effects of these Ca^{2+} waves can modulate immature hair cell action potentials and promote refinement of their synaptic connections (Johnson *et al.*, 2017).

Following development, the role of P2Y receptors within the inner sulcus remains unclear due to the limited amount of research conducted, along with several contradictory findings. On one hand, the expression of P2Y receptors was reported to be absent in the adult rat inner sulcus (Huang *et al.*, 2010), and ATP/UTP-inducible Ca^{2+} oscillations were either significantly reduced or not detected at all following hearing onset (Tritsch and Bergles, 2010; Chan and Rouse, 2016). However, it has also been suggested that P2Y receptors are maintained in the adult inner sulcus as Ca^{2+} responses were induced following ATP, and UTP, application (Sirko, Gale and Ashmore, 2019). Further investigation is required to better define P2Y receptors and their function within the adult cochlear inner sulcus.

Additionally, senescence-related changes in the expression and function of P2Y purinergic receptors are yet to be researched within the cochlea. This could have important implications for the development of ARHL as numerous other tissues have displayed a link between

changes in P2Y purinergic receptors and the development of age-related neurodegenerative disease (Burnstock, 2008). For example, alterations in P2Y receptor activity in the ageing brain has been linked to pathological mechanisms associated with Parkinson's disease and Alzheimer's disease (Erb *et al.*, 2015; Iring *et al.*, 2022). More specifically, $P2Y_1$ receptors were found to co-localise with pathologic structures associated with Alzheimer's disease, such as neuritic plaques and reactive astrocytes (Moore *et al.*, 2000), and $P2Y_1$ antagonist application largely reduced disease-associated hyperactivity within these pathogenic structures (Delekate *et al.*, 2014). Additionally, P2Y receptor antagonists are being considered as treatments for these neurodegenerative diseases (Cieślak and Wojtczak, 2018), further highlighting their involvement in age-related disease.

This chapter aims to define the progressive changes in P2Y receptor expression and activity within the murine cochlear inner sulcus cells. Three age groups were studied to compare any change in P2Y receptor properties between pre-hearing (postnatal day 7), adult (1-month-old) and aged (17+ months old) cochleae.

3.2 Results

3.2.1 Progressive changes in P2Y receptor expression in the cochlea

Organs of Corti from neonatal (postnatal day 7, P7), adult (1-month-old) and aged (17-22-month-old) mice were immunolabelled with antibodies against $P2Y_1$, $P2Y_2$ and $P2Y_4$ receptors (see Chapter 2, General Methods). This was performed to determine whether the supporting cells in the organ of Corti undergo age-related changes in the expression of P2Y receptors. Additionally, mice of C57BL/6N (6N) background were compared with C3H/HeJ mice (C3H) to investigate whether any age-related changes in P2Y receptor expression were associated with mouse strains showing signs of early onset or late onset ARHL, respectively. For all antibodies tested, the labelling in the organ of Corti is shown from both a top-down view and a lateral side-on view to better illustrate the location of protein expression (Figure 3.1A). Bright field images of the epithelium have also been taken from the top-down view to better show the position of the cells labelled in later images (Figure 3.1B, C).

3.2.1.1 $P2Y_1$ receptor expression

At P7, the organs of Corti of 6N and C3H mice displayed similar expression of $P2Y_1$ receptors in the Kölliker's organ cells (Figure 3.1D, E, F, G). This is consistent with previous work showing $P2Y_1$ receptors contribute to the generation of spontaneous Ca^{2+} transients within Kölliker's organ at this neonatal age (Babola *et al.*, 2020). At 1-month, immunolabelling experiments showed a loss of expression of $P2Y_1$ receptors in the cochlear inner sulcus of both 6N and C3H mice (Figure 3.1D, E, F, G). This again would be expected as spontaneous Ca^{2+} transients are absent after hearing onset (Tritsch and Bergles, 2010). Similar $P2Y_1$ receptor expression was observed between 1-month-old and 17-22-month-old mice from both 6N and C3H strains (Figure 3.1D, E, F, G).

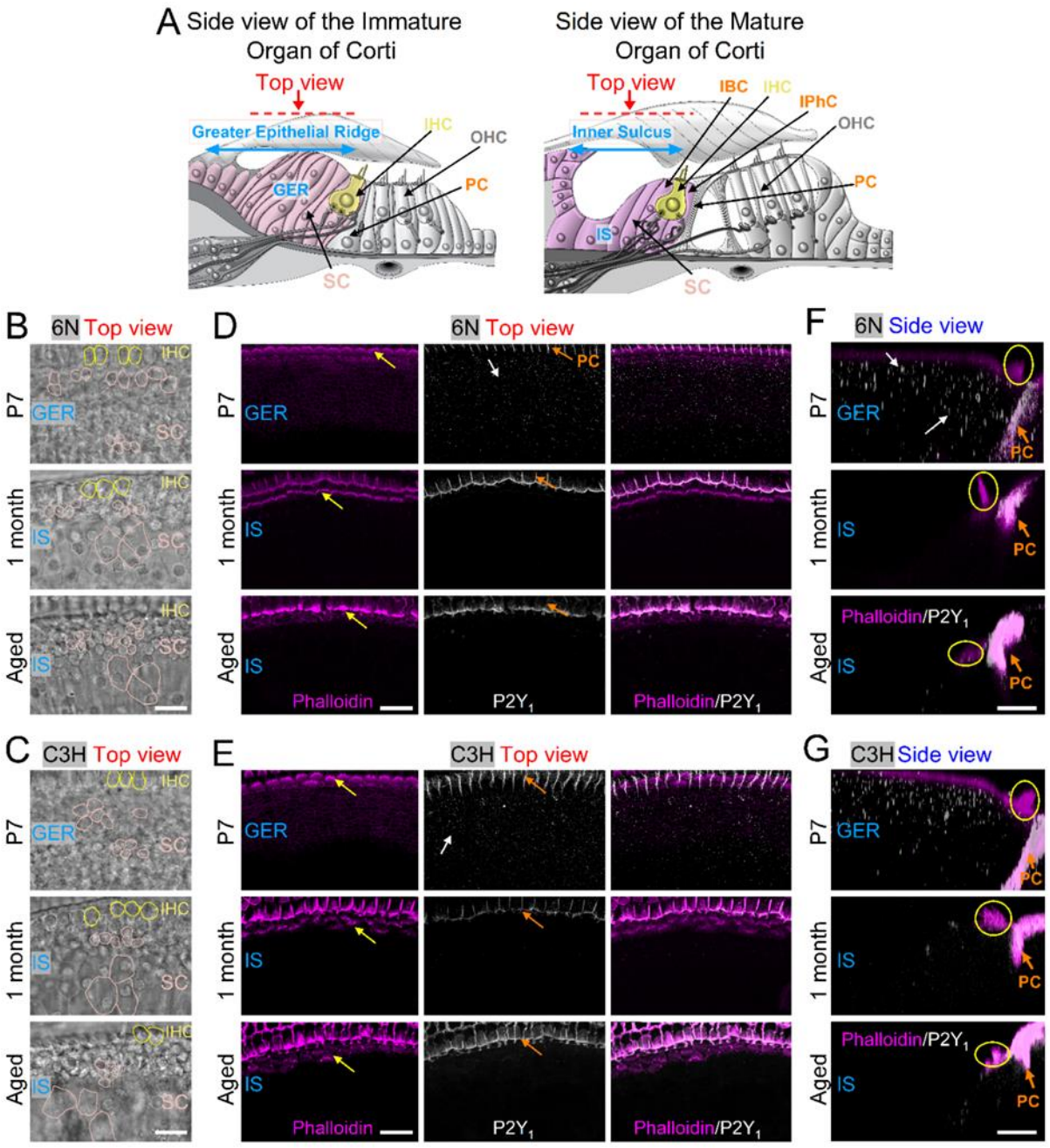

Figure 3.1: $P2Y_1$ receptor expression in the ageing cochlea of 6N and C3H mice

A: Diagram showing a cross-section side-view of a pre-hearing (left) and mature (right) organ of Corti. IHC: inner hair cell; OHC: outer hair cell; IPhC: inner phalangeal cell; IBC: inner border cell; PC: pillar cell; GER: greater epithelial ridge; IS: inner sulcus; SC: supporting cells of the GER and IS, which also include IPhCs and IBCs. The 'Immature' and 'Mature' designations refer to before and after the onset or hearing, respectively, which in mice occurs at around P12. The image on the left was modified from (Ceriani *et al.*, 2019b). The images below represent either the top view (red arrow) or the side view of the GER and IS. **B**, **C**: Brightfield images of the organ of Corti in P7 (top), 1-month-old (middle) and aged (bottom) C57BL/6N (**B**) and C3H/HeJ (**C**) mice taken from the top-view orientation used for the fluorescence images in panels **D** and **E**; these images highlight the location of the different supporting

cell types (SC) in the GER and IS and the IHCs. Note that for simplicity, only a few SCs are highlighted in panels **B** and **C**. Scale bars are 20 μm. **D**, **E**: Maximum intensity projections of confocal *z*-stacks showing images of the GER and IS viewed from the top (red arrow in panel **A**) in P7 (top panels), 1-month-old (middle panels) and aged (17–22 months: bottom panels) 6N (**D**) and C3H (**E**) mice. Left columns show the actin-marker phalloidin (magenta), which is labelling the hair bundles of the IHCs (yellow arrows) and the membrane of some of the supporting cells. Middle columns show the $P2Y_1$ puncta-like labelling (white) in the supporting cells from the bulk of the GER and IS (white arrows). $P2Y_1$ was also expressed in the pillar cells (PCs: orange arrows) which were not investigated in this study. Right panels show the merged images. Scale bars are 20 μm. **F** and **G**: Maximum intensity projections of confocal z-stack images of the GER and IS viewed from the side (see panel **A**). Phalloidin: magenta; $P2Y_1$: white. Note that Phalloidin primarily labels actin in the hair bundle of the IHCs (yellow circles) and the intercellular junctions of pillar cells (PC). Scale bars are 10 μm. Whole figure and legend taken from (Hool *et al.*, 2023).

3.2.1.1 $P2Y_2$ and $P2Y_4$ receptor expression

The organs of Corti of P7 6N and C3H mice displayed comparable expression of $P2Y_2$ and $P2Y_4$ receptors in the Kölliker's organ cells (Figure 3.2 and 3.3). This suggests $P2Y_2$ and $P2Y_4$ receptors could also contribute to ATP-induced Ca^{2+} responses within the immature organ of Corti (Piazza *et al.*, 2007; Huang *et al.*, 2010). At 1-month, immunolabelling experiments showed a loss of expression of $P2Y_2$ and $P2Y_4$ receptors in the cochlear inner sulcus of both 6N and C3H mice (Figure 3.2 and 3.3). This again would be expected as spontaneous Ca^{2+} transients are absent after hearing onset (Tritsch and Bergles, 2010). The supporting cells from 17-22-month-old 6N mice displayed an upregulation of $P2Y_2$ and $P2Y_4$ receptor expression compared to those present in the 1-month-old inner sulcus (Figure 3.2 and 3.3). However, this upregulation was minimal or strongly delayed in inner sulcus cells from 17-22-month-old C3H mice.

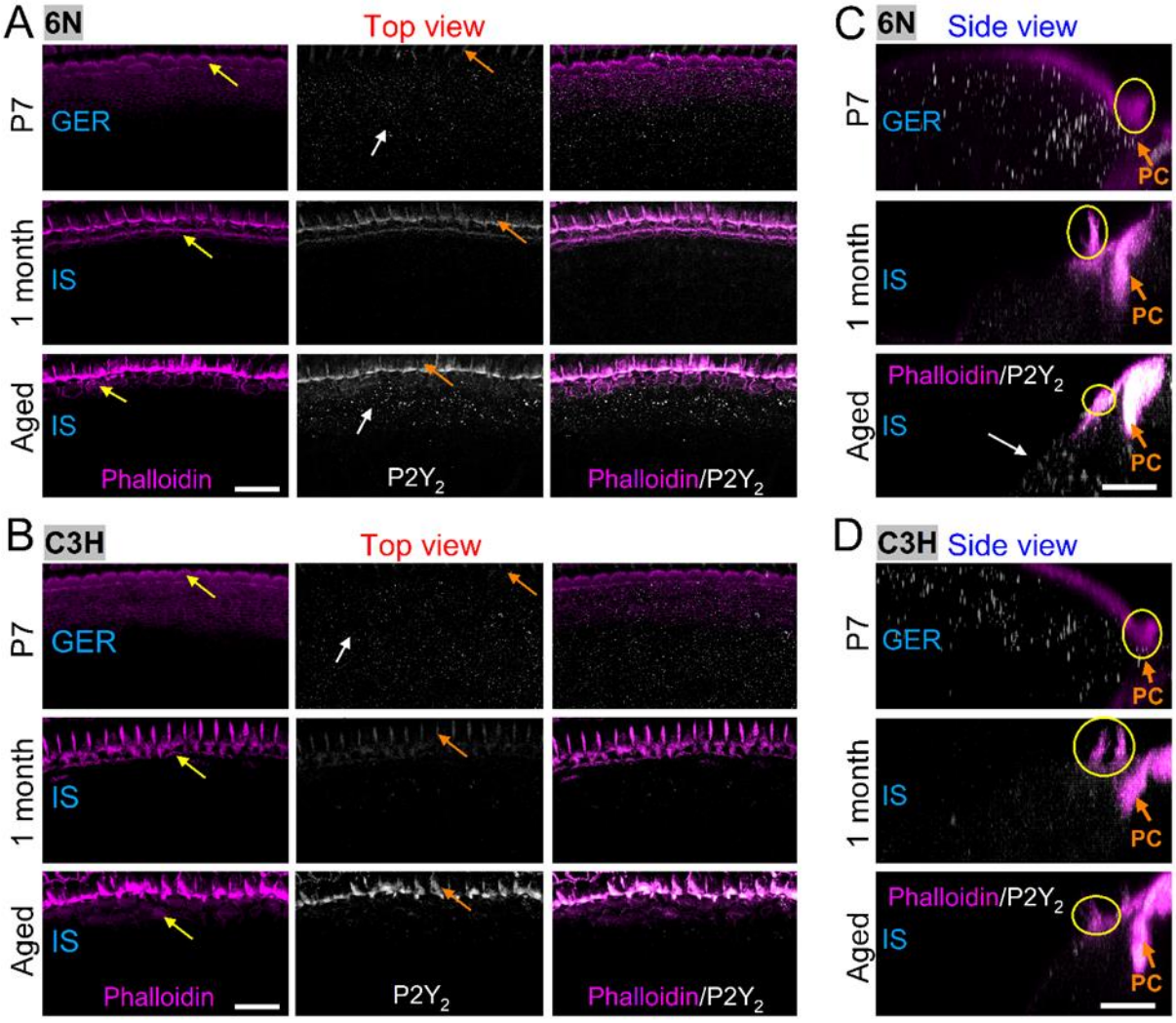

Figure 3.2: $P2Y_2$ receptor expression in the ageing cochlea of 6N and C3H mice

A, **B**: Maximum intensity projections of confocal *z*-stacks showing images of the greater epithelial ridge (GER) and inner sulcus (IS) viewed from the top (red arrow in Figure 3.1A) in P7 (top panels), 1-month-old (middle panels) and aged (17–22 months: bottom panels) C57BL/6N (**A**) and C3H/HeJ (**B**) mice. Left column: actin-marker phalloidin (magenta); middle column: $P2Y_2$ (white). Right panels show the merged images. For the identification of the cellular organisation and labels, see Figure 3.1. Scale bars are 20 µm. **C**, **D**: Maximum intensity projections of confocal *z*-stack images of the GER and IS viewed from the side (see Figure 3.1). Phalloidin: magenta; $P2Y_2$: white. Scale bars are 10 µm. Whole figure and legend taken from (Hool *et al.*, 2023).

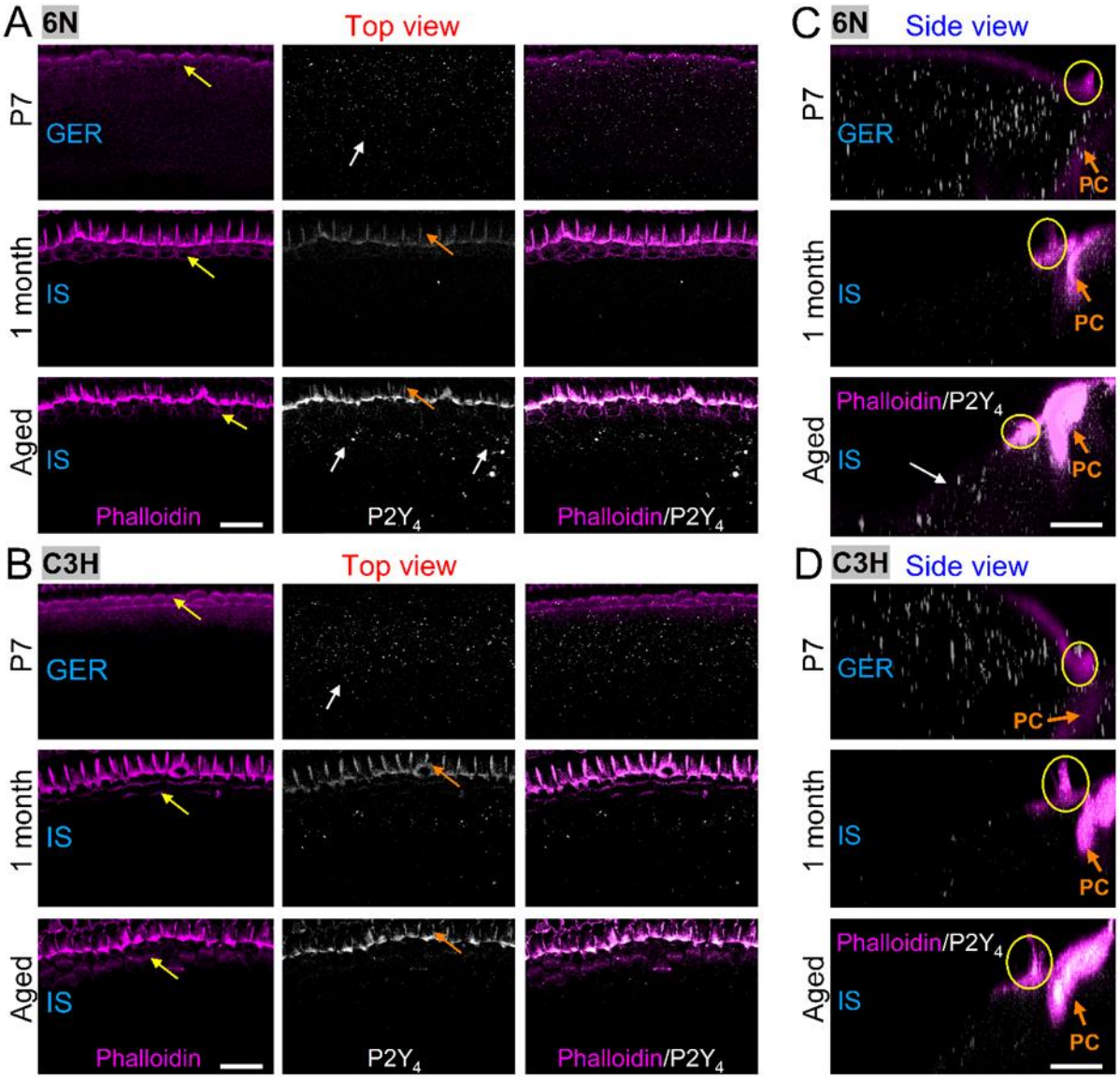

Figure 3.3: $P2Y_4$ receptor expression in the ageing cochlea of 6N and C3H mice

A, **B**: Maximum intensity projections of confocal *z*-stacks showing images of the GER and IS viewed from the top (red arrow in Figure 3.1A) in P7 (top panels), 1-month-old (middle panels) and aged (17–22 months: bottom panels) 6N (**A**) and C3H (**B**) mice. Left column: actin-marker phalloidin (magenta); middle column: $P2Y_4$ (white). Right panels show the merged images. For the identification of the cellular organization and labels, see Figure 3.1. Scale bars are 20 µm. **C**, **D**: Maximum intensity projections of confocal *z*-stack images of the GER and IS viewed from the side (see Figure 3.1). Phalloidin: magenta; $P2Y_4$: white. Scale bars are 10 µm. Whole figure and legend taken from (Hool *et al.*, 2023).

3.2.2 Progressive changes in P2Y receptor function in the cochlea

In order to study P2Y-mediated intracellular Ca^{2+} responses in the supporting cells, the cochlear explants from neonatal (postnatal day 7), adult (1-month-old) and aged (18-24-months-old) mice were incubated with the ratiometric fluorescent Ca^{2+} indicator Fura-2. This was performed to determine whether the supporting cells in the organ of Corti undergo age-related changes in the function of P2Y receptors. For these experiments, C57BL/6N and C3H/HeJ mice were investigated together with C57BL/6N-repaired mice, which are co-isogenic with C57BL/6N mice but have the *Cdh23*^{ahl} allele repaired with CRISPR/Cas9 (Mianné *et al.*, 2016).

Three of the most abundant endogenous ligands for the P2Y receptor family include adenosine 5'-triphoshate (ATP), adenosine 5'-diphosphate (ADP) and uridine 5'-triphosphate (UTP) (Jacobson *et al.*, 2009). ATP is a general P2 receptor agonist known to activate all three P2Y receptors we intend to study ($P2Y_1$, $P2Y_2$ and $P2Y_4$) as well as other P2Y and P2X receptor subtypes (Burnstock, 2004). It has been reported that the concentration of ATP in the endolymph and perilymph of the cochlea at rest is 10-20 nM (Muñoz *et al.*, 1995). However, this is expected to fluctuate, and is likely increased during development as ATP is being constantly released by Kölliker's organ cells (Piazza *et al.*, 2007). Additionally, it is also known that ATP is released into the extracellular cochlea fluids following insults such as high levels of noise exposure or hypoxia (Muñoz *et al.*, 1995; Chan and Rouse, 2016). Therefore, 100 nM was selected as the concentration of ATP to use in these experiments to elicit P2Y-mediated Ca^{2+} responses in the supporting cells of the cochlea. However, the majority of other studies in the literature use 1-100 µM of ATP (Piazza *et al.*, 2007; Tritsch and Bergles, 2010; Sirko, Gale and Ashmore, 2019) which is much larger than the ATP concentration expected to exist *in vivo.* Nonetheless, it was apparent that it was not necessary to use such a high ATP concentration as we observed Ca^{2+} responses in cochlear supporting cells with 100 nM (Figure 3.4).

3.2.2.1 ATP-induced intracellular Ca^{2+} responses increase in the aged inner sulcus

The extracellular application of 100 nM ATP onto the sensory epithelium from postnatal day 7 6N mice induced increases in intracellular Ca^{2+} concentration which propagated across the cells of Kölliker's organ in waves (Figure 3.4B). This was anticipated as it is well established that P2Y receptors are expressed in Kölliker's organ prior to hearing onset (Babola *et al.*, 2020; Huang *et al.*, 2010). ATP is known to stimulate P2Y-mediated Ca^{2+} release from the endoplasmic reticulum, and the gap junction network connecting these cells will facilitate the spread of this Ca^{2+} response across the epithelium (Ceriani, Pozzan and Mammano, 2016). Alongside this, spontaneous intracellular Ca^{2+} waves were also observed in Kölliker's organ cells, unrelated to the application of ATP. *In vivo*, these cells are known to spontaneously release ATP which activates their own P2Y receptors and induces spontaneous intracellular Ca^{2+} waves (Piazza *et al.*, 2007; Tritsch *et al.*, 2007). Neonatal supporting cells also exhibit oscillatory activity comprising of periodic, transient increases in Ca^{2+} levels upon continuous stimulation with ATP. Therefore, age-related differences in both individual Ca^{2+} spikes, and Ca^{2+} oscillations, were investigated to evaluate both the size and dynamics of Ca^{2+} responses in the ageing cochlea.

In 1-month-old organs of Corti, the application of 100 nM ATP induced minimal increases in intracellular Ca^{2+} in the supporting cells of the inner sulcus (Figure 3.4C). The average, and maximum, ATP-induced Ca^{2+} response was significantly reduced in 1-month-old explants compared to those recorded at P7 ($P < 0.0001$) (Figure 3.4O, P). Additionally, ATP-induced Ca^{2+} responses remained minimal in supporting cells from 6-month-old 6N mice and, when compared with the 1-month-old explants, no significant difference was found between either the average or maximum ATP-inducible Ca^{2+} responses.

However, 12-month-old inner sulcus cells showed a significant increase in average and maximum ATP-induced Ca^{2+} responses compared to those from 1-month-old explants (Figure 3.4O, P), and this was even more pronounced in the senescent age group ($P < 0.0001$) (18-24-months-old). These Ca^{2+} responses also appeared to resemble more closely those observed

in the neonatal explants as they manifested as both Ca^{2+} spikes and oscillations (an oscillation being classed as a repetitive Ca^{2+} spike where Ca^{2+} levels rise and fall cyclically) (Figure 3.4Q).

The reason for an upregulation in P2Y receptor function in the 6N aged cochlea is unclear. To understand whether this upregulation was linked to the degree of hearing loss, age-related changes in P2Y receptor function were first compared between the 6N (early onset ARHL) and C3H mouse (late onset ARHL) strains. No significant difference was found in the average or maximum ATP-induced Ca^{2+} responses between the neonatal explants from 6N and C3H mice (Figure 3.4N, O and P), and similar to the 6N mice, the 1-month-old C3H explants showed a significant reduction in ATP-induced Ca^{2+} responses compared to the neonatal cells ($P < 0.0001$). However, unlike the 6N strain, the 12-month-old C3H inner sulcus cells did not show a significant upregulation in the average or maximum ATP-induced Ca^{2+} responses when compared to the 1-month-old cells (Figure 3.4O and P). Furthermore, in the senescent age group (18-24-months-old) the C3H inner sulcus cells exhibited a significantly smaller upregulation in ATP-induced Ca^{2+} responses compared to the upregulation observed in the 6N cells. There was also no significant increase in the frequency of ATP-induced Ca^{2+} oscillations in the senescent C3H inner sulcus compared to the 1-month-old adult (Figure 3.4Q). Taken together, these results suggest that the C3H mouse strain undergoes much less of (or a delayed) upregulation of P2Y receptor function with ageing in comparison to the 6N strain. This conclusion raises the possibility that these age-related changes in the function of P2Y receptors might be associated with the progression of ARHL. However, there is also the possibility that they might be a secondary effect of ARHL and have no influence on its progression.

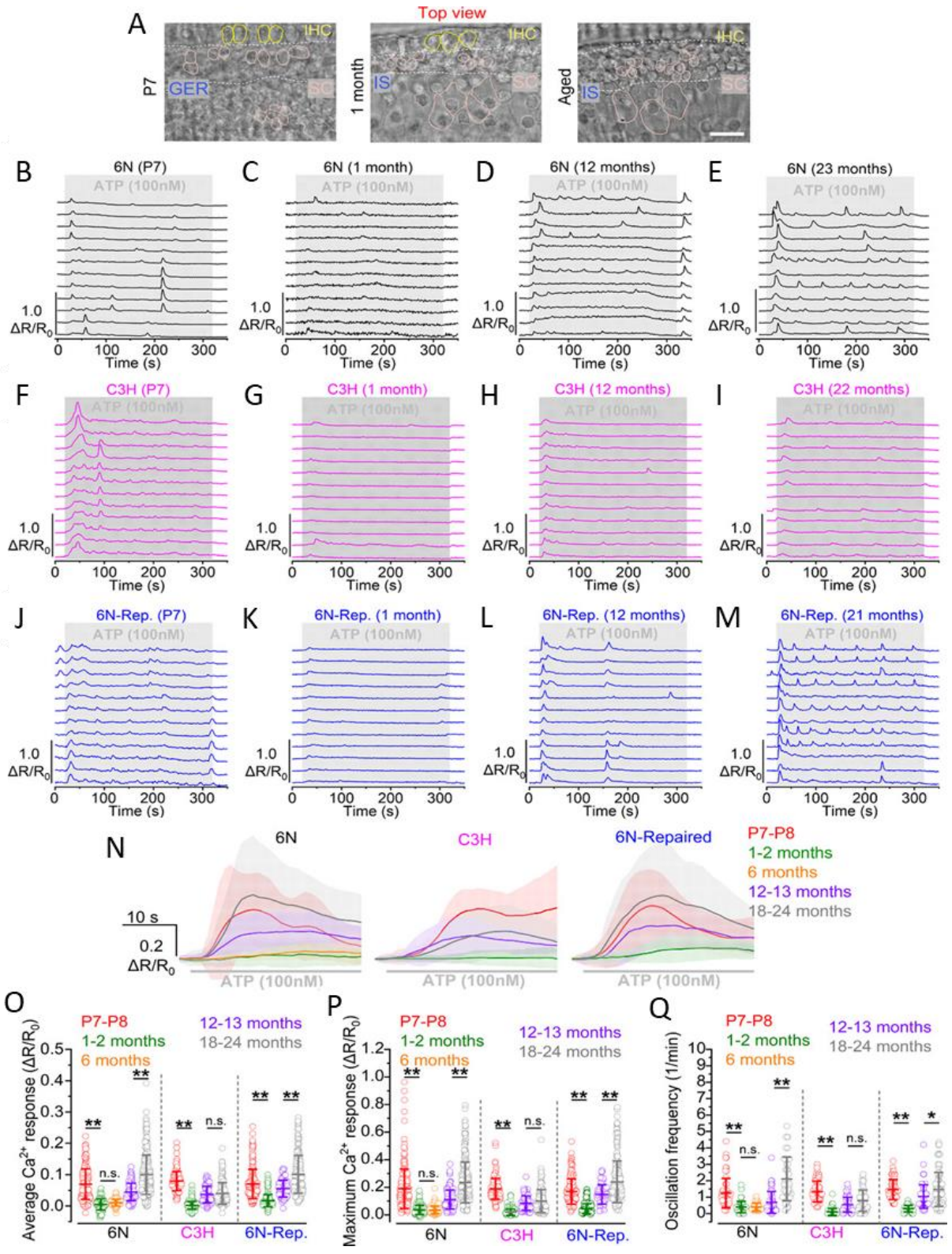

Figure 3.4: ATP-induced Ca^{2+} responses in ageing 6N, C3H and 6N-repaired mouse inner sulcus cells

A: Brightfield images of the organ of Corti in P7 (left), 1-month-old (middle) and aged (right) mice from Figure 3.1 B (immunolabelling experiments) showing the area of the GER and IS used for the Ca^{2+} imaging experiments, which includes the supporting cells close to the IHCs (area in between the

white dashed lines). Scale bars are 20 µm. **B**–**M**: Representative Ca^{2+} responses in supporting cells induced by the extracellular application of 100 nM ATP (grey area) in 6N (**B**–**E**, black), C3H (**F**–**I**, magenta), and 6N-Repaired (6N-Rep.: **J**–**M**, blue) mice at different ages reported above each set of traces. Synchronised peaks in several traces after the increase at the onset of stimulation (evident in panels **B**, **F** and **L**) reflect the propagation of Ca^{2+} waves across multiple cells. **N**: Comparison of the average Ca^{2+} responses from supporting cells at the onset of ATP application from 6N (left), C3H (middle), and 6N-Repaired (right) mice at different ages. Continuous traces represent averages, while the shaded area is the SD. Numbers of individual ROIs (i.e. supporting cells) for mice at P7–P8, 1–2 months, 12–13 months, and 18–24 months are: 6N, 212 (8 mice), 144 (7), 134 (3), 276 (10); C3H, 127 (3), 194 (7), 127 (4), 173 (9); Repaired, 176 (6), 171 (5), 88 (3), 250 (8). For 6N mice, an additional set of experiments was performed in 6-month-old animals (130 ROIs from 4 mice). **O**, **P**: Comparison of the average (**O**) and maximum (**P**) Ca^{2+} response of each cell to 100 nM ATP application in the three mouse strains at different ages. Open circles represent single data points. Significance values are indicated by the asterisks ($^{**}P < 0.0001$, Wilcoxon rank sum test, ART two-way ANOVA). **Q**: Comparison of the oscillation frequency in supporting cells during application of 100 nM ATP. For this quantification, we only used experiments from panels **O** and **P** in which ATP perfusion was longer than 100 s. Numbers of individual ROIs (i.e. supporting cells) for mice at P7–P8, 1–2 months, 12–13 months, and 18–24 months are: 6N, 60 (3 mice), 52 (3), 55 (2), 48 (3); C3H, 66 (3), 71 (3), 65 (4), 56 (5); Repaired, 66 (3), 65 (4), 77 (3), 132 (6). For 6N mice, an additional set of experiments was performed in 6-month-old animals (55 ROIs from 4 mice). Open circles represent single data points. Significance values are indicated by the asterisks ($^{*}P = 0.031$, $^{**}P < 0.0001$, Wilcoxon rank sum test, ART two-way ANOVA). Whole figure and legend taken from (Hool *et al.*, 2023).

In order to evaluate whether the *Cdh23*^{ahl} allele in 6N hair cells was indirectly involved in the upregulation of P2Y receptors, the progressive changes in P2Y receptor function were compared between 6N and 6N-repaired mouse strains. As mentioned above, the 6N-repaired mouse line is co-isogenic to the 6N mouse strain, except the 6N-repaired strain has the mutation in *Cadherin 23* corrected via CRISPR/Cas9-mediated homology directed repair (Mianné *et al.*, 2016). This correction reduces the severity of early onset ARHL observed in 6N mice and gives the 6N-repaired mice significantly better ABR thresholds at older ages in the high-frequency regions (>12kHz) (Figure 2.1) (Jeng *et al.*, 2021). The 6N-repaired inner sulcus cells displayed a similar upregulation of ATP-induced Ca^{2+} responses in the senescent explants to that observed by 6N explants (Figure 3.4J-N). No significant difference was found in the size or dynamics of these Ca^{2+} responses between 6N or 6N-repaired aged inner sulcus cells (Figure 3.4O-Q). These data suggest the observed age-related alterations in P2Y-mediated purinergic signalling is unlikely to be influenced by the *Cdh23*^{ahl} allele. However, the C57BL strain, irrespectively to the *Cdh23*^{ahl} allele, was more susceptible to changes in supporting cells compared to the C3H mice.

To better understand the dynamics of these senescence-specific Ca^{2+} responses, different concentrations of ATP were applied to inner sulcus cells from 6N mice aged 18-24-months old. From this, it could be inferred what concentrations of ATP would be required *in vivo* in the endolymph to generate Ca^{2+} responses. Spikes and sustained oscillations in intracellular Ca^{2+} could be induced from application of 30 – 300 nM ATP (Figure 3.5A). The application of higher ATP concentrations (1 µM) triggered a rise in intracellular Ca^{2+} levels followed by a plateau or damped oscillations (Figure 3.5A). The EC_{50} (the concentration required to produce 50% of the response) was calculated to be 60-70 nM ATP for both the average and maximum Ca^{2+} responses from aged supporting cells (Figure 3.5C and D).

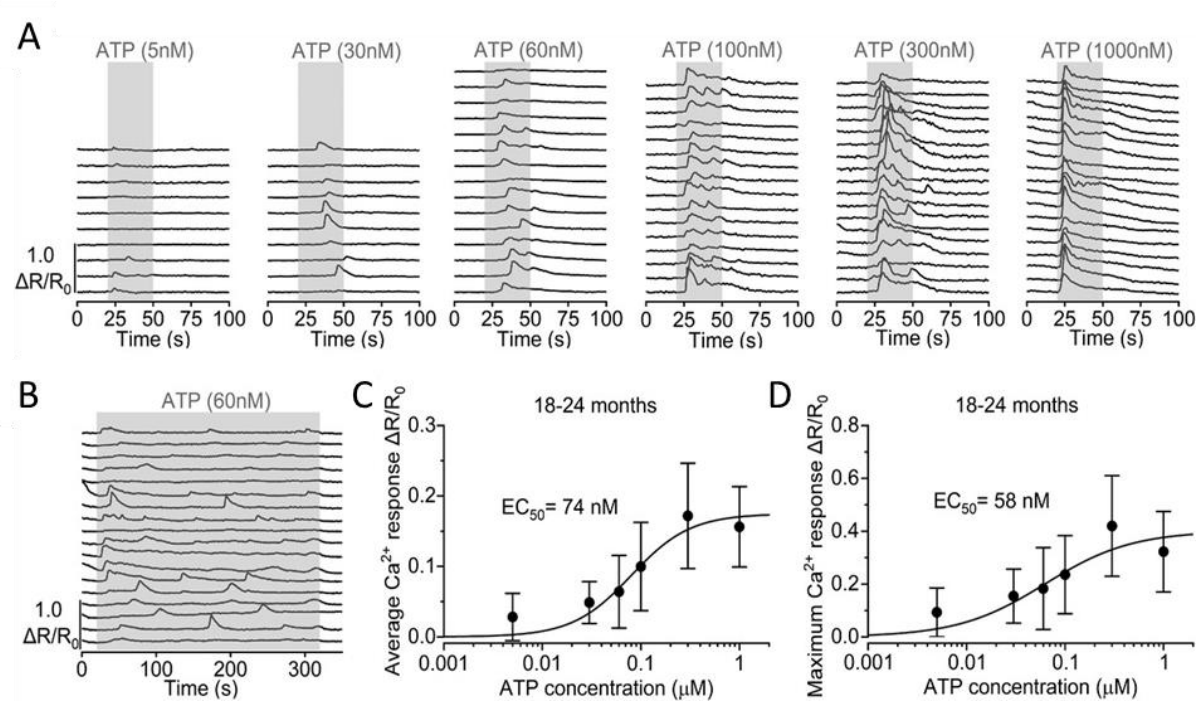

Figure 3.5: Dose-dependent ATP-induced Ca^{2+} signalling in supporting cells from aged 6N mice

A: Representative Ca^{2+} responses to different concentrations of ATP in supporting cells induced by ATP perfusion (grey area) in aged (18–24 months) 6N mice. **B**: Prolonged stimulation (5 min) with 60 nM ATP, highlighting the occurrence of slow oscillations. **C**, **D**: Dose-response curves for the average (**C**) and maximal (**D**) Ca^{2+} response as a function of the ATP concentration. Data are plotted as mean ± SD. The continuous lines represent a fit with a Hill function:

$$R = R_{\max} \frac{[\mathrm{ATP}]^n}{[\mathrm{ATP}]^n + \mathrm{EC_{50}}^n},$$

where EC_{50} = 74 ± 6 nM and n = 1.62 ± 0.23 (**C**) and EC_{50} = 58 ± 10 nM and n = 1.07 ± 0.22 (**D**). Numbers of individual supporting cells (ROIs) recorded from 18–24-month-old mice and from lower to higher concentrations are: 31 (3 mice), 56 (3), 130 (6), 276 (10), 66 (3), 56 (5). Whole figure and legend taken from (Hool *et al.*, 2023).

3.2.2.2 ATP-induced intracellular Ca^{2+} responses rely on Ca^{2+} release from intracellular stores

The activation of P2Y purinergic receptors induces an intracellular G-protein coupled signalling cascade which drives Ca^{2+} efflux into the cytoplasm from the endoplasmic reticulum (Housley, 2000). Therefore, to confirm whether the observed intracellular Ca^{2+} responses are a result of activating P2Y receptors, thapsigargin was used to block the SERCA ATPase pump. This ATPase pump is located on the endoplasmic reticulum and is responsible for building up the Ca^{2+} stores by taking up Ca^{2+} from the cytoplasm (Thastrup, 1990). Therefore, thapsigargin will deplete Ca^{2+} stores within the endoplasmic reticulum and prevent any P2Y-mediated intracellular Ca^{2+} responses. Extracellular thapsigargin completely abolished any intracellular Ca^{2+} rise or oscillations induced following the application of 100 nM ATP to aged inner sulcus cells (Figure 3.6). This suggests the Ca^{2+} responses induced by application of nanomolar concentrations of ATP are a result of the activation of P2Y receptors stimulating Ca^{2+} release from the ER into the cytoplasm, and are not due to Ca^{2+} influx into the cell from the extracellular space via ionotropic P2X purinergic receptors. Furthermore, it has already been reported that thapsigargin abolishes ATP-mediated intracellular Ca^{2+} responses in the pre-hearing Kölliker's organ (Piazza *et al.*, 2007; Babola *et al.*, 2020).

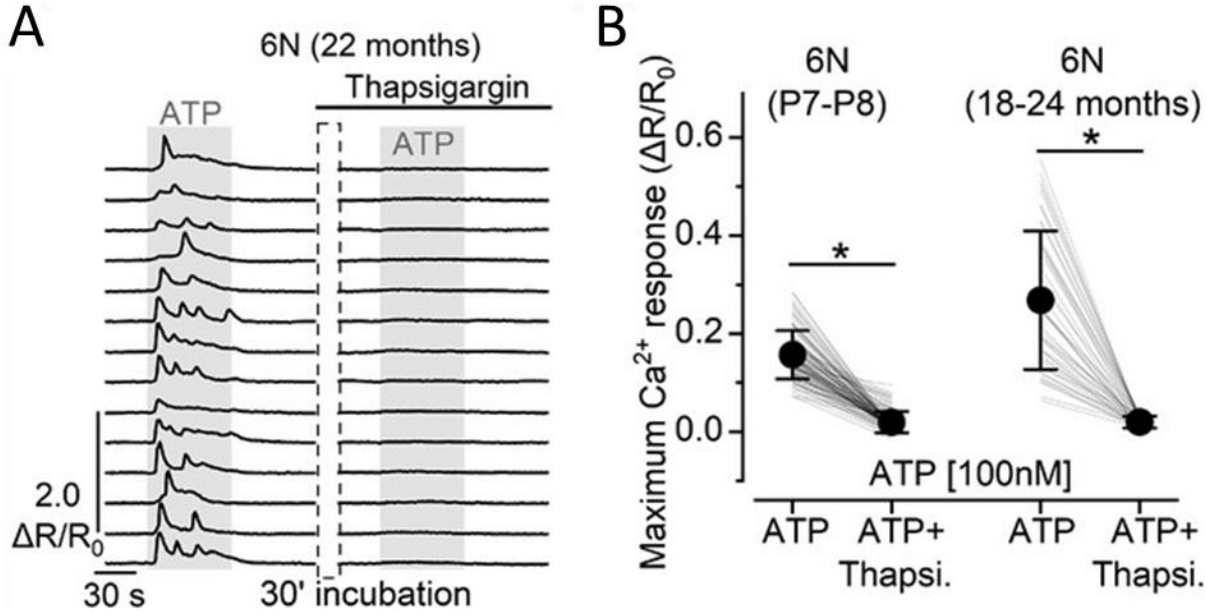

Figure 3.6: ATP-induced Ca^{2+} signals in supporting cells of aged mice depend on intracellular Ca^{2+} stores

A: Representative Ca^{2+} responses in supporting cells induced by ATP perfusion (100 nM, grey area) in an aged 6N mouse before (left) and after (right) 30-min incubation in 2 µM Thapsigargin. **B**: Maximal ATP-induced Ca^{2+} response before and after Thapsigargin incubation. Thapsigargin incubation abolished the Ca^{2+} responses ($P < 0.0001$, Wilcoxon signed-rank test). Numbers of individual supporting cells (ROIs): P7–P8, 102 (3 mice); 18–24 months old, 46 (3 mice). Whole figure and legend taken from (Hool *et al.*, 2023).

3.2.2.3 ADP-induced intracellular Ca^{2+} responses are unchanged in the aged cochlea

Adenosine 5'-diphosphate (ADP) is known to activate $P2Y_1$, but not $P2Y_2$ and $P2Y_4$ (Burnstock, 2004; von Kügelgen and Hoffmann, 2016). The use of this agonist allowed the observation of intracellular Ca^{2+} responses due to $P2Y_1$ alone without the influence of the other two receptors known to be expressed in the inner sulcus cells (Figure 3.2 and 3.3). The extracellular application of 1uM ADP onto the organs of Corti from postnatal day 7 mice induced similar intracellular Ca^{2+} responses to those observed after ATP application (Figure 3.7A-F). However, ADP application triggered Ca^{2+} responses in 1-month-old inner sulcus cells and this was not observed following ATP application at this age. Furthermore, these ADP-induced Ca^{2+} responses remain unchanged and are maintained in the aged inner sulcus cells. No significant difference was found between the maximum or average Ca^{2+} responses from 6N inner sulcus cells aged 1-month-old and 18-24-months-old (Figure 3.7E, F). To confirm that the Ca^{2+} responses are due to ADP activating $P2Y_1$ receptors, the $P2Y_1$ specific antagonist MRS2500 was applied. This antagonist completely abolished any ADP-induced Ca^{2+} responses in the aged inner sulcus cells (Figure 3.7G, H). Therefore, it is likely that these ADP-induced Ca^{2+} responses are a result of $P2Y_1$ receptor activation. However, the immunolabelling images show no $P2Y_1$ receptor expression at 1-month old or 18-24 months old (Figure 3.1).

This means the immunolabelling and Ca^{2+} imaging experiments give contradictory conclusions about the presence of $P2Y_1$ receptors in the adult and aged inner sulcus. One explanation for this could be that the antibody was not validated on a $P2Y_1$ knock out mouse and so it is not certain as to whether the labelling was reliable. Alternatively, there could be other receptors which become expressed in the adult and aged inner sulcus which both respond to ADP, and are influenced by the MRS2500 antagonist. This will be discussed further in later chapters.

Nevertheless, both of these data report no difference between the expression or function of $P2Y_1$ receptors in the adult cochlea (1-month-old) compared to the aged cochlea (18-24 months old). Therefore, it was decided to investigate other P2Y receptors to try and figure out what was driving the senescence-specific increase in ATP-inducible Ca^{2+} responses reported earlier.

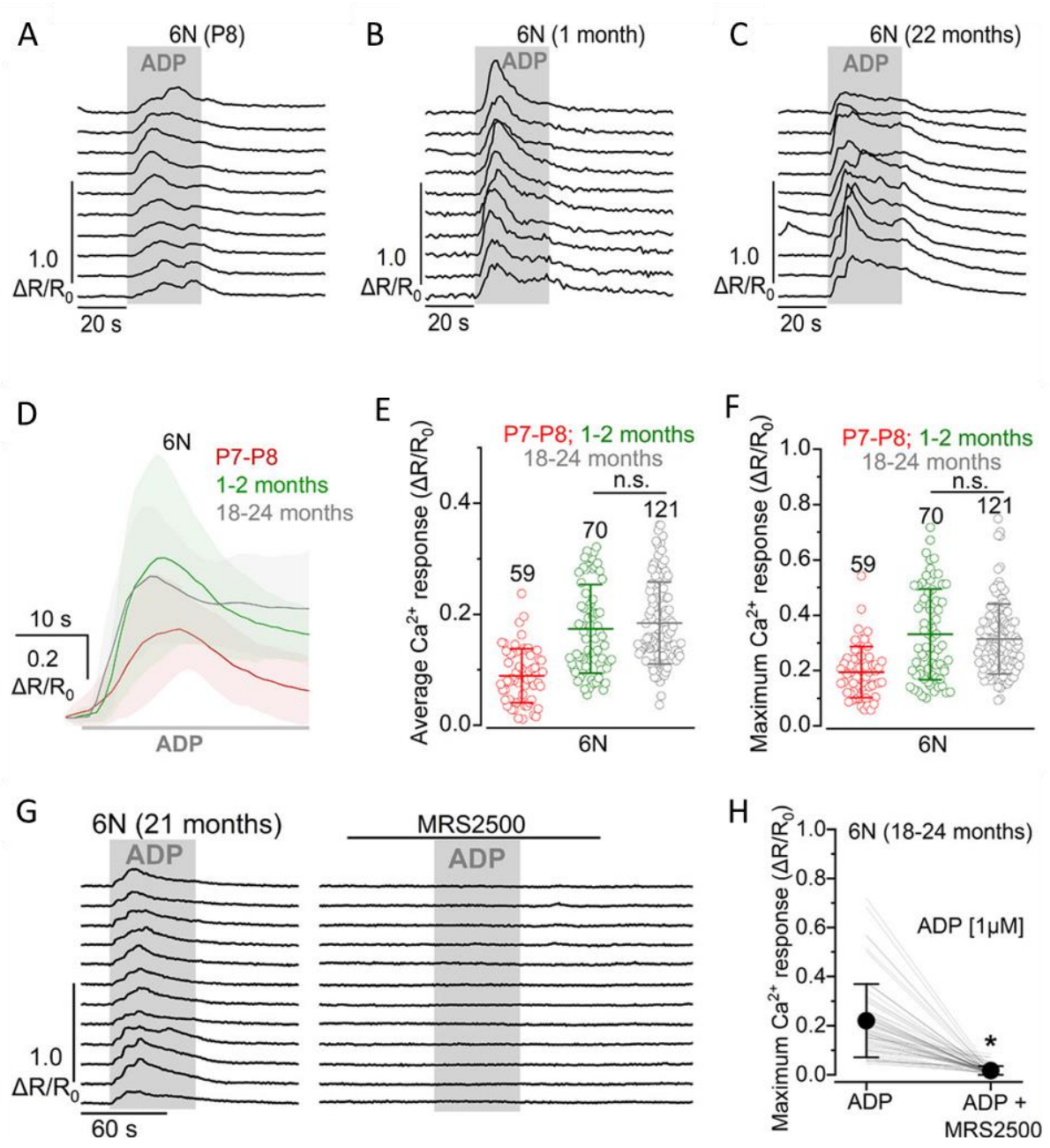

Figure 3.7: ADP-induced Ca^{2+} responses in supporting cells of the 6N mouse cochlea

A–**C**: Representative Ca^{2+} responses in supporting cells induced by the extracellular application of 1 µM ADP (grey area) in 6N mice at different age ranges shown above the recordings. **D**: Comparison of the average Ca^{2+} response at the onset of ADP application (grey bar beneath the traces) in cochlear supporting cells of 6N mice in the three different age ranges tested. Continuous traces represent averages, while the shaded area is the SD. Numbers of individual supporting cells (ROIs): P7–P8, 59 ROIs (3 mice); 1–2 months old, 70 ROIs (4), and 18–24 months old, 121 ROIs (5). **E**, **F**: Comparison of the average (**E**) and maximum (**F**) Ca^{2+} response to 1 µM ADP application in 6N mice at different ages. Number of supporting cells used is shown above the averages (± SD) and single data points (plotted as open circles). **G**: Representative Ca^{2+} responses in supporting cells induced by 1 µM extracellular

ADP (grey area) in aged 6N mice. The application of ADP together with the $P2Y_1$ antagonist MRS2500 (1 µM, top black horizontal line) blocked the ADP-induced Ca^{2+} response. **H**: Effect of $P2Y_1$ antagonist MRS2500 on the size of the ADP-induced Ca^{2+} response in cochlear supporting cells from aged mice from 64 supporting cells (ROIs) from 3 mice. Significance values are indicated by the asterisks ($P < 0.0001$, Wilcoxon signed-rank test). Whole figure and legend taken from (Hool *et al.*, 2023).

3.2.2.4 UTP-induced intracellular Ca^{2+} responses are increased in the aged cochlea

UTP is known to activate $P2Y_2$ and $P2Y_4$ receptors, but not $P2Y_1$ receptors (von Kügelgen and Hoffmann, 2016). Application of 300 nM UTP to 6N organs of Corti from postnatal day 7 mice, 1-month-old and aged cells induced similar intracellular Ca^{2+} responses to those observed after ATP application. Both the neonatal (P7/8) and aged (18-24 months old) inner sulcus cells displayed intracellular Ca^{2+} oscillations in response to UTP (Figure 3.8A and C). While supporting cells from 1-month-old 6N mice showed little or no Ca^{2+} responses to this agonist (Figure 3.8B). As observed with ATP, no difference was observed between the Ca^{2+} responses recorded from 6N and C3H mouse strains in the neonatal (P7/8) and adult (1-month-old) age groups (Figure 3.8G-I). However, inner sulcus cells from aged 6N mice displayed significantly larger UTP-induced Ca^{2+} responses when compared to C3H mice of the same age (Figure 3.8G-I). This data again suggests that the upregulation of P2Y receptor function observed in the aged inner sulcus appears to be more pronounced in mice with more severe ARHL.

To further confirm that UTP-induced Ca^{2+} responses are a result of $P2Y_2$ and $P2Y_4$ receptor activation, the specific $P2Y_2$ receptor antagonist AR-C 118925XX (Rafehi *et al.*, 2017) and the $P2Y_4$ receptor agonist MRS4062 (Maruoka *et al.*, 2011) were extracellularly applied (Figure 3.9). When AR-C 118925XX was applied together with UTP, it abolished the UTP-induced Ca^{2+} responses in the inner sulcus cells of 6N aged mice, indicating that these Ca^{2+} oscillations rely on the $P2Y_2$ receptor. Additionally, application of MRS4062 elicited similar intracellular Ca^{2+} responses to those seen following UTP application. This suggests that UTP is also activating the $P2Y_4$ receptors as the UTP-induced responses are comparable to $P2Y_4$-specific responses. Taken together, these results suggest that the $P2Y_2$ and $P2Y_4$ receptors are responsible for the upregulation of UTP-induced Ca^{2+} responses in the aged inner sulcus.

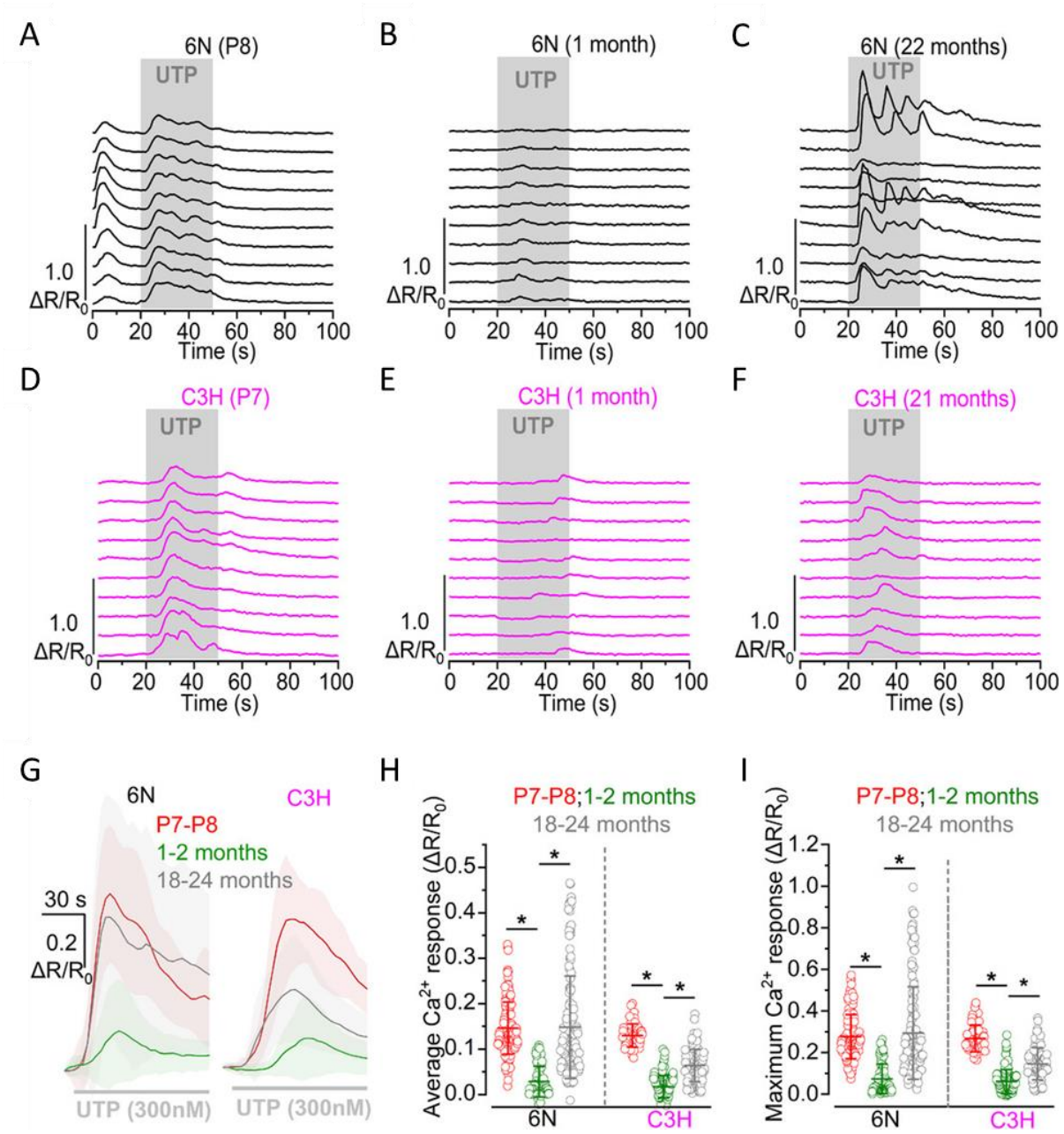

Figure 3.8: Age dependence of UTP-induced Ca^{2+} responses in ageing mice

A–**F**: Representative Ca^{2+} responses in supporting cells induced by the superfusion of 300 nM UTP (grey area) in 6N (**A**–**C**, black) and C3H (**D**–**F**, magenta) mice at the different age ranges shown above the recordings. **G**: Comparison of the average Ca^{2+} response at the onset of UTP application (grey bar beneath the traces) in cochlear supporting cells of 6N (left) and C3H (right) mice. Continuous traces represent averages, while the shaded area is the SD. Numbers of individual supporting cells (ROIs) for P7–P8, 1- to 2-month-old and 18- to 24-month-old mice, are: 6N, 151 (5 mice), 104 (5 mice), 148 (7 mice); C3H, 66 (3 mice), 128 (5 mice), 125 (7 mice). The average frequency of UTP-induced Ca^{2+} oscillations for 6N mice at different ages was: P7–P8, 3.75 ± 1.29 oscillations/min; 1–2 months, 1.33 ± 1.29 oscillations/min; 18–24 months, 3.83 ± 2.35 oscillations/min. The average frequency of UTP-induced Ca^{2+} oscillations for C3H mice at different ages was: P7–P8, 3.32 ± 1.24 oscillations/min;

1–2 months, 1.24 ± 1.05 oscillations/min; 18–24 months, 1.57 ± 0.85 oscillations/min. **H**, **I**: Comparison of the average (**H**) and maximum (**I**) Ca^{2+} response to 300 nM UTP application in 6N and C3H mice at different ages. Single data points are plotted as open circles. Numbers of individual supporting cells (ROIs) and mice is as described in panel **G** above. Significance values are indicated by the asterisks ($^{*}P < 0.0001$, Wilcoxon rank sum test, ART two-way ANOVA). Whole figure and legend taken from (Hool *et al.*, 2023).

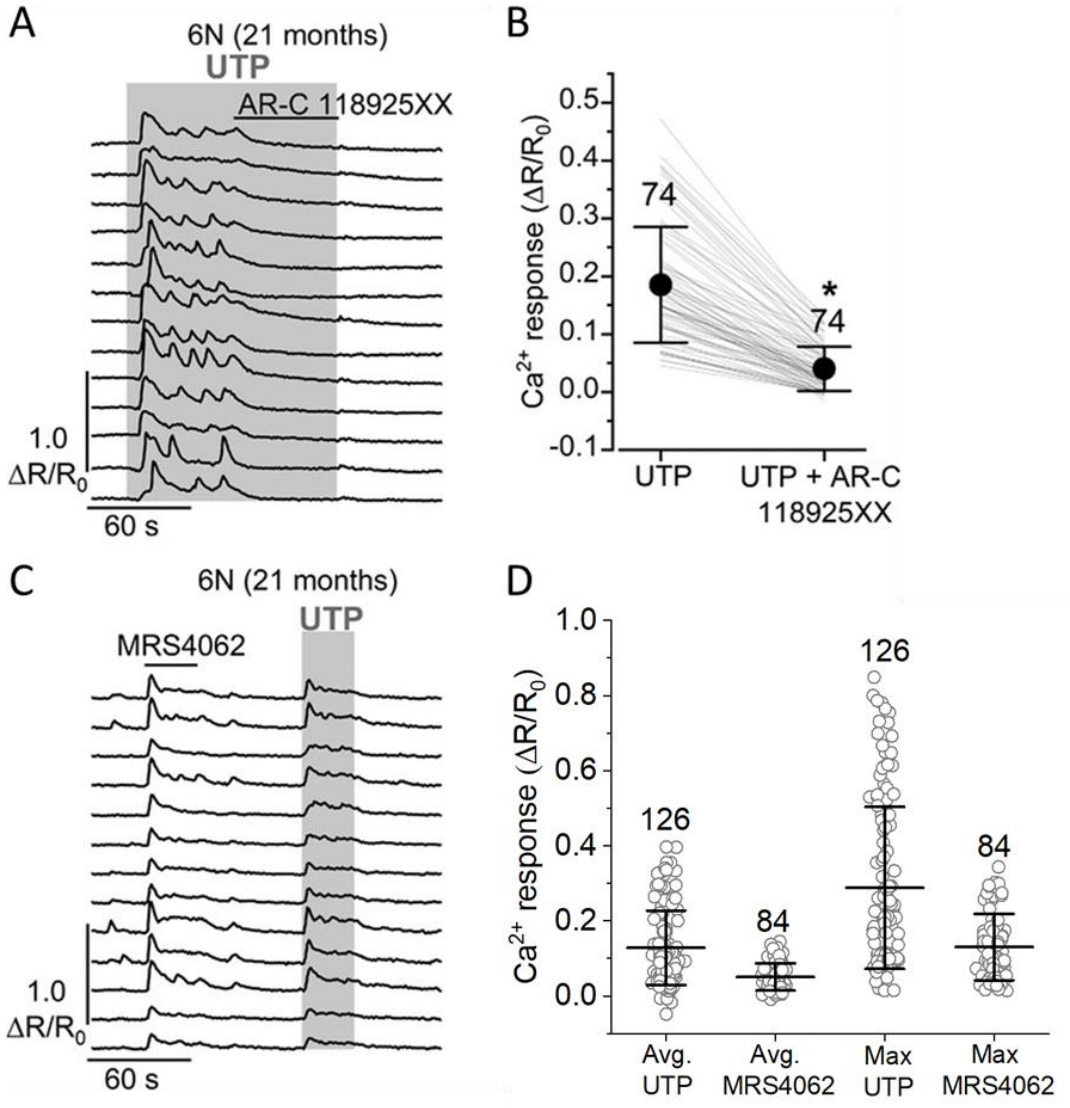

Figure 3.9: Pharmacology of UTP-induced Ca^{2+} responses in supporting cells

A: Representative Ca^{2+} responses in supporting cells induced by the extracellular application of 300 nM UTP (grey area) in aged 6N mice. The application of UTP together with the $P2Y_2$ antagonist ARC-118925XX (15 µM, top black horizontal line) caused a reduction of the UTP-induced Ca^{2+} response and stopped Ca^{2+} oscillations. **B**: Average UTP-induced Ca^{2+} responses during the last 10 s of UTP application and when UTP was applied together with the $P2Y_2$ antagonist ARC-118925XX in cochlear supporting cells from aged mice (74 ROIs from 4 mice). Significance values are indicated by the asterisks ($P < 0.0001$, Wilcoxon signed-rank test). **C**: Representative Ca^{2+} responses in supporting cells induced by the $P2Y_4$ agonist MRS4062 (10 µM, top black horizontal line) in aged 6N mice. This initial response was followed by the application of 300 nM UTP alone (grey area), to confirm that the supporting cell was responsive to UTP. **D**: Average and maximum MRS4062-induced Ca^{2+} response in comparison to the average and maximum UTP-induced Ca^{2+} response in cochlear supporting cells from aged mice. Open symbols are measurements from individual supporting cells (ROIs): 126 or 84 cells from 3 mice. Whole figure and legend taken ad modified from (Hool *et al.*, 2023).

3.3 Discussion

It is well established that purinergic P2Y receptors are expressed by the Kölliker's organ cells in the immature cochlea (Huang *et al.*, 2010; Babola *et al.*, 2020). The activation of these receptors has been shown to induce rises in intracellular Ca^{2+} levels which can propagate across the Kölliker's organ as Ca^{2+} waves (Piazza *et al.*, 2007; Ceriani, Pozzan and Mammano, 2016). This mechanism is believed to be crucial for the correct development of the organ of Corti, as spontaneous intercellular Ca^{2+} transients modulate the immature hair cell spiking which drives both synaptic maturation (Johnson *et al.*, 2017) and refinement of central auditory pathways (Babola *et al.*, 2018; Babola *et al.*, 2020). Even though it is clear P2Y receptors play an important role during development, very little is known about their role in the adult organ of Corti. Moreover, no research has investigated whether P2Y purinergic receptor function is altered in the aged cochlea. Seeing as the pathology behind age-related conditions such as Alzheimer's disease and Parkinson's disease have reported associations with changes in P2Y receptor functioning (Erb *et al.*, 2015), investigating the progressive changes in P2Y receptors of the ageing cochlea might reveal information regarding ARHL pathophysiology. Therefore, this chapter discusses data collected regarding the expression and function of P2Y receptors in the ageing cochlea.

3.3.1 P2Y receptors in the pre-hearing Kölliker's organ

The immunolabelling images show that $P2Y_1$, $P2Y_2$ and $P2Y_4$ receptors are all expressed across the Kölliker's organ cells of both 6N and C3H neonatal organs of Corti. These results are supported by the ratiometric Ca^{2+} imaging recordings. Kölliker's organ cells from P7 organs of Corti displayed intracellular Ca^{2+} transients both spontaneously and in response to ATP (general P2 receptor agonist), UTP ($P2Y_2$ and $P2Y_4$ receptor agonist) and ADP ($P2Y_1$ receptor agonist). The Ca^{2+} transients were confirmed to be a result of P2Y-mediated Ca^{2+} release from the endoplasmic reticulum as they were abolished by the SERCA ATPase pump blocker thapsigargin.

Even though the immunolabelling and Ca^{2+} imaging experiments in the neonatal cochlea suggest P2Y receptors are responsible for driving intracellular Ca^{2+} transients, it remains

unclear how each of the individual P2Y receptor subtypes contribute to the observed ATP-induced Ca^{2+} responses. The non-specific P2 agonist ATP should activate $P2Y_1$, $P2Y_2$ and $P2Y_4$ receptors, and so it is likely they all contribute to the observed Ca^{2+} responses. It would have been beneficial to perform an additional experiment to see how blocking each P2Y receptor subtype individually would affect the size and dynamics of the ATP-induced Ca^{2+} responses. For example, the $P2Y_1$ receptor antagonist was only applied alongside ADP ($P2Y_1$ receptor agonist) and so the entire Ca^{2+} response was abolished because it was generated by ADP activating $P2Y_1$ receptors alone. However, applying the $P2Y_1$ receptor antagonist alongside ATP should leave $P2Y_2$ and $P2Y_4$ receptors unaffected and able to produce Ca^{2+} responses. This would allow us to infer how much of the ATP-induced Ca^{2+} response is produced by $P2Y_1$ receptor activation.

The $P2Y_2$ antagonist was applied alongside UTP ($P2Y_2$ and $P2Y_4$ receptor agonist) and so should have not affected the activation of $P2Y_4$ receptors. However, we observed a complete loss of Ca^{2+} response to UTP when AR-C 118925XX was applied. This raises concerns about the specificity of the antagonist as it would be expected that the $P2Y_4$ receptors would still respond to UTP. This uncertainty regarding the true pharmacology of P2Y receptors could also explain the discrepancies within the literature around which P2Y receptor subtype is driving the immature spontaneous Ca^{2+} transients in the cochlea. For example, UTP (agonist for $P2Y_2$ and $P2Y_4$, but not for $P2Y_1$) was reported to trigger large Ca^{2+} oscillations across the Kölliker's cells of the rat cochlea (Piazza *et al.*, 2007). In addition to this, a significantly larger Ca^{2+} response was observed in the Kölliker's cells following ATP administration compared to ADP administration. ATP is known to be the principal agonist for $P2Y_2$ and $P2Y_4$ receptors, whereas $P2Y_1$ receptors have a weak response to ATP and respond most strongly to ADP (von Kügelgen and Hoffmann, 2016). Therefore, this suggests $P2Y_2$ and $P2Y_4$ receptors are responsible for the ATP-induced Ca^{2+} transients observed within Kölliker's organ before hearing onset. However, it has also been hypothesised that $P2Y_1$ is the main receptor responsible for the spontaneous purinergic-induced Ca^{2+} signals in supporting cells of the immature cochlea (Babola *et al.*, 2020). It was reported that all spontaneous activity is absent when the $P2Y_1$ receptor activity is blocked via an antagonist, even though Huang et al., 2010 show no $P2Y_1$ expression in Kölliker's organ.

One possible explanation for this discrepancy could be the formation of hetero-oligomers containing numerous different subtypes of P2Y receptor. These complexes are known to form readily at the cell membrane and have shown to alter the typical pharmacology expected from complexes containing one subtype of P2Y receptor (Ecke *et al.*, 2008). For example, $P2Y_1$ receptors were found to associate with $P2Y_2$ and $P2Y_4$ receptors in granulocytes, and these hetero-oligomers responded to both ADP and UTP (Ribeiro-Filho *et al.*, 2016). It is well established that $P2Y_1$ receptors respond to ADP but not to UTP, and $P2Y_2$ and $P2Y_4$ respond to UTP but not ADP (von Kügelgen and Hoffmann, 2016). Therefore, it would be beneficial to investigate whether the $P2Y_1$, $P2Y_2$ and $P2Y_4$ receptors in the cochlea also co-localise as hetero-oligomers and exhibit alterations in their typical pharmacology.

3.3.2 P2Y receptors in the adult inner sulcus

The immunolabelling data suggest that the expression of all three P2Y receptor subtypes are lost from the 1-month-old adult inner sulcus cells in both the 6N and C3H mice. This is again supported by the ratiometric Ca^{2+} imaging data. The application of ATP and UTP induced minimal changes in intracellular Ca^{2+} concentration across the cells of the adult inner sulcus, suggesting the absence of P2Y receptors. However, the application of ADP to the 1-month-old inner sulcus did induce elevations of intracellular Ca^{2+} which were abolished by the $P2Y_1$ receptor antagonist MRS2500. This suggests the presence of $P2Y_1$ purinergic receptors and contradicts the immunolabelling images. Therefore, it is unclear from the data collected here whether $P2Y_1$ receptors are maintained in the adult inner sulcus.

It would be beneficial to validate the $P2Y_1$ receptor antibody using a $P2Y_1$ knock-out mouse to be sure that the labelling is reliable. It is possible that the antibody specificity is poor and is not detecting expression at older ages or has shown non-specific labelling at P7. However, if the immunolabelling is validated, it could mean that there are other P2Y purinergic receptors present contributing to the ADP-induced Ca^{2+} responses in the adult cochlea. As discussed in the previous section, the specificity of the P2Y antagonists is questionable because AR-C 118925XX ($P2Y_2$ antagonist) appeared to block the activity of both $P2Y_2$ and $P2Y_4$ receptors. Therefore, there is the possibility that the $P2Y_1$ antagonist MRS2500 might also be blocking the activity of other P2Y receptors. ADP is also known to activate $P2Y_{12}$

receptors and so potentially these could become upregulated in the adult inner sulcus and contribute to the ADP-induced Ca^{2+} responses. This could also explain the lack of $P2Y_1$ receptors in the immunolabelling images from the adult inner sulcus.

However, it would be expected that if another purinergic receptor was upregulated in the adult inner sulcus (such as $P2Y_{12}$) that it would also respond to ATP. This might not be the case for $P2Y_{12}$ as ATP is only known to be a weak partial agonist for this receptor, so potentially, the 300nM ATP was not enough to trigger much of a Ca^{2+} response. Therefore, it is possible that any $P2Y_1$ or $P2Y_{12}$ receptors expressed in the adult inner sulcus might have not been detected by the immunolabelling, and might only be able to induce Ca^{2+} responses following ADP application due to agonist selectivity.

Other studies in the literature also gives contradictory data on whether P2Y receptors are expressed in the adult inner sulcus. Both the expression of P2Y receptors and ATP/UTP-inducible Ca^{2+} oscillations were reported to be absent in the inner sulcus cells following hearing onset (Huang *et al.*, 2010; Tritsch and Bergles, 2010; Chan and Rouse, 2016). However, it has also been reported that P2Y receptors are maintained in the adult inner sulcus, as Ca^{2+} oscillations were observed in response to ATP and UTP application (Sirko, Gale and Ashmore, 2019). Overall, there is still uncertainty about whether P2Y receptors are maintained in the adult inner sulcus. The complexity of their unique pharmacological profiles, along with the formation of P2Y receptor heterodimers which will further complicate their pharmacology, means further experiments will be needed to better understand this topic.

3.3.3 P2Y receptors in the aged inner sulcus

We report an upregulation of $P2Y_2$ and $P2Y_4$ receptor expression in the aged inner sulcus cells, when compared to the adult. Furthermore, we observed an upregulation of ATP and UTP-induced Ca^{2+} oscillations in these aged inner sulcus cells. As mentioned previously, UTP is the primary agonist for $P2Y_2$ and $P2Y_4$ receptors, indicating their possible involvement in the Ca^{2+} responses. Furthermore, the application of AR-C 118925XX ($P2Y_2$ antagonist) abolished ATP- and UTP-induced Ca^{2+} responses in the aged inner sulcus cells, indicating $P2Y_2$ receptors participate in this response. Also, the application of MRS4062 ($P2Y_4$ agonist) triggered similar

intracellular Ca^{2+} responses to those seen following ATP and UTP application, suggesting $P2Y_4$ receptors are also involved. Conversely, there was no upregulation of $P2Y_1$ receptor expression, or ADP-induced Ca^{2+} responses, in the aged inner sulcus. This data together indicates that the aged inner sulcus cells only appear to upregulate $P2Y_2$ and $P2Y_4$ receptor expression and function.

These age-related changes in P2Y receptors were investigated in both 6N and C3H strains. Interestingly, both the age-related upregulation in $P2Y_2$ and $P2Y_4$ receptor expression, and the increase in ATP and UTP-induced Ca^{2+} oscillations, were more pronounced in the 6N and 6N-repaired mice than the C3H mice. In other words, it appears that the senescence-related increase in P2Y receptors in the inner sulcus is associated with mouse strains exhibiting a more severe low-frequency hearing loss (6N and 6N-repaired strains) rather than the C3H strain. Similar patterns have also been observed in ageing hair cells and their innervations. For example, hallmarks of ageing hair cells, including changes in innervation and cell size, have also been reported to be more pronounced in 6N than C3H mice (Jeng *et al.*, 2020a; Jeng *et al.*, 2021). Therefore, it is likely that the inner sulcus cells also undergo senescence-related changes which affect their functioning, and the level of this might be associated with the progression of hearing loss. However, these differences in P2Y receptor upregulation with ARHL severity could also be due to strain-related differences, so further research is required to confirm a link between P2Y receptors and ARHL.

It is unclear why aged inner sulcus cells might upregulate $P2Y_2$ and $P2Y_4$ receptors in association with hearing loss progression. However, these receptors do not appear to be present in adult mice (1-month-old), suggesting that their upregulation is likely not associated with typical cochlear function. One possible explanation for their upregulation in the aged cochlea might involve the increase in cochlear damage signalling pathways due to senescence-related trauma. It has been reported in the immature cochlea that hair cells release ATP following insult, and this activates $P2Y_2$ and $P2Y_4$ receptors on surrounding supporting cells (Hensen's and Claudius' cells) producing intracellular Ca^{2+} waves (Gale *et al.*, 2004). This Ca^{2+} signalling pathway has been found to activate ERK1/2 and encourage hair cell death in response to cochlear insult (Lahne and Gale, 2008). It is unknown whether this damage response signalling pathway is present in the non-senescent, adult inner sulcus. Nevertheless, the accumulation of damage known to occur during ageing of the auditory

system may drive an upregulation of P2Y receptor expression in the inner sulcus to assist in the propagation of insult-associated Ca^{2+} signalling. Both pathological changes in hair cell characteristics, and age-related hearing loss, have been reported to occur in 6N mice from as early as 6 months of age (Jeng *et al.*, 2020a; Jeng *et al.*, 2021). Since age-related cochlear changes are well-established by 12 months of age, and this is a time when P2Y receptors are upregulated, this suggests a possible role for P2Y receptors in assisting the management of senescence-induced cochlear functional changes.

A further explanation for the upregulation of P2Y receptor function in the aged cochlea could be linked to an attempt to mimic development and limit senescence-related damage. Both the P2Y receptor expression and associated Ca^{2+} responses observed in the aged inner sulcus closely resemble those seen in the pre-hearing Kölliker's organ (Tritsch *et al.*, 2007; Johnson *et al.*, 2017). These events are completely absent in the inner sulcus of the adult cochlea. Another instance of this has been reported in the senescent hair cells which display efferent re-innervation (Jeng *et al.*, 2021; Lauer *et al.*, 2012). It is well established that the inner hair cells only retain innervation from efferent fibres up until just before the onset of hearing (Simmons *et al.*, 2011). However, senescent hair cells were reported to become re-innervated by these fibres in a manner very similar to the neonatal hair cell innervation phenotype (Lauer *et al.*, 2012). It is unknown as to why the ageing cochlea might revert back to express more developmental characteristics, as no benefit to this process is yet to be detected. Nevertheless, it would be beneficial to better understand whether this recapitulation is a coincidence unrelated to the ageing of the cochlea, or whether it is some kind of attempt to mimic development and limit senescence-related damage.

3.3.4 Summary

Overall, this chapter has investigated the progressive changes in P2Y receptor expression and function in the supporting cells of the ageing inner sulcus of the cochlea. The data collected on neonatal and adult cochleae further support previous findings. For example, the expression of P2Y receptors and associated intracellular Ca^{2+} responses in the pre-hearing Kölliker's organ appear to be, for the most part, lost in the inner sulcus after hearing onset. Furthermore, we show new data regarding the upregulation of $P2Y_2$ and $P2Y_4$ receptor

expression and function in the senescent inner sulcus. The reason behind this remains unclear, however, we hypothesise it is linked to the progression of ARHL as the degree of P2Y receptor upregulation was more pronounced in mice known to exhibit severe ARHL.

Chapter 4. Age-related changes in gap junction channels of mouse cochlear supporting cells

4.1 Introduction

Gap junction membrane channels allow intercellular diffusion of ions and small molecules between neighbouring cells (Bennett and Goodenough, 1978). They occur when two connexon complexes on adjacent cells align their membrane pores and create a continuous passageway between the two intracellular spaces. Connexons contain six connexin proteins at the cell membrane which assemble as a hexametric ring with a pore in the centre between the cytosol and extracellular space (Bruzzone, White and Paul, 1996; Beyer, Paul and Goodenough, 1990). Connexons can form either homomeric or heteromeric complexes consisting of one or numerous different connexin proteins respectively (Kumar and Gilula, 1996). The different combination of connexin proteins within a connexon have been shown to influence how they function, e.g. their pore size and selectivity (Veenstra, 1996). Typically, multiple gap junction channels (GJCs) congregate together at the cell membrane in groups forming GJC plaques (Lopez *et al.*, 2001). These GJC plaques can contain thousands of individual gap junction channels and span several micrometres wide (Lauf *et al.*, 2002).

In the organ of Corti, the majority of the supporting cells express GJC plaques composed of connexin 26 (Cx26) and connexin 30 (Cx30) (Kikuchi *et al.*, 1995; Zhao *et al.*, 2006). This widespread expression of GJCs forms a transport network across the epithelium. Molecules such as IP_3, ATP, Ca^{2+}, K^+ and glucose use this network to travel between cells across the organ of Corti (Hernandez *et al.*, 2007; Kikuchi *et al.*, 2000; Chang *et al.*, 2008). The diversity in molecules proposed to use this transport network implies it is involved in multiple different aspects of cochlear function and signalling. For example, the GJC network has been shown to be involved in ionic homeostasis within the organ of Corti to maintain the driving force for hair cell depolarisation (Santos-Sacchi and Dallos, 1983; Wangemann, 2006). Additionally, intercellular signalling cascades also use the GJC network to spread downstream signalling molecules from cell to cell. One example of this is the purinergic receptor signalling cascade which propagates intracellular Ca^{2+} waves across the inner sulcus cells during development, which has been shown to be crucial for the generation of coordinated inner hair cell firing, synaptic maturation and sensory domain refinement in the auditory pathway (Tritsch *et al.*, 2007; Babola *et al.*, 2021). The array of important processes involved in cochlear functioning which utilise the GJC network can explain why mutations affecting Cx26 or Cx30 are the most

common causes of non-syndromic hearing loss (del Castillo and del Castillo, 2017; Chan and Chang, 2014; Chen *et al.*, 2022).

Even though connexin-related mutations are well researched as a cause for inherited hearing loss (Jagger and Forge, 2015; Wingard and Zhao, 2015), less is known regarding whether changes in the gap junction network could also contribute to age-related hearing loss. Tajima et al. 2020 showed that the cochlear GJC plaques of 32-week-old C57BL/6J mice were significantly shorter, and displayed a more fragmented organisation, when compared with 4-week-old C57BL/6J cochlear GJC plaques (Tajima *et al.*, 2020). However, it is not known whether this affected the GJC's ability to function, and so the consequences of these structural changes remain unknown. Although, it was reported that there was minimal hair cell damage and hearing loss at 32 weeks (when GJC plaque structure was altered), but by 36 weeks, the mice had developed severe hearing loss. This data led the authors to hypothesise that the fragmentation of the GJC plaques negatively influenced their functional efficiency. A reduction in transportation of molecules necessary to support hair cell function may have been implicated in the development of the hearing loss. In support of this, reductions in GJC plaque size in other tissues such as the heart are already known to negatively impact intercellular communication and have been linked to disease (Luke and Saffitz, 1991; Kaprielian *et al.*, 1998). However, it is necessary to examine this in more detail as it is not known how these changes impact GJC permeability in the cochlea. In addition to this, looking at mice older than 32-weeks would determine whether this GJ plaque fragmentation continues to worsen and whether it is part of the progressive pathological changes in the auditory organ.

This chapter will focus on investigating age-related changes in the gap junction channels within the supporting cells of the organ of Corti. Specifically, the expression and structural organisation of GJC plaques will be compared between young adult and aged mice. Furthermore, the permeability of GJCs will also be compared across these age groups via Lucifer yellow fluorescence imaging. It is anticipated that any age-related changes in the structure or function of the gap junction channel network could influence cochlear function, and potentially, the development of age-related hearing loss.

4.2 Results

4.2.1 Progressive changes in gap junction plaque organisation and expression

Organs of Corti from young adult (1-month-old), adult (12-months-old) and aged (17-22-months-old) mice were immunolabelled with antibodies against Cx26 and Cx30, which are the two major components of cochlear gap junction plaques (Kikuchi *et al.*, 1995; Zhao *et al.*, 2006). This allowed for the investigation of age-related changes in gap junction plaque expression and structural organisation in the supporting cells of the organ of Corti. Additionally, mice of C57BL/6N (6N) background were compared with C3H/HeJ mice (C3H) to determine whether any progressive changes in gap junction plaque expression were associated with mouse strains showing signs of early onset, or late onset ARHL, respectively.

4.2.1.1 Gap junction plaque location in the ageing organ of Corti

In the 1-month-old 6N organ of Corti, gap junction channel plaques were found to be expressed on the majority of non-sensory supporting cells, and absent in hair cells (Figure 4.1). Furthermore, most plaques appear to contain a combination of both Cx26 and Cx30, with only the Deiters' cell plaques containing predominantly Cx30. These observations align with what has already been reported and show similar characteristics for gap junction expression in the adult mouse organ of Corti (Jagger and Forge, 2015; Forge *et al.*, 2003).

12-month-old and 17-22-month-old mouse organs of Corti were also immunolabelled for Cx26 and Cx30. There appears to be no age-related differences in the location of gap junction plaques between the 1-month-old, 12-month-old and 17-22-month-old cochleae in both 6N mice (Figure 4.2) and C3H mice (Figure 4.3). As observed in the 1-month-old organ of Corti, Cx26 and Cx30 are co-expressed within gap junction plaques across the majority of non-sensory supporting cells in the older age groups investigated. Additionally, the expression of Cx30 alone is maintained in the Deiters' cells in all age groups.

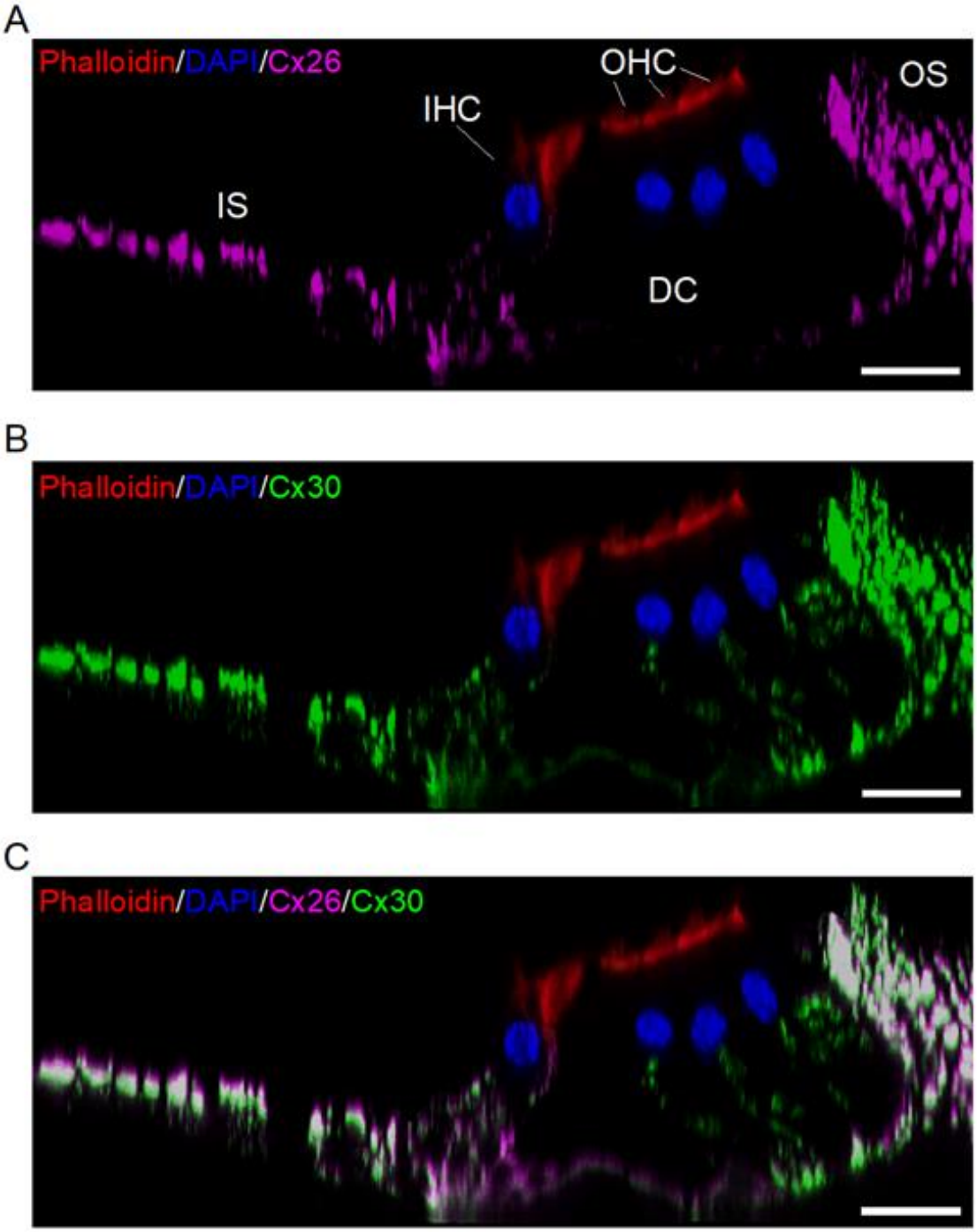

Figure 4.1: Connexin 26 and connexin 30 expression in the organ of Corti of 1-month-old 6N mice

Lateral projections of immunolabelled murine organs of Corti from 1-month-old 6N mice. The stereocilia and nuclei of the hair cells were labelled using phalloidin to stain F-actin (red) and DAPI (blue) respectively. Nuclei of supporting cells were removed to better show labelling of gap junction plaques. **A:** Connexin 26 labelling (Cx26, magenta) was observed in the inner sulcus (IS) and outer sulcus cells (OS). **B:** Connexin 30 labelling (Cx30, green) was observed in the inner sulcus, outer sulcus and Deiters' cells (DC). **C:** Merge of A and B. Scale bars: 20 µm.

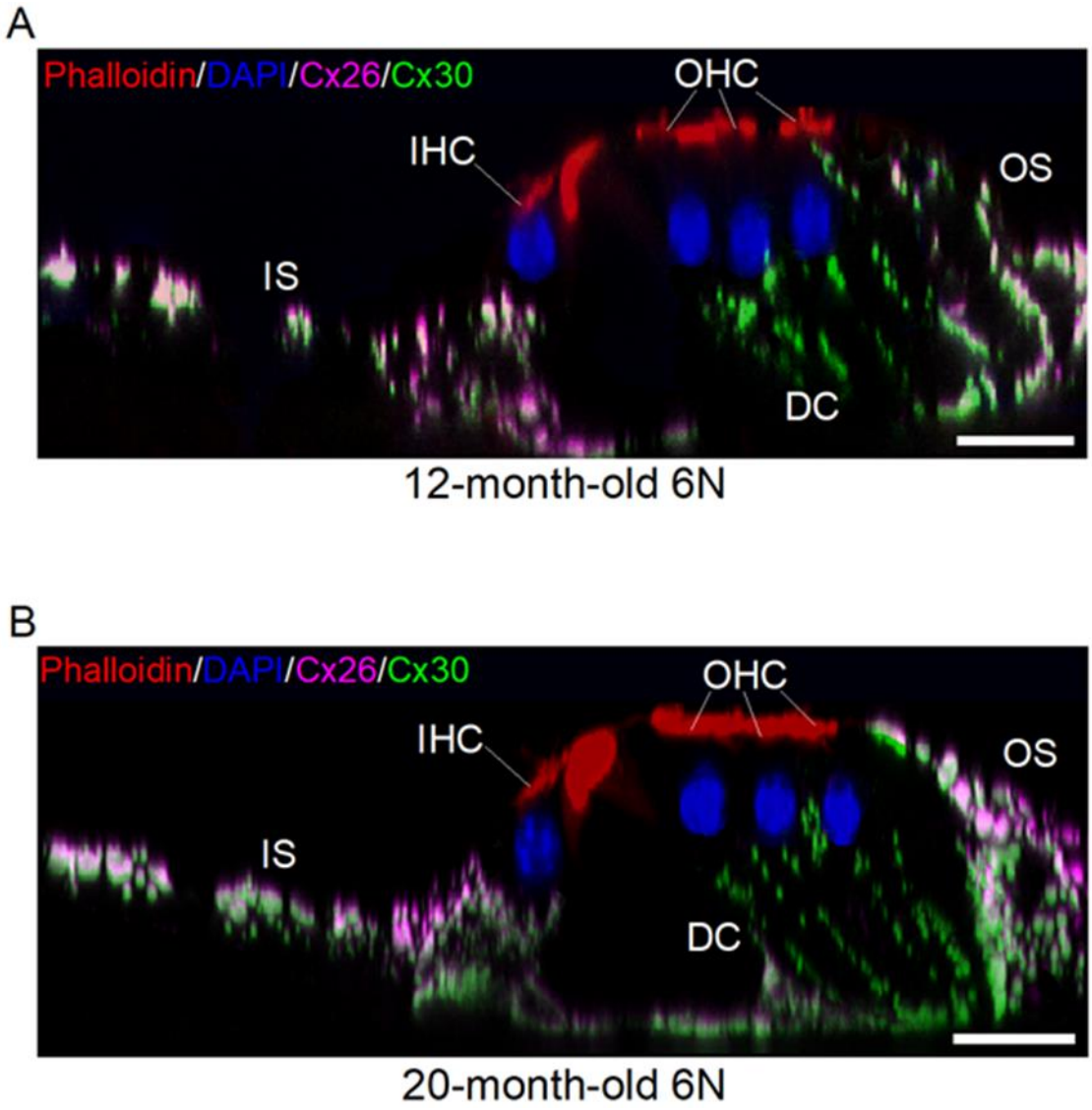

Figure 4.2: Connexin 26 and connexin 30 expression in the organ of Corti of 12-month-old and 20-month-old 6N mice

Lateral projections of immunolabelled murine organs of Corti from 12-month-old (**A**) and 20-month-old 6N mice (**B**). The labelling of Cx26 (magenta) and Cx30 (green) show gap junction plaques expressed in the supporting cells. The inner sulcus cells (IS) and outer sulcus cells (OS) show expression of gap junction plaques containing both Cx26 and Cx30. The Deiters' cells express gap junction plaques containing Cx30 only. Phalloidin (staining F-actin, red) labels the hair cell stereocilia bundles and DAPI (blue) labels the hair cell nuclei. Nuclei of supporting cells were removed to better show labelling of gap junction plaques. Scale bars: 20 µm.

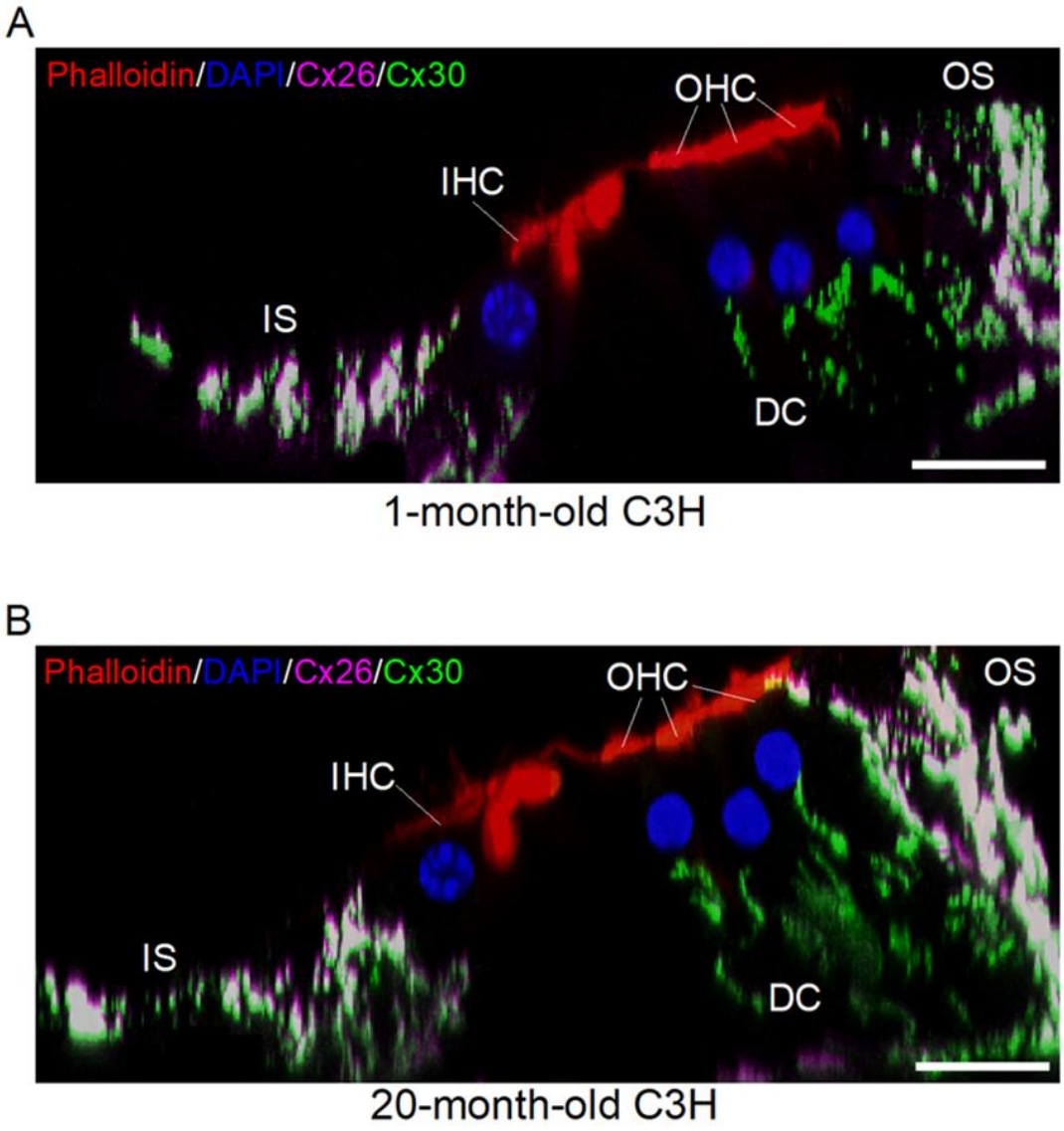

Figure 4.3: Connexin 26 and connexin 30 expression in the organ of Corti of 1-month-old and 20-month-old C3H mice

Lateral projections of immunolabelled murine organs of Corti from 1-month-old (**A**) and 20-month-old C3H mice (**B**). The labelling of Cx26 (magenta) and Cx30 (green) show gap junction plaques expressed in the supporting cells. The inner sulcus cells (IS) and outer sulcus cells (OS) show expression of gap junction plaques containing both Cx26 and Cx30. The Deiters' cells express gap junction plaques containing Cx30 only. Phalloidin (staining F-actin, red) labels the hair cell stereocilia bundles and DAPI (blue) labels the hair cell nuclei. Nuclei of supporting cells were removed to better show labelling of gap junction plaques. Scale bars: 20 µm.

4.2.1.2 Gap junction plaque organisation in the ageing organ of Corti

When studying plaque organisation, it was decided to focus on the cells of the inner sulcus as they form a single cell layer and so each cell-cell connection would be easier to visualise. The supporting cells directly adjacent to the IHCs were not included in any analysis as their cell borders are more difficult to define as some stack on top of each other (Figure 4.4, 4.5, 4.6).

Inner sulcus cells within 1-month-old 6N organs of Corti showed Cx26 and Cx30 co-expression in large plaques around the cell border (Figure 4.4). The plaques appear to typically organise into a hexagon/pentagon shape around each cell, with ~1-3 large plaques located at each cell-cell junction (Figure 4.4D). These observations align with what is already published regarding the organisation of typical gap junction plaques in the healthy adult inner sulcus. Previous immunolabelling and freeze-fracture imaging experiments have also described gap junction plaque structure between inner sulcus cells as having 'long profiles' and covering large portions of the membrane connecting the two cells (Forge *et al.*, 2003; Kamiya *et al.*, 2014).

The 12-month-old and 17-22 month-old inner sulcus cells similarly showed co-expression of Cx26 and Cx30 in their gap junction plaques (Figure 4.5, Figure 4.6). However, in comparison to the 1-month-old gap junction plaques, the organisation and size of the plaques in the 12-month-old and 17-22-month-old inner sulcus cells appeared different. There seemed to be a higher quantity of plaques per cell in the inner sulcus cells from the older age groups, and these plaques looked to be much smaller in size (Figure 4.5D, Figure 4.6D). This change appeared to occur similarly in both 6N and C3H mouse strains (Figure 4.7).

Additionally, a progressive increase in cell size in the 12-month-old and 17-22 month-old inner sulcus cells was also observed. The aged cells appeared to have expanded to cover a larger area in comparison to the young adult. This age-specific change in cell morphology has not been reported before, but it must be considered in this chapter as it could influence the organisation of the gap junction plaques.

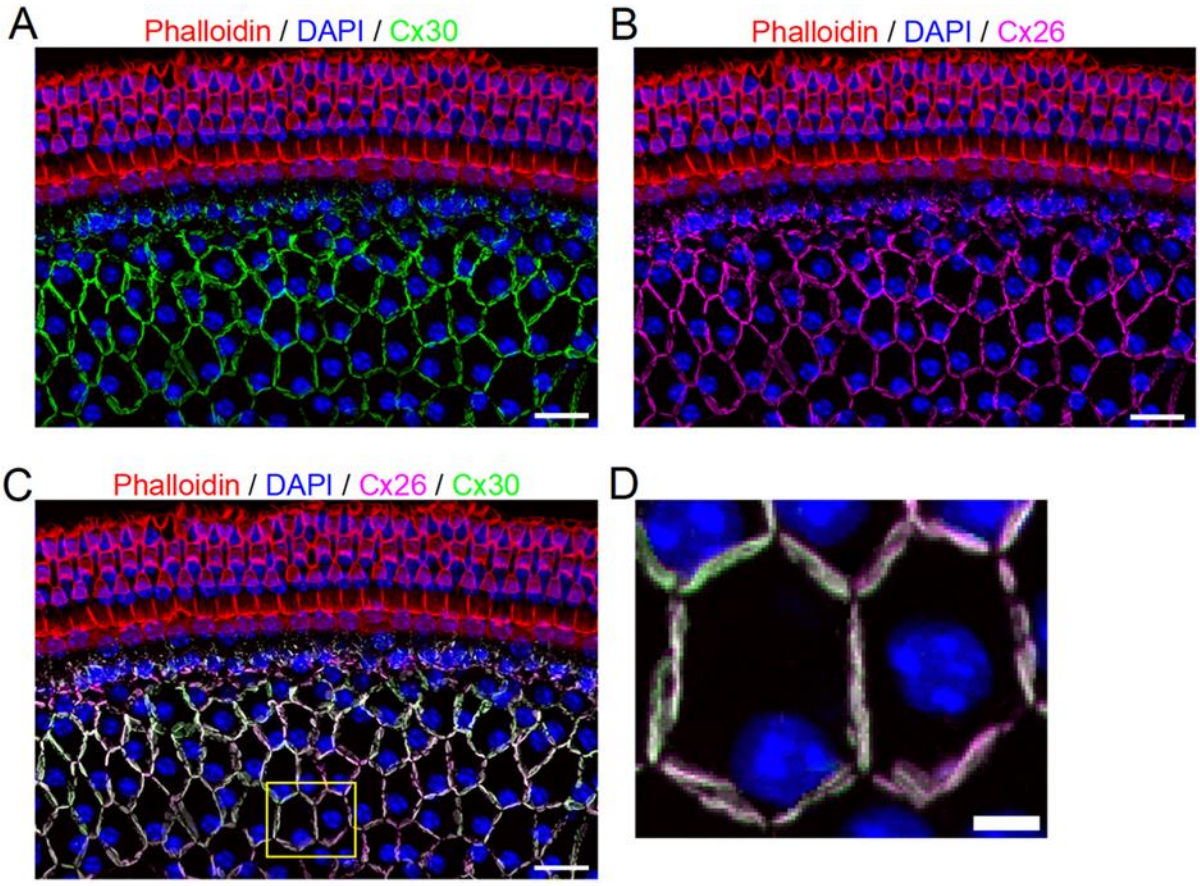

Figure 4.4: Gap junction plaque organisation in the 1-month-old 6N inner sulcus

A, **B**, **C**: Maximum intensity projections of confocal *z*-stacks from images of a 1-month-old 6N mouse organ of Corti. Immunolabelling for Cx30 (green) and Cx26 (magenta) is shown alongside phalloidin staining of F-actin (red) to show the hair cells and DAPI staining (blue) to show the nuclei. The inner sulcus cell borders co-express Cx26 (magenta) and Cx30 (green) within their gap junction plaques. Scale bars: 20 µm. **D**: Magnified image of the yellow box highlighted in **C** showing the organisation of gap junction plaques into pentagon/hexagon formation around the border of each cell. Scale bar: 5 µm.

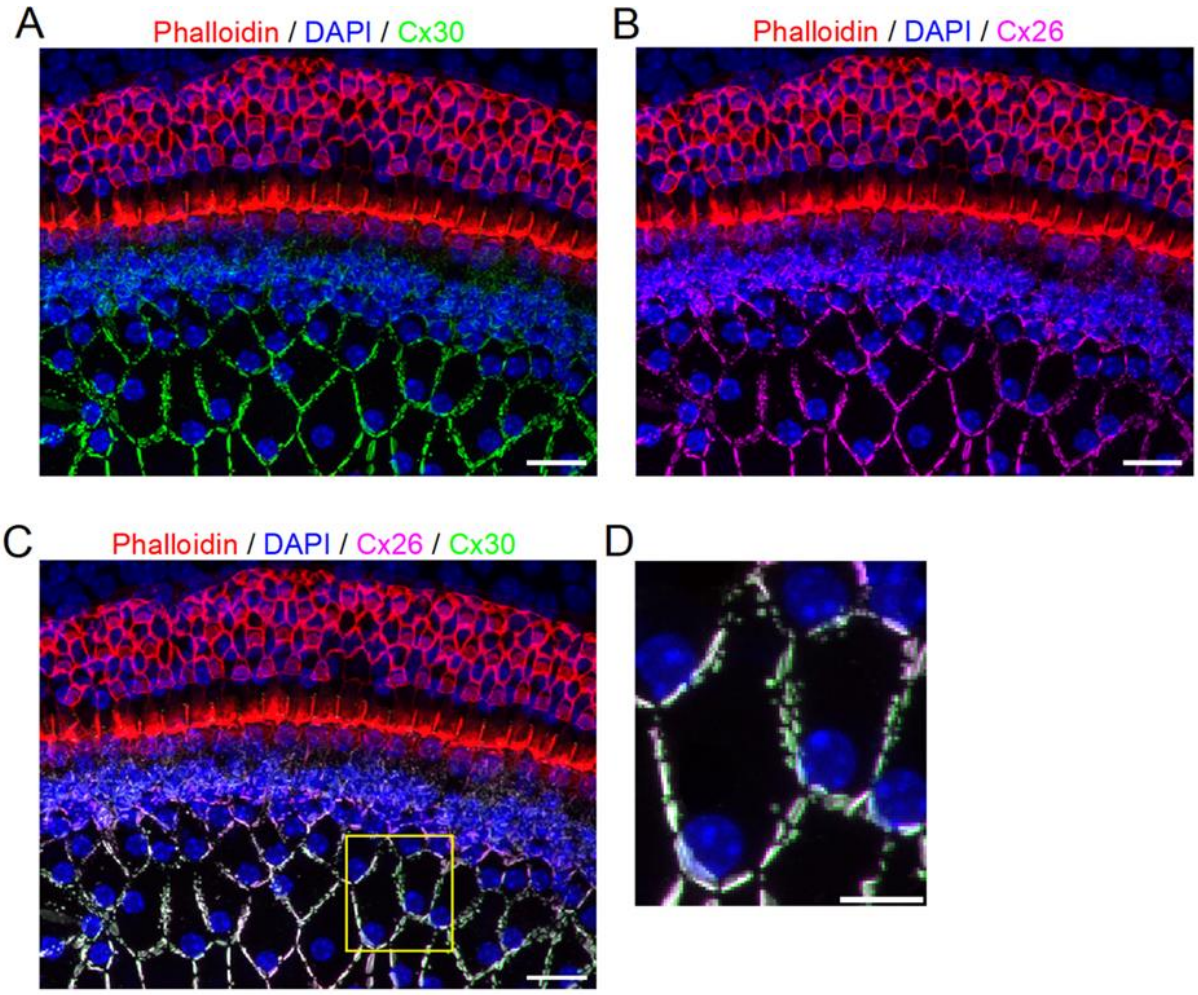

Figure 4.5: Gap junction plaque organisation in 12-month-old 6N inner sulcus

A, **B**, **C**: Maximum intensity projections of confocal *z*-stacks from images of a 12-month-old 6N mouse organ of Corti. Immunolabelling for Cx30 (green) and Cx26 (magenta) is shown alongside phalloidin staining of F-actin (red) to show the hair cells and DAPI staining (blue) to show the nuclei. The inner sulcus cell borders co-express Cx26 (magenta) and Cx30 (green) within their gap junction plaques. Scale bars: 20 µm. **D**: Magnified image of the yellow box highlighted in **C** showing the organisation of gap junction plaques into pentagon/hexagon formation around the border of each cell. Scale bar: 10 µm.

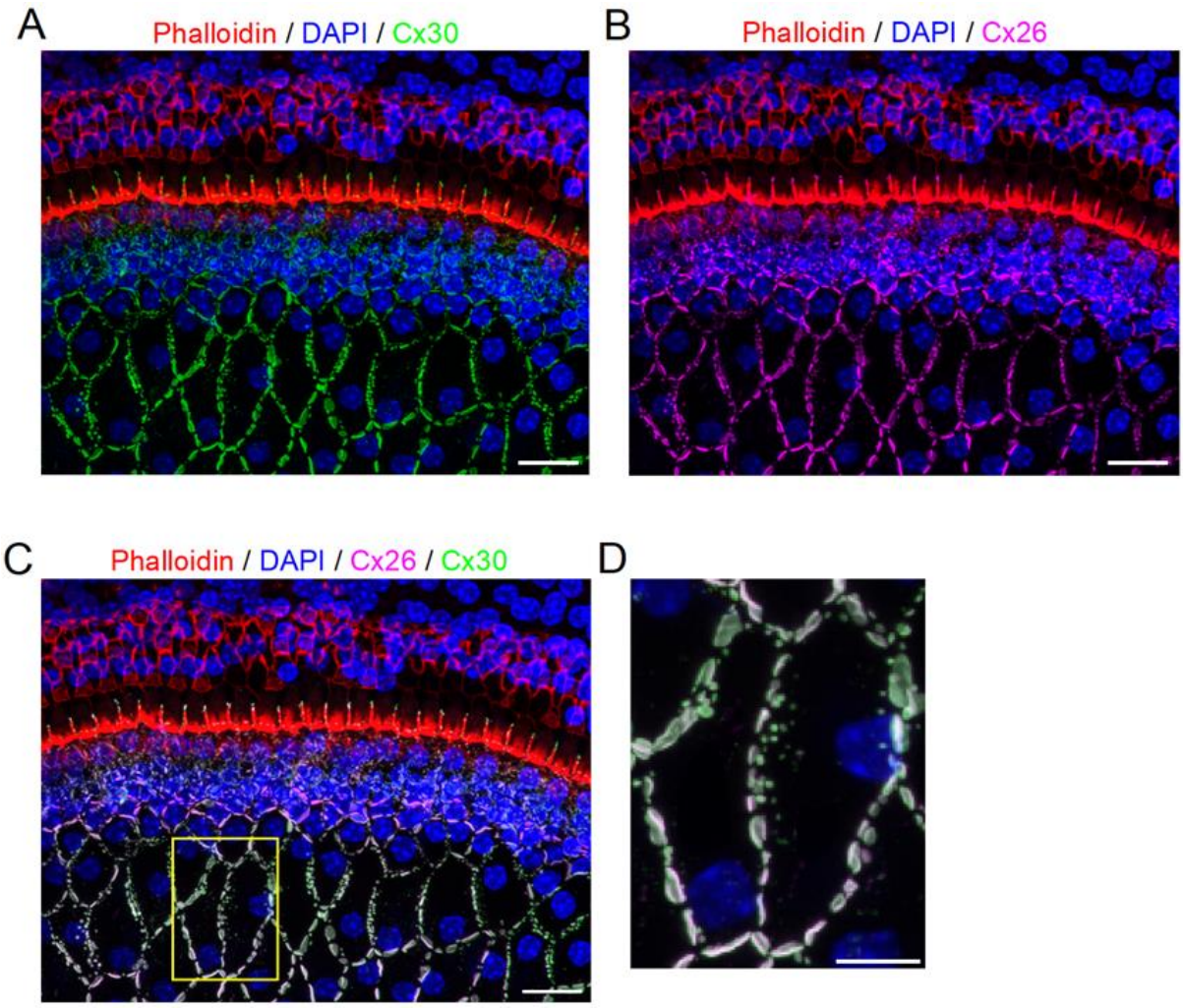

Figure 4.6: Gap junction plaque organisation in 20-month-old 6N inner sulcus

A, **B**, **C**: Maximum intensity projections of confocal *z*-stacks from images of a 20-month-old 6N mouse organ of Corti. Immunolabelling for Cx30 (green) and Cx26 (magenta) is shown alongside phalloidin staining of F-actin (red) to show the hair cells and DAPI staining (blue) to show the nuclei. The inner sulcus cell borders co-express Cx26 (magenta) and Cx30 (green) within their gap junction plaques. Scale bars: 20 µm. **D**: Magnified image of the yellow box highlighted in **C** showing the organisation of gap junction plaques into pentagon/hexagon formation around the border of each cell. Scale bar: 10 µm.

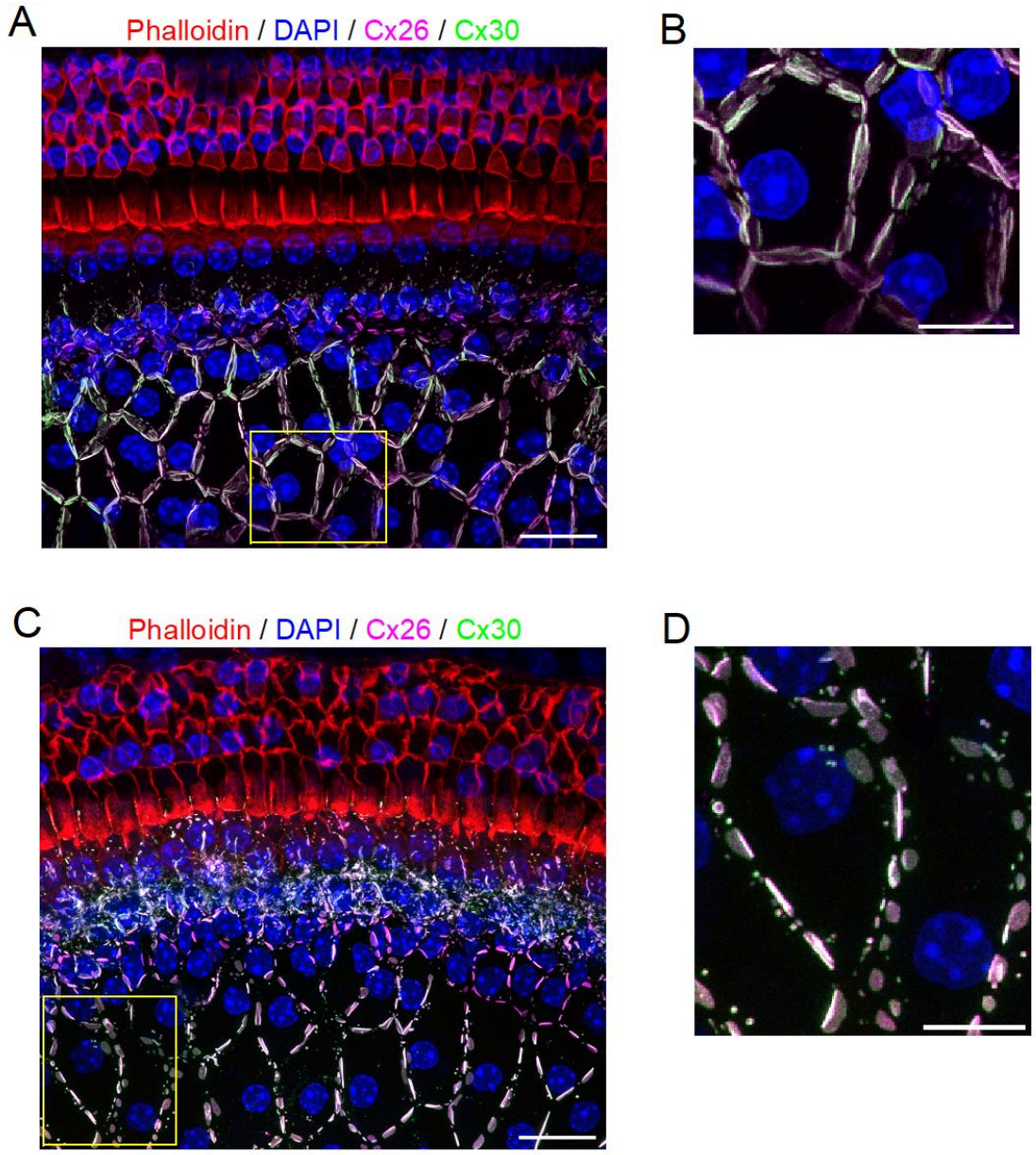

Figure 4.7: Gap junction plaque organisation in the 1-month-old and 20-month-old C3H inner sulcus

A, **C**: Maximum intensity projections of confocal *z*-stacks from images of a 1-month-old (**A**) and a 20-month-old (**C**) C3H mouse organs of Corti. Immunolabelling for Cx30 (green) and Cx26 (magenta) is shown alongside phalloidin staining of F-actin (red) to show the hair cells and DAPI staining (blue) to show the nuclei. The inner sulcus cell borders co-express Cx26 (magenta) and Cx30 (green) within their gap junction plaques. Scale bars: 20 µm. **B, D**: Magnified image of the yellow boxes highlighted in **A** and **C** showing the organisation of gap junction plaques into pentagon/hexagon formation around the border of each cell. Scale bars: 10 µm.

4.2.1.3 Gap junction plaque fragmentation in the ageing organ of Corti

In order to quantify the observed changes in gap junction plaque organisation with age, the individual plaque length was measured and compared between 1-month-old, 12-month-old and 17-22-month-old 6N inner sulcus cells (Figure 4.8). It has been reported that GJ plaque length within inner sulcus cells can approximately range from 3 µm up to 10 µm, with the mean plaque length being calculated as 5.10 µm (Tajima *et al.*, 2020) and 6.25 µm (Kamiya *et al.*, 2014). Our data has provided similar measurements, with the 6N 1-month-old inner sulcus cells possessing a median plaque length of 5.57 µm and mean of 5.73 µm (Figure 4.8). Furthermore, the majority of plaques measure above 2 µm in length. It is only in $CX26^{R75W+}$ (dominant negative Cx26 mutation) mice that GJ plaques have been measured to be smaller than 2 µm and appear 'vesicle-like' (Kamiya *et al.*, 2014). This is likely due to issues with plaque assembly with the lack of functional Cx26 in that mutant. Therefore, immunostained objects were categorised as 'plaques' or 'fragments' depending on whether they were above or below the limit of 2 µm length. This distinction allowed the investigation of whether there was a difference in the abundance of these smaller fragment-like objects, but also in the length of the 'healthy' plaques. Anytime the word 'plaque' is used for the rest of this chapter it refers to objects longer than 2 µm.

The median plaque lengths for 6N 1-month-old, 12-month-old and 17-22-month-old cells were calculated to be 5.57 µm, 3.60 µm and 3.01 µm respectively. There was a significant decrease in the median plaque length between 1-month-old and 12-month-old inner sulcus cells, 12-month-old and 17-22-month-old inner sulcus cells, and between 1-month-old and 17-22-month-old inner sulcus cells ($P < 0.0001$) (Figure 4.8A). Furthermore, there was a progressive increase in both the number of 'fragments' and 'plaques' per cell with age. The 17-22-month-old cells have significantly more fragments and plaques per cell than both the 1-month-old and the 12-month-old groups ($P < 0.05$) (Figure 4.8B, C). Additionally, the 12-month-old group has significantly more fragments and plaques per cell than the 1-month-old age group. This suggests that with age, the inner sulcus cells exhibit a higher frequency of gap junction plaques and fragments which are shorter in length.

However, as mentioned previously, the size of the inner sulcus cells increases with age. So, it might be expected that larger cells would contain more individual plaques or fragments.

Therefore, the combined number of plaques and fragments per cell was calculated and normalised to the length of the cell. This still found a significant increase in normalised plaque and fragment count per cell between 1-month-old, 12-month-old and 17-22-month old cells ($P < 0.05$) (Figure 4.8D), further suggesting the frequency of plaques and fragments per cell progressively increases with age.

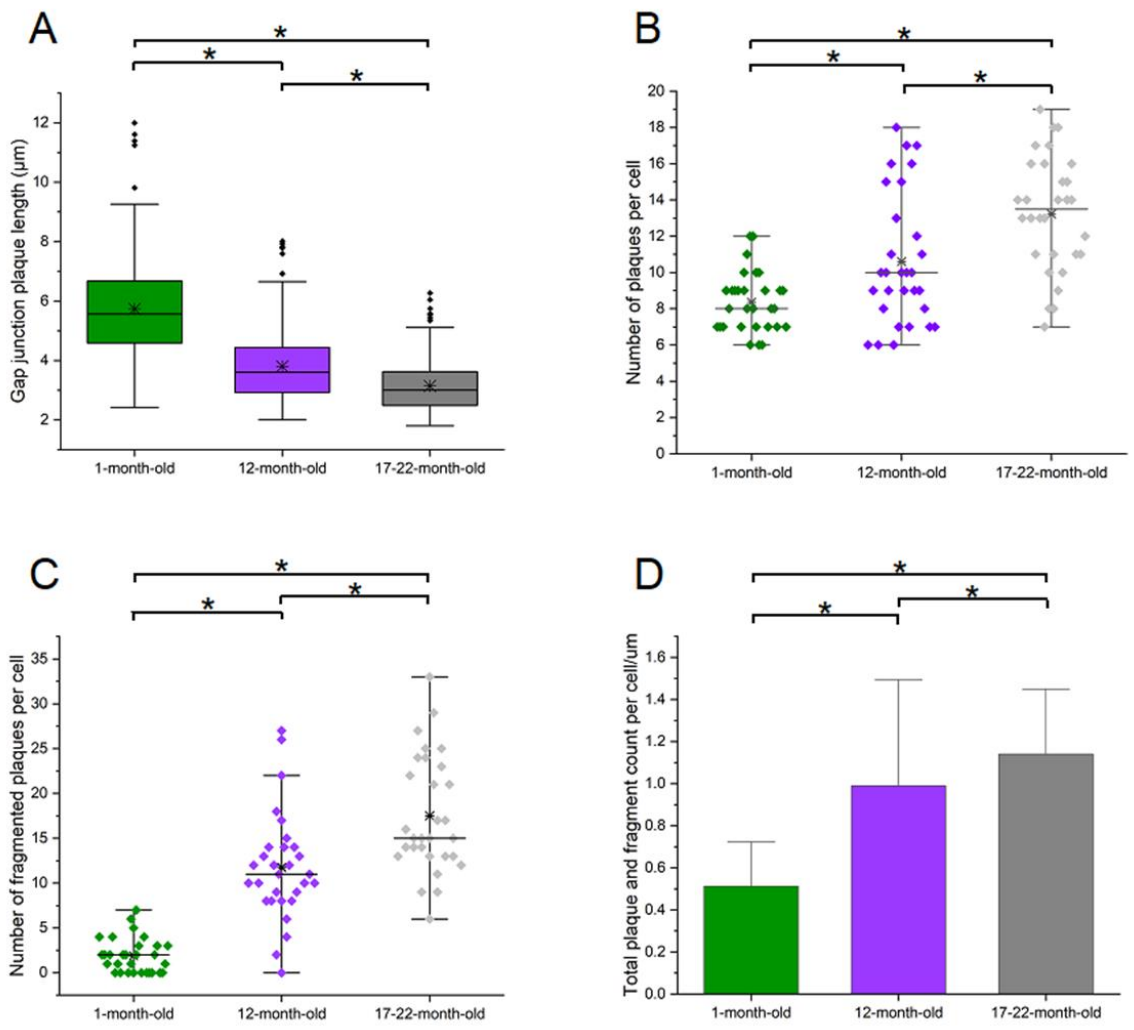

Figure 4.8: There is a higher frequency of shorter gap junction plaques in the aged inner sulcus cells

A: Length of gap junction plaques from 6N cochlear inner sulcus cells in three age groups: 1-month-old (green), 12-months-old (purple) and 17-22-months-old (grey). Mean plaque length is labelled by the star. Median plaque length is the central line of each box plot. n=3 mice analysed for each age group. Ten inner sulcus cells from each mouse were analysed, giving 240, 312 and 388 plaques total for 1-month, 12-month and 17-22 month old groups respectively. There is a significant decrease in the median plaque length between 1-month-old and 12-month-old inner sulcus cells, 12-month-old and 17-22-month-old inner sulcus cells and between 1-month-old and 17-22-month-old inner sulcus cells. Significance values are indicated by the asterisks (*$P < 0.0001$, Kruskal-Wallis ANOVA). **B, C:** The number of gap junction plaques (measuring above 2 µm) (**B**) and gap junction fragments (measuring below 2 µm) (**C**) per cochlear inner sulcus cell from three age groups: 1-month-old (green), 12-months-old (purple) and 17-22-months-old (grey). Diamonds represent the individual data points. Median plaque length is the central line of each whisker plot. n=3 mice analysed for each age group. Ten inner sulcus cells from each mouse were analysed. There is a significant increase in the median number of both plaques and fragments between 1-month-old and 12-month-old inner sulcus cells, and also between 12-month-old and 17-22-month-old inner sulcus cells. Significance values are indicated by

the asterisks (*$P < 0.05$, Kruskal-Wallis ANOVA). **D**: The total number of gap junction plaques and fragments per cochlear inner sulcus cell were measured in three age groups: 1-month-old (green), 12-months-old (purple) and 17-22-months-old (grey). This value was normalised to the length of the cell. Mean number of gap junction plaques and fragments per cell are show as the top of the coloured bar for each age group. n=3 mice analysed for each age group. Ten inner sulcus cells from each mouse were analysed. There is a significant increase in the mean plaque length between 1-month-old and 12-month-old inner sulcus cells, 12-month-old and 17-22-month-old inner sulcus cells and between 1-month-old and 12-month-old inner sulcus cells. Significance values are indicated by the asterisks (*$P < 0.05$, one-way ANOVA).

4.2.2 Progressive changes in gap junction plaque permeability

To test the difference in GJ permeability due to the change in plaque morphology with time, whole-cell dye injection of Lucifer yellow was performed in 1-month-old and 19-20-month-old inner sulcus cells from 6N mouse organs of Corti. Dye diffusion into neighbouring cells via the gap junction channels could then be analysed to determine whether gap junction channel permeability was altered with age. Lucifer yellow dye (molecular weight: 443 Da; charge, −2) has been utilised previously to investigate gap junction channel coupling in the organ of Corti (Santos-Sacchi and Dallos, 1983; Zwislocki *et al.*, 1992; Jagger and Forge, 2006). Homotypic mouse, rat and human Cx26 gap junction channels are all permeable to Lucifer yellow (Manthey *et al.*, 2001; Beltramello *et al.*, 2003; Marziano *et al.*, 2003). However, homotypic mouse and rat Cx30 gap junction channels do not allow Lucifer yellow diffusion (Manthey *et al.*, 2001; Marziano *et al.*, 2003). The differences between the cytoplasmic domains of these connexins were shown to directly influence the selectivity, permeability and voltage gating of Cx26 and Cx30 (Manthey *et al.*, 2001).

The formation of Cx26/Cx30 heterotypic gap junction channels will produce different permeability properties compared to the homotypic channels. It has been reported that HeLa cells transfected with rat cDNA for both Cx26 and Cx30 were impermeable to Lucifer yellow (Marziano *et al.*, 2003). However, HeLa cells transfected with human cDNA for both Cx26 and Cx30 showed permeability to Lucifer yellow (Yum *et al.*, 2007). This could potentially be due to interspecies differences in connexins, but also could be due to Cx26 homotypic channels forming in the HeLa cells, alongside the heterotypic channels, to allow dye diffusion. This latter hypothesis is suggested to explain why the inner sulcus cells and Hensen's cells both showed Lucifer yellow diffusion in rats at P12 (Jagger and Forge, 2006), even though these cells are known to express both Cx26 and Cx30.

All of the immunolabelled gap junction plaques in the previous section of this thesis show co-expression of both Cx26 and Cx30. This makes it highly likely that these cells contain Cx26/Cx30 heterotypic gap junction channels within the plaques, alongside Cx26 and Cx30 homotypic gap junction channels. Therefore, it was anticipated that because Lucifer yellow is only permeable via some subtypes of the gap junction channel, it may help to reveal any age-related changes in the type of gap junction channels present.

4.2.2.1 Lucifer yellow dye diffusion in inner sulcus cells

For each whole-cell patch clamp recording, the dye was injected and diffusion was monitored for 25 minutes. This length of time was chosen as it became apparent that Lucifer yellow diffusion speed was very slow (Figure 4.9). By the end of the 25 minutes, dye had reached an average of 11 cells across both age groups. It was expected that the reason for such slow dye diffusion was that Lucifer yellow is only permeable via homotypic Cx26 channels, and so the homotypic Cx30 channels and potentially the heterotypic Cx26/Cx30 channels were not allowing dye diffusion. The immunolabelling images, along with the slow speed of dye diffusion, both suggest that the majority of gap junction channels may be Cx26/Cx30 heterotypic gap junction channels.

A subset of inner sulcus cells showed no dye diffusion into neighbouring cells throughout the full recording. This could simply be because the chosen cell is uncoupled from the rest of the epithelium. This inconsistency in dye diffusion was also found in numerous other studies investigating Lucifer yellow dye diffusion in the organ of Corti (Santos-Sacchi, 1986; Jagger and Forge, 2006). Therefore, when analysing gap junction channel permeability, only cells which showed evidence of dye diffusion were considered.

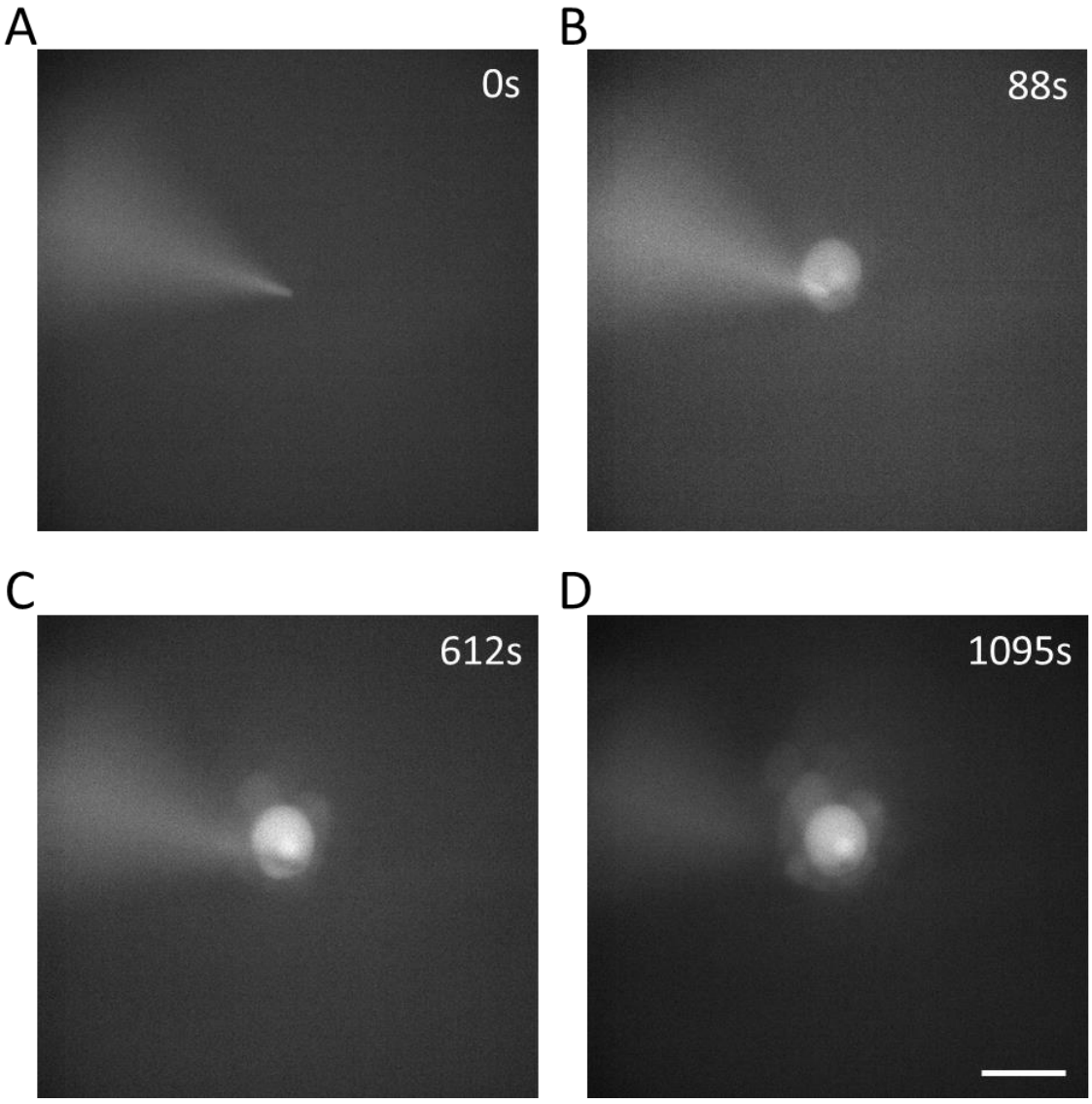

Figure 4.9: The diffusion of Lucifer yellow dye across inner sulcus cell gap junctions is very slow

Individual frames taken from an example recording of Lucifer yellow dye injection into a single inner sulcus cell from a 1-month-old 6N mouse. **A:** The first frame of the recording. The fluorescent patch pipette containing the dye is in contact with the chosen cell membrane before whole cell mode has been achieved. **B**: A frame taken from 88 seconds into the recording after entering whole-cell mode where the dye has entered the patched cell. **C**: A frame taken from 612 seconds into the recording where the dye has diffused into neighbour cells directly adjacent to the patched cell. **D**: A frame taken from 1095 seconds where the dye has diffused even further into second and third order cells. Scale bar in **D** also applies to **A**, **B** and **C**: 30 µm.

4.2.2.1 Lucifer yellow diffusion is unchanged with age in inner sulcus cells

From both the 1-month-old and 19-20-month old injected inner sulcus cells the dye was able to reach second order or third order cells within 25 minutes. As discussed in the Methods chapter (Section 2.5.3), first order cells are directly adjacent to the injected cell, second order cells are adjacent to first order cells, and third order cells are adjacent to second order cells. Of the ten 1-month-old cells injected, eight displayed dye diffusion into second order cells and two displayed dye diffusion into third order cells. Conversely, of the nine 19-20-month-old cells injected, six displayed dye diffusion into second order cells and three displayed dye diffusion into third order cells. This suggests the inner sulcus cells of both age groups have similar permeability to Lucifer yellow. In addition to this, the number of cells the dye entered was counted at the end of each 25-minute-long recording. No significant difference was calculated in the number of cells which had taken up Lucifer yellow between the 1-month-old and 19-20-month-old cells ($P = 0.3458$) (Figure 4.10A). Additionally, the total area displaying fluorescence due to dye diffusion was also measured at the end of each recording. No significant difference was identified between the area of fluorescent cells between the 1-month-old cells and the 19-20-month-old cells ($P = 0.1041$) (Figure 4.10B). This again suggests no age-related differences in the permeability of inner sulcus cells to Lucifer yellow.

The similarity between the extent of Lucifer yellow dye diffusion between the two age groups suggests the level of gap junction-mediated cell-cell coupling is unchanged. To further investigate this, the membrane resistance of the cells was compared between 1-month-old and 19-20-month-old inner sulcus cells. The value of the resistance incorporates the membrane resistance of the patched cell, but is also influenced by other neighbouring cells which are electrically coupled via the gap junction channels. Therefore, this value is an indirect measurement of cells GJ connectivity. Lucifer yellow was not added to the intracellular solution for these recordings. The cells from both age groups displayed a wide range of membrane resistances (19 to 190 MΩ) indicating that the cells across the epithelium of the inner sulcus display varied degrees of coupling (Figure 4.10C). This is consistent with what is already known regarding the membrane resistance of an inner sulcus cell as P25-P35 C57BL/6N inner sulcus cells have previously been shown to have membrane resistances

ranging from 30 to 660 MΩ (Sirko, Gale and Ashmore, 2019). Here, no significant difference was found between the membrane resistances of 1-month-old and 19-20-month-old inner sulcus cells (*P* = 0.4599), suggesting that the large variation in cell-cell coupling is maintained with age.

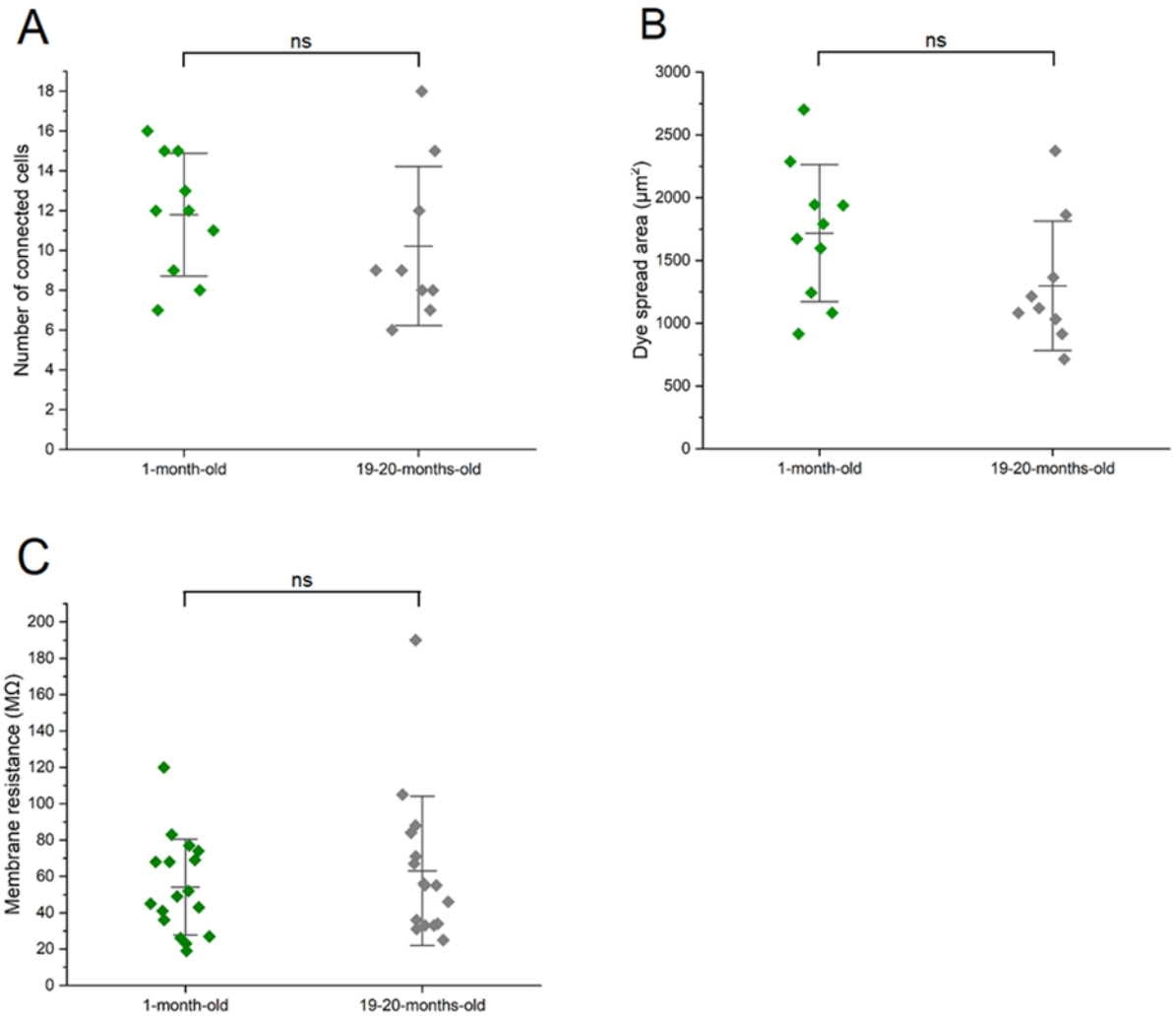

Figure 4.10: The inner sulcus cells display similar permeability to Lucifer yellow at 1-month-old and 19-20-months-old

A: Number of neighbour cells showing fluorescence due to dye diffusion counted 25 minutes after injection into a single cell. Error bars show mean ± SD. N=10 cells in 1-month-old group (green data points) and n=9 cells in 19-20-month-old group (grey data points). (Two-sample t test, *P* = 0.3458). **B:** The total area showing fluorescence due to dye diffusion measured 25 minutes after dye injection into a single cell. Error bars show mean ± SD. N=10 cells in 1-month-old group (green data points) and n=9 cells in 19-20-month-old group (grey data points). (Two-sample t test, *P* = 0.1041). **C**: The membrane resistance measured from inner sulcus cells. Error bars show mean ± SD. N=17 cells in 1-month-old group (green data points) and n=16 cells in 19-20-month-old group (grey data points). (Two-sample t test, *P* = 0.4599).

4.2.2.2 Lucifer yellow diffusion directionality is unchanged with age in inner sulcus cells

Next, the direction of dye diffusion was analysed to determine if there was a difference in GJ connectivity along the radial (i.e. pillar-modiolar) and longitudinal (i.e. apex-to-base) axis of the cochlea. The distance of dye spread was measured along two orthogonal axes and in three directions. This included modiolar diffusion (towards the modiolus), pillar diffusion (towards pillar cells and the hair cell rows) and radial diffusion (movement laterally along the inner sulcus away from the patch pipette) (Figure 4.11A). Depending on the position of the patch pipette, diffusion was either measured in the apical radial direction or the basal radial direction (always away from the pipette). No significant difference was found between the distance of dye diffusion radially (P = 0.4534) (Figure 4.11B) or towards the hair cells (P = 0.6744) (Figure 4.11C) between the two age groups.

Regarding diffusion towards the modiolus, two of the nine cells aged 19-20-months did not diffuse at all in this direction (Figure 4.11D). This could have been because the cells in this area were uncoupled from the rest of the epithelium. However, it is unlikely to be the case because of a preference for diffusion in other directions as the other seven cells in this group show diffusion towards the modiolus. Nevertheless, when these two points were included in the analysis there was a significant increase in modiolar diffusion in the 1-month-old group compared to the 19-20-month-old group ($P < 0.05$). Overall, this suggests that Lucifer yellow freely and passively diffuses from cell to cell without a preferential direction, indicating homogenous distribution in cell-cell coupling across the inner sulcus.

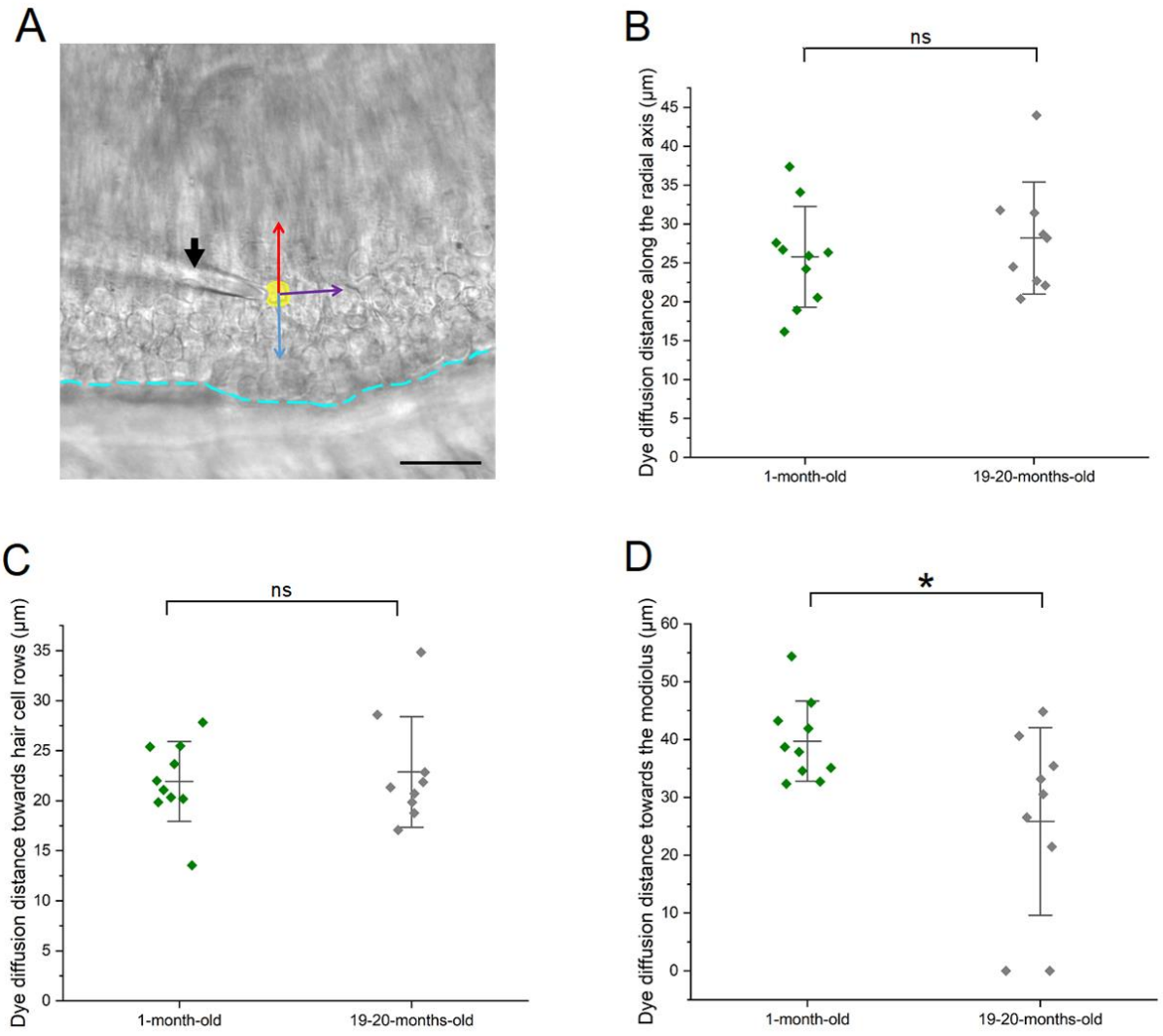

Figure 4.11: There is no directional preference for dye diffusion in inner sulcus cells at both 1-month-old and 19-20-months-old

A: Brightfield image of the organ of Corti. The cyan dotted line shows the divide between the inner sulcus above and the hair cell rows below. A patch pipette (black arrow) is shown contacting the injected inner sulcus cell (yellow). The maximum dye diffusion distance from the centre of the injected cell was measured in three directions: towards the modiolus (red arrow), radially along the inner sulcus away from the patch pipette (purple arrow) and towards the hair cell rows (blue arrow). Scale bar: 20 µm. **B:** Dye diffusion in the radial direction was measured for each recording. (Two-sample t test, $P = 0.4534$). **C**: Dye diffusion towards the hair cell rows was measured for each recording. (Two-sample t test, $P = 0.6744$). **D**: Dye diffusion in the modiolar direction was measured for each recording. (Two-sample t test, $^*P < 0.05$). Green data points represent recordings from 1-month-old inner sulcus cells and grey data points are from 19-20-month-old cells. Error bars show mean ± SD.

4.2.2.3 Lucifer yellow diffusion speed is unchanged with age in inner sulcus cells

Lucifer yellow dye diffusion was plotted as relative changes in fluorescence intensity (ΔF/F0). Where F is the fluorescence intensity and F0 is an average of the fluorescence in the first five frames of each recording. This was calculated for all cells in each recording and for an additional region of interest placed over the patch pipette (See Methods 2.5.3). Then, the ΔF/F0 for each cell was subtracted from that of the pipette to correct for the reduction in fluorescence over time due to photobleaching.

From looking at the traces, it became apparent that there were large variations between the ΔF/F0 across all recordings from both age groups (Figure 4.12). For analysis, the average ΔF/F0 traces for each cell order (distance from the patched cell) were compared between the two age groups. This comparison was made at a specific timeframe (1300 seconds after whole cell mode was established) and took an average ΔF/F0 of five frames at this time point. Each one of these average ΔF/F0 values was also normalised to the fluorescence in the patched cell (this was determined by calculating the 90^{th} percentile of the patched cell ΔF/F0 values before 1300 seconds). As seen in the traces in Figure 4.12A-F, the average ΔF/F0 values were very varied across both age groups (Figure 4.12G-1). No significant difference was found between the average normalised fluorescence values of first order (P = 0.9756) or second order cells (P = 0.9360) in the 1-month-old and the 19-20-month-old inner sulcus.

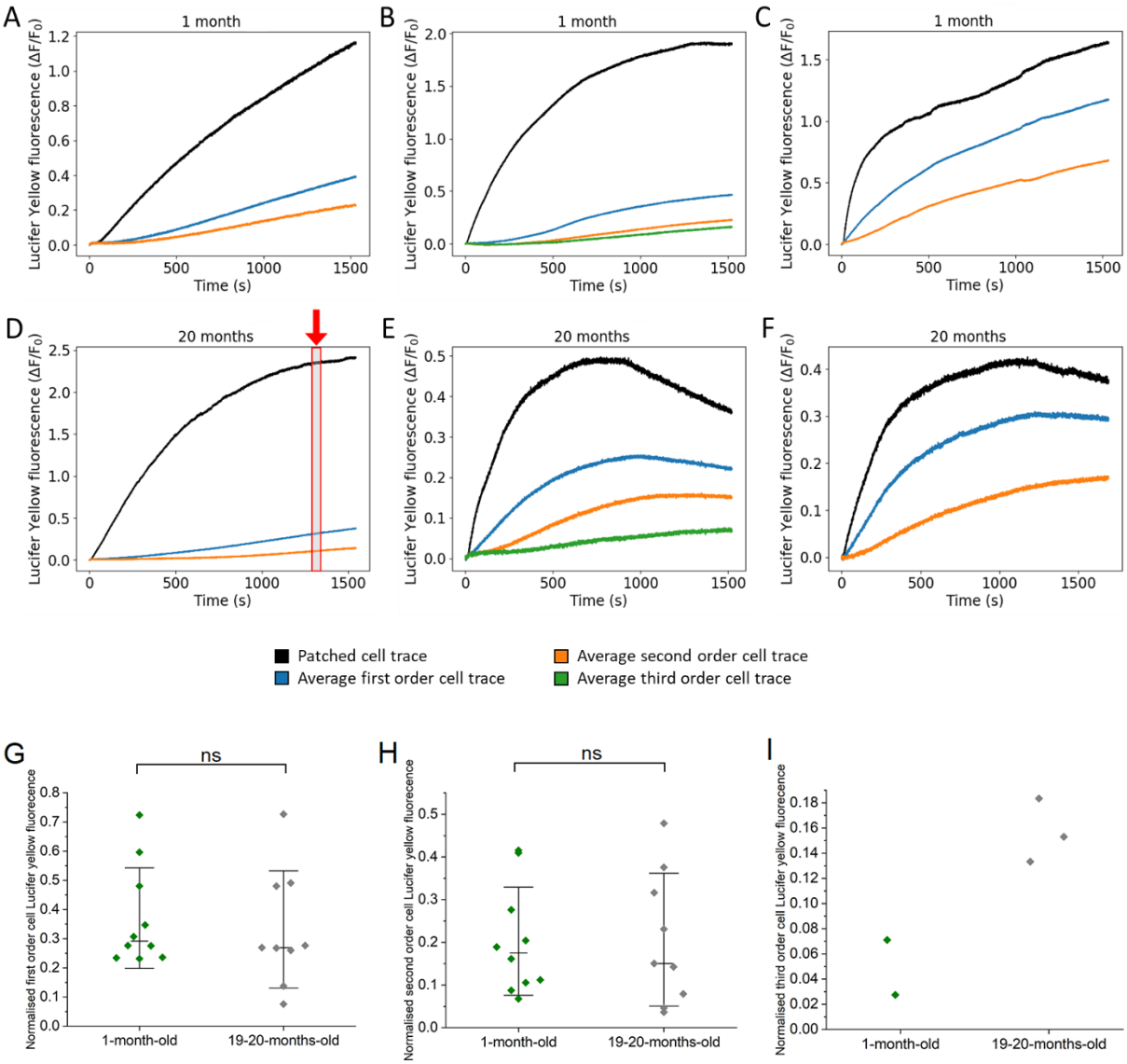

Figure 4.12: The ΔF/F0 traces show large variations from both 1-month-old and 19-20-months-old inner sulcus cells

Example Lucifer yellow fluorescence ΔF/F0 traces from whole-cell injection recordings from 1-month-old (**A**, **B**, **C**) and 19-20-month-old (**D**, **E**, **F**) inner sulcus cells. **D**: The box and red arrow at 1300 seconds show the five frames taken and averaged, and then normalised to the fluorescence in the patched cell (this was determined by calculating the 90th percentile of the patched cell ΔF/F0 values before 1300 seconds). These values were then used as the normalised Lucifer yellow fluorescence in **G**, **H** and **I**. **G**: No significant difference was found between the normalised Lucifer yellow fluorescence of first order cells from 1-month-old and 19-20-month old 6N mice. (Two-sample t test, P = 0.9756). **H**: No significant difference was found between the normalised Lucifer yellow fluorescence of second order cells from 1-month-old and 19-20-month old 6N mice. (Two-sample t test, P = 0.9360). **I**: The normalised Lucifer yellow fluorescence of third order cells did not have a large enough n number to perform statistical analysis as not enough recordings reached this order (n=2 for 1-month-old cells and n=3 for 19-20-month-old cells). Error bars show mean ± SD.

To test possible differences in the diffusion speed among the two ages, a time constant was calculated by fitting the fluorescence traces with the following exponential growth function:

$$a \cdot (1 - e^{-\frac{x}{t}})$$

For this analysis, the average ΔF/F0 traces for each cell order were fit with the function.

However, because the spread of Lucifer yellow dye was slow, some of the traces did not exhibit a plateau within the 25 minutes of recording (Figure 4.12), making the fit difficult to converge and giving extremely large time constant values. Nevertheless, all time constant values were plotted and included within the analysis. For example, for the average ΔF/F0 traces of first order cells, three out of the ten recordings from 1-month-old mice had large time constant values, and one out of the nine recordings from 19-20-month-old mice had a large time constant value (Figure 4.13A). Furthermore, the 19-20-month-old cells displayed a significant decrease in the first order cell time constants in comparison to the 1-month-old cells ($P < 0.05$). This would suggest that the dye moves more quickly from the patched cell into neighbouring cells in the older age group, which would also imply the aged gap junction channels have an increased permeability compared to the young adults. In addition to this, for the second order cell time constants, no significant difference was found between the 1-month-old cells and the 19-20-month-old cells ($P = 0.0662$) (Figure 4.13B). Six out of the ten recordings from 1-month-old cells, and two out of the nine recordings from the 19-20-month-old cells, displayed extremely large time constant values.

Overall, there does appear to be a trend suggesting that the 1-month-old inner sulcus cells display slower diffusion speed of Lucifer yellow dye into neighbouring cells as a higher proportion of the 1-month-old time constants were very large. However, it is very likely that the slow speed of dye diffusion as a whole has made it more difficult to identify subtler changes in dye diffusion speed between age groups.

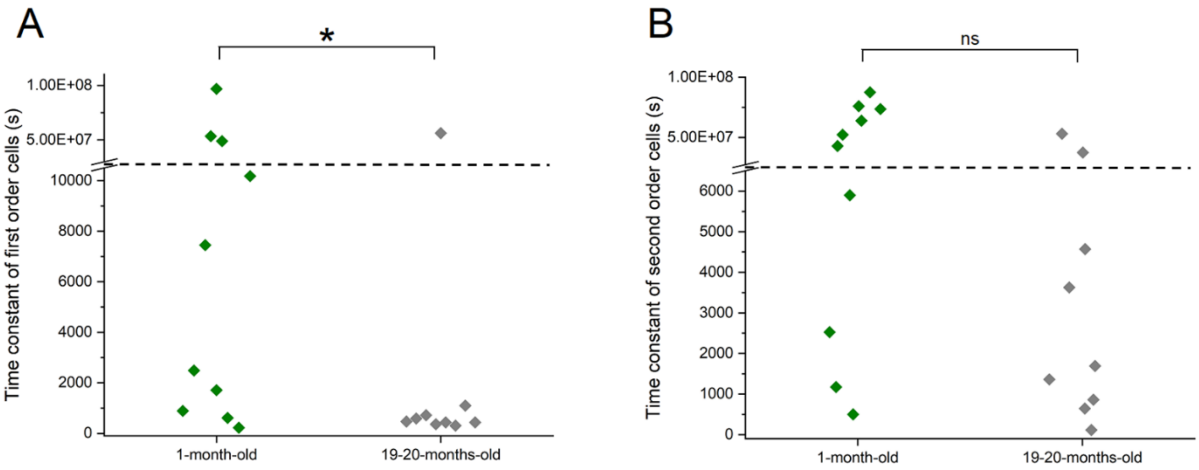

Figure 4.13: Dye diffusion speed time constants of 1-month-old and 19-20-months-old inner sulcus cells

A: Time constant values calculated from the average ΔF/F0 traces of first order cells from 1-month-old and 19-20-month old 6N mice. 19-20-month-old cells displayed a significant decrease in the first order cell time constants in comparison to the 1-month-old cells (Mann-Whitney test, $*P < 0.05$). **B**: Time constant values calculated from the average ΔF/F0 traces of second order cells from 1-month-old and 19-20-month old 6N mice. No significant difference was found between the time constant of second order cells from 1-month-old and 19-20-month old 6N mice. (Mann-Whitney test, $P = 0.0662$).

4.3 Discussion

A network of gap junction channels connects the supporting cells of the organ of Corti and facilitates the movement of ions and small molecules across the epithelium (Hernandez *et al.*, 2007; Kikuchi *et al.*, 2000; Chang *et al.*, 2008; Jagger and Forge, 2015). Any mutations affecting the synthesis, trafficking or permeability of these membrane channels is well known to have a negative effect on cochlear function and lead to hearing loss (del Castillo and del Castillo, 2017; Chan and Chang, 2014; Chen *et al.*, 2022). This is believed to be because the gap junction transport network is implicated in numerous important processes required for the correct development and functioning of the organ of Corti. For instance, the delivery of metabolites such as glucose (Chang *et al.*, 2008), the propagation of intercellular signalling cascades during development (Anselmi *et al.*, 2008) and the recycling of ions such as K^+ to maintain ionic homeostasis within the cochlea (Kikuchi *et al.*, 2000; Wangemann, 2006). Even though it is clear these GJCs are critical for the maintenance of cochlear function, minimal research has been performed to investigate whether this could also be implicated in age-related hearing loss. Therefore, this chapter investigated whether gap junction channel plaques in the organ of Corti undergo changes in their structural organisation and function with age.

4.3.1 Gap junction plaque organisation is altered in the aged inner sulcus

Here, it was found that C57BL/6N murine cochlear inner sulcus cell gap junction plaques become significantly smaller and more fragmented with age. Specifically, a progressive decrease in plaque length was measured across 1-month-old, 12-month-old and 17-22-month-old inner sulcus cells. This aligns with previous work which showed that in comparison to one-month-old C57BL/6J mice, eight-month-old mice had significantly shorter gap junction plaques which exhibited a 'scattered structure' (Tajima *et al.*, 2020). Furthermore, their qRT-PCR showed no age-related difference in Cx26 (*GJB2* gene) or Cx30 (*GJB6* gene) mRNA expression, whereas western blots show a significant decrease in Cx26 and Cx30 protein levels with age. Therefore, they hypothesised that this decrease in plaque length was likely due to

an age-related increase in the degradation and instability of plaques rather than a downregulation of connexin expression.

Most gap junctions have short half-lives lasting from 1-5 hours (Beardslee *et al.*, 1998; Fallon and Goodenough, 1981). This means that the plaques are continuously being remodelled as older connexons are degraded and replaced with new ones. In the Golgi apparatus, most newly-assembled connexons travel along microtubules to the plasma membrane (Lauf *et al.*, 2002). They are then recruited towards gap junction plaques via interactions with the actin cytoskeleton mediated by the actin binding protein zona occludens (Hervé *et al.*, 2014). The connexons then dock onto the outer edges of the pre-existing plaques and form intercellular channels with adjacent connexons on the neighbouring cell. Alongside this, older connexons are endocytosed from the centre of the plaque and sent for lysosomal degradation (Gaietta *et al.*, 2002). It is not known as to why GJ plaques are so dynamic, one possible explanation might be that the continual remodelling makes it easier to alter the extent of cell-cell coupling in response to physiological stimuli.

Nevertheless, the observed age-related decrease in gap junction plaque length might be a result of dysfunction of gap junction remodelling. Any changes in how new connexins are recruited or how old connexins are removed will affect the size of the GJC plaque. As mentioned above, plaque remodelling is a complex process involving the actin cytoskeleton, microtubules and a range of scaffolding/support proteins in the plaque. Therefore, age-related dysfunction in any of these components could be what is driving the observed changes in GJC plaque size. For example, a decrease in zona occludens expression has been shown to cause large GJC plaque size as it is believed that this protein regulates how quickly new connexons are added to the plaque (Hunter *et al.*, 2005). Age-related changes in gap junction channel remodelling has not been the focus of much research in any tissues. However, the individual components important for this complex mechanism have been investigated in senescence. For example, the actin cytoskeleton is known to undergo a reduction in actin expression and changes in dynamics with old age (Moshier, Cornell and Majumdar, 1993; Kasper *et al.*, 2009). Therefore, age-related changes in a component required for gap junction plaque remodelling could be influencing the observed reductions in plaque size.

Tajima et al., 2020 also report changes in the organisation of gap-junction-associated lipid rafts and suggest that this could be contributing to the observed decrease in plaque size, and

maybe plaque disassembly, in the aged inner sulcus. Typically, Cx26/Cx30 gap junction plaques have the location of their lipid rafts restricted to tricellular junctions (regions which are adjacent to the end of three separate plaques) (Figure 4.14) (Defourny, Thelen and Thiry, 2019; Defourny and Thiry, 2021). These lipid rafts are rich in actin filaments and adhesion molecules and so newly-assembled connexons from the Golgi are believed to be trafficked to this location before being added to the existing plaques (Defourny and Thiry, 2021; Locke, Liu and Harris, 2005). However, instead of orderly lipid rafts at located at tricellular junctions, the eight-month-old inner sulcus cells displayed scattered localisation of their lipid rafts at random points along the gap junction plaques (Tajima *et al.*, 2020). Therefore, it is possible that the reduction in gap junction plaque size and integrity is due to age-related changed in lipid rafts which negatively impact gap junction plaque remodelling. Overall, in future work it would be beneficial to investigate age-related changes in the expression and location of other components associated with gap junction plaque remodelling to understand why there is an increase is disassembly with age in the cochlea.

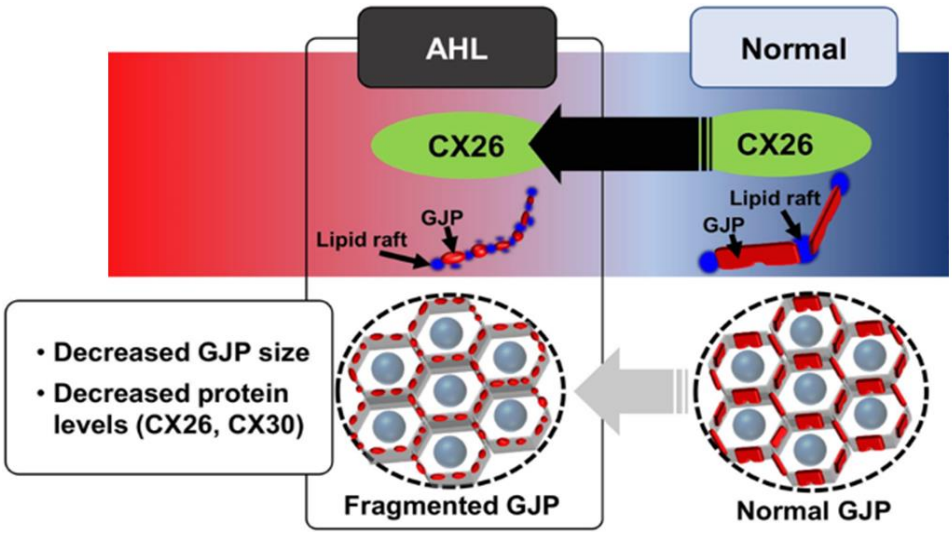

Figure 4.14: Age-related changes in gap junction plaques and associated lipid rafts in the organ of Corti

Normal gap junction plaques (GJPs) organise into long planar structures along the edge of the inner sulcus cells (red). They also have regular organisation of lipid rafts in the gaps between gap junction plaques (blue). In age-related hearing loss (ARHL) the size of gap junction plaques becomes shorter, and the location of their lipid rafts appears to be more scattered and disorganised. Figure from (Tajima *et al.*, 2020).

4.3.2 Gap junction plaque permeability in the aged inner sulcus

Whole cell injection of the fluorescent dye Lucifer yellow was utilised to investigate whether gap junction channels exhibited changes in their permeability, as well as their organisation, in the aged inner sulcus. No significant difference was found between the dye diffusion distance or directionality between 1-month-old and 19-20-month-old C57BL/6N murine cochlear inner sulcus cells. However, a significant decrease in in the dye diffusion time constant of first order cells from 19-20-month-old cells was discovered compared to 1-month-old cells, suggesting GJ channels from the older age group were more permeable to Lucifer yellow. Although, no significant difference was observed between the time constants of the second order cells.

Overall, this implies that the observed changes in gap junction plaque size have minimal effects on the permeability of Cx26 homotypic channels. However, it is well established that alterations in gap junction plaque organisation and size do in fact influence permeability. For instance, cells with larger gap junction plaques have been found to exhibit greater electrical coupling via electrophysiological recordings (Bukauskas *et al.*, 2000; Johnson *et al.*, 1974). Additionally, HeLa cells transfected with Cx26 and Cx30 showed reduced Neurobiotin transfer (a tracer permeable to both Cx26 and Cx30 gap junction channels) in cells with smaller gap junction plaques (Kamiya *et al.*, 2014). Furthermore, a decrease in gap junction plaque size has been associated with disease in other tissues. For example, within the heart, the lack of synchronised muscle contraction associated with aryhthmias has been linked to smaller gap junction plaques limiting cell-cell coupling and the efficient spread of electrical signals (Luke and Saffitz, 1991; Kaprielian *et al.*, 1998).

Therefore, it would be expected that the changes observed here in the organisation of aged inner sulcus cell gap junction plaques would also influence their permeability. One explanation for this could be that the diffusion of Lucifer yellow dye may not have been a sensitive enough measure to detect these changes. The main reason for this is likely that its impermeable to gap junction channels containing Cx30 (Manthey *et al.*, 2001; Marziano *et al.*, 2003), which make up a large proportion of gap junction channels within the organ of Corti. This meant that it could have only been the homotypic Cx26 channels being considered in the analysis in this chapter, which excludes the homotypic Cx30 channels and the heterotypic

Cx26/Cx30 channels. The dye moved quite slowly into neighbouring cells suggesting the levels of Cx26 homotypic channels were low in both age groups. Therefore, it would suggest this experiment is actually not considering the majority of gap junction channels in these inner sulcus cells, which could explain the inability to see many age-related changes in gap junction permeability.

Nevertheless, this meant it was possible to measure age-related changes in permeability across homotypic Cx26 gap junction channels alone. This was advantageous as Tajima et al., 2020 hypothesised that the decrease in gap junction plaque length they observed with age in the inner sulcus was potentially due to the degradation of plaques following the progressive conversion of hydrophilic Cx26 to hydrophobic Cx26. This would promote the association of the plaques with lipid rafts and impact how and where new connexons are recruited to the existing gap junction plaques. Therefore, it would be expected that the plaque fragmentation would be most extreme at Cx26 homotypic channels. However, the dye diffusion reported here suggests that there is likely to be too few of these homotypic channels present in the plaques for many age-related changes in permeability to be detected.

Even though studying homotypic Cx26 channels alone was beneficial in some ways, performing additional dye diffusion experiments alongside Lucifer yellow would have allowed measurement of permeability in other channel subtypes. Neurobiotin has been utilised to measure gap junction permeability within the cochlea (Jagger and Forge, 2006; Jagger, Nickel and Forge, 2014). It is known to be permeable to homotypic Cx26, homotypic Cx30 and heterotypic Cx26/Cx30 gap junction channels (Manthey *et al.*, 2001; Marziano *et al.*, 2003). However, for Neurobiotin to be visualised it requires the explant to be fixed and labelled with fluorescent streptavidin, meaning live imaging of the diffusion cannot be performed. This is effective for testing whether cells are coupled or not, but will not be as sensitive at detecting aspects such as dye diffusion speed. Nevertheless, performing this alongside the Lucifer yellow experiments could still have provided additional information regarding the other subtypes of gap junction channel.

Moreover, dye diffusion speed seems to be an important parameter as even though it is apparent Lucifer yellow transfer was not a very sensitive method to study GJC permeability, a significant decrease was still identified between the first order cell time constants of aged cells compared to young adult cells. This would suggest that the aged cells display faster

diffusion of Lucifer yellow into neighbouring cells, implying a potential increase in Cx26 homotypic channels or even a change in the selectivity of the Cx26/Cx30 heterotypic channels. This difference might have been missed if the dye diffusion were not live imaged, as with the potential use of Neurobiotin. However, again the slow speed of dye diffusion meant that it was difficult to identify significant differences between the time constants of second order cells, and third order cells rarely showed signs of dye diffusion within the 25-minute recording.

4.3.3 Summary

In conclusion, this chapter has investigated age-related changes in gap junction channel plaque organisation and permeability in the inner sulcus of the cochlea. The immunolabelling experiments show that young adult inner sulcus cells display large gap junction plaques covering large portions of the cell membranes, alongside dye diffusion experiments showing low permeability to Lucifer yellow. In addition to this, the chapter presents new data showing that gap junction plaque organisation becomes progressively more fragmented with age in 12-month-old and 17-20-month-old inner sulcus cells. It is not clear why gap junction plaques might become shorter in aged cells, one potential explanation could be that these cells undergo age-related changes in their ability to remodel their gap junction plaques. However, this change in organisation was not found to impact the permeability of the gap junction plaques to Lucifer yellow. Additional experiments should be performed to further analyse changes in gap junction permeability which might have been missed in the experiments performed in this thesis.

Chapter 5. General Discussion

The majority of research into the pathophysiology behind age-related hearing loss (ARHL) has focused on the progressive loss of inner hair cells, outer hair cells and spiral ganglion neurons (Spongr *et al.*, 1997; Viana *et al.*, 2015; Jeng *et al.*, 2021; Jeng *et al.*, 2020b). However, the mechanisms which actually precede and trigger this sensory cell loss are poorly understood, making it difficult to generate targeted treatments for ARHL. The supporting cells of the organ of Corti promote hair cell longevity and are required to maintain our sense of hearing (Wan, Corfas and Stone, 2013). Minimal research has been conducted to investigate whether these glia-like non-sensory cells also undergo an age-related decline in function alongside sensory hair cells. Here it was hypothesised that any age-related dysfunction in the supporting cells would affect their ability to aid hair cell functioning, and this might exacerbate the progressive hair cell loss driving ARHL. Therefore, the overarching aim of this thesis was to evaluate whether the cochlear supporting cells underwent age-related changes in their protein expression and function.

Two main functions of the supporting cells have been extensively discussed in this thesis. The first being the P2Y purinergic receptor signalling cascade initiated in the supporting cells during cochlear development (Tritsch *et al.*, 2007; Babola *et al.*, 2020). The intracellular Ca^{2+} transients produced following P2Y receptor activation are thought to have downstream effects on the driving force for inner hair cell depolarisation, and therefore, modulate the immature spontaneous inner hair cell action potentials which are crucial for synaptic maturation (Clause *et al.*, 2014; Müller *et al.*, 2019). Secondly, the majority of supporting cells express gap junction channel plaques which couple the intracellular spaces of neighbouring cells (Kikuchi *et al.*, 1995). This creates a transport network across the cochlear epithelium which is believed to promote hair cell longevity by facilitating ion and metabolite homeostasis (Zhang *et al.*, 2005; Chang *et al.*, 2008). Age-related changes in either of these mechanisms in the supporting cells were anticipated to influence the functioning of the hair cells and therefore could be involved in age-related hearing loss.

5.1 P2Y purinergic receptors in the ageing mammalian organ of Corti

In Chapter 3 of this thesis, age-related changes in P2Y receptor expression and associated intracellular Ca^{2+} transients were investigated in the cochlear inner sulcus cells. Specifically, $P2Y_1$, $P2Y_2$ and $P2Y_4$ receptors were all found to be expressed in the immature inner sulcus (Kölliker's organ) where they were responsible for generating ATP-induced intracellular Ca^{2+} waves. This mechanism was lost in the adult inner sulcus as it is believed to only be required during development to modulate the immature hair cell action potentials and promote synaptic maturation (See Introduction section 1.1.1.2.1) (Tritsch *et al.*, 2007; Clause *et al.*, 2014). However, aged inner sulcus cells displayed an upregulation of $P2Y_2$ and $P2Y_4$ receptor expression and associated intracellular Ca^{2+} transients. It is unclear as to why an upregulation of P2Y receptors might occur in the aged inner sulcus when they are not required in the adult cochlea, and in Section 3.3 a few hypotheses to explain this were suggested including the cochlea attempting to recapitulate immature characteristics to limit further age-related damage. Nevertheless, the actual function of P2Y receptors at this age remains uncertain and further work is required to better understand this mechanism.

One area of future work, which could advance our understanding of age-related P2Y receptor upregulation, is the use of conditional knock-out mice. In this thesis, using an immunological and pharmacological approach, it was reported that only $P2Y_2$ and $P2Y_4$ receptors were re-expressed with age, but not $P2Y_1$ receptors which are also present during development. This selective re-upregulation suggests the different receptor subtypes might be involved in different mechanisms, with only $P2Y_2$ and $P2Y_4$ being implicated in age-related processes. However, the functioning of the individual receptor subtypes could not be fully investigated in this thesis because the antagonists were not completely specific (e.g. $P2Y_2$ antagonists also blocked $P2Y_4$ activity), or it is possible that the formation of P2Y heterodimers might have influenced the pharmacology of individual receptors (Ecke *et al.*, 2008; Ribeiro-Filho *et al.*, 2016). Nevertheless, removing a single subtype of P2Y receptor via conditional knock-out mice could help provide information regarding how each receptor contributes to these Ca^{2+} transients, and also, why only certain subtypes are upregulated in the aged inner sulcus.

Alongside this, tamoxifen inducible knock-out mice would allow the deletion of individual P2Y receptor subtypes in adult mice, thus bypassing the role of these receptors in the developing cochlea. This approach would allow the investigation of the specific role of $P2Y_2$ and $P2Y_4$ receptors in the aged cochlea. In Chapter 3, it was reported that P2Y receptor upregulation was more pronounced in mice with more severe ARHL (C57BL/6N) than in those with good hearing (C3H/HeJ). This suggests a link between P2Y receptor upregulation and the severity of ARHL. However, C57BL/6N and C57BL/6N-repaired had comparable levels of P2Y receptor upregulation, even though the C57BL/6N-repaired display significantly less severe ARHL compared to C57BL/6N (Noben-Trauth, Zheng and Johnson, 2003). Therefore, it is likely that there are multiple different mechanisms influencing ARHL progression and the upregulation of P2Y receptors is potentially implicated in one of them. It would be interesting to see whether blocking this P2Y upregulation would have any effect on ARHL progression, and if so does it exacerbate or alleviate it.

In addition to this, it would be beneficial to study these P2Y-receptor-mediated Ca^{2+} transients both *ex vivo* and *in vivo*. For the *ex vivo* experiments used in this thesis, the organ of Corti had to be removed from its natural physiological environment. This would be expected to impact the cells being studied as normal cochlear function is known to largely rely on the specific ionic compartments and coupling of all supporting cells forming a syncytium. The loss of the endolymph and damage to cell-cell connections from the dissection process is therefore expected to influence the cell activity observed *ex vivo*. Furthermore, intracellular Ca^{2+} transients across the supporting cells are also stimulated by damage to the epithelium (Gale *et al.*, 2004). Therefore, it is not known whether some of the transients observed in the present work were spontaneous (similar to those during development known to modulate hair cell firing) or induced by damage. *In vivo* Ca^{2+} imaging techniques on live immature mice have recently been developed by other members in the Marcotti lab here at the University of Sheffield. This procedure uses two-photon microscopy to image Ca^{2+} transients in reporter mice where GCaMP6 is selectively expressed in the cells of interest. Therefore, another potential area for future work would be to repeat these experiments *in vivo* to evaluate whether we see the same characteristics of Ca^{2+} transients as we do *ex vivo*.

5.2 Gap junction channels in the ageing mammalian organ of Corti

In Chapter 4 of this thesis, age-related changes in the structural organisation and permeability of gap junction channel (GJC) plaques were studied in the cochlear inner sulcus cells. As discussed in the Introduction chapter (Section 1.1.1.2.2), the majority of supporting cells express GJC plaques composed of connexin 26 (Cx26) and connexin 30 (Cx30) (Kikuchi *et al.*, 1995; Lautermann *et al.*, 1998), which facilitate the transport of ions and metabolites across the epithelium (Zhang *et al.*, 2005; Chang *et al.*, 2008). Here, it was discovered that with increasing age between 1-month-old, 12-months-old and 17-20-months-old inner sulcus cells, there was a higher quantity of shorter gap junction plaques per cell. It was hypothesised that this alteration in plaque size was due to age-related changes in proteins required for GJC plaque remodelling, as this would influence how channels are added or removed from the plaques. Therefore, it would be interesting to study progressive changes in the expression of proteins involved in GJC plaque remodelling in the cochlea to investigate whether this could be what is driving the plaque fragmentation.

GJC plaque size and organisation have been shown to influence their permeability (Kaprielian *et al.*, 1998; Kamiya *et al.*, 2014). This could have important implications for ARHL as it is already well established that dysfunction of supporting cell gap junction channels is a common cause of non-syndromic hearing loss (del Castillo and del Castillo, 2017; Chan and Chang, 2014; Chen *et al.*, 2022). Therefore, any progressive change in GJC permeability with age would be expected to impact ARHL progression. However, no differences were found between the distance or directionality of Lucifer yellow dye diffusion between 1-month-old and 19-20-month-old inner sulcus cells, suggesting gap junction channel permeability is similar across both age groups. As discussed in Chapter 4, it became apparent that this dye diffusion technique was not very sensitive for cochlear GJCs as it was only permeable via Cx26 and not Cx30. Therefore, alternative experiments are required to better evaluate how the observed changes in GJC plaque structure affect their permeability.

Fluorescence recovery after photobleaching (FRAP) is an example of another method which could be utilised to better measure GJC permeability. The full organ of Corti epithelium would

be loaded with a cell permeable dye (such as Calcein-AM) which is only converted into a fluorescent form after being taken up into cells. After loading, a defined section of the epithelium is photo-bleached and then dye redistribution into the bleached cells is monitored to evaluate how coupled those cells are by GJCs. One advantage of this technique is that no dye injection is required and so the cell integrity is maintained across the epithelium. This is particularly important for measuring gap junction permeability as it has been shown that mechanical forces applied during whole-cell patch clamp experiments can influence supporting cell coupling in the cochlea (Zhao and Santos-Sacchi, 1998).

Alternatively, supporting cell gap junction coupling could also be inferred using other whole-cell patch clamp electrophysiology measurements. One example already used in Chapter 4 is the input membrane resistance which indirectly represents the extent of gap junction coupling between the patched cell and the rest of the epithelium. Low input membrane resistances indicate the patched cell has many open gap junction channels allowing it to be electrically coupled to the others in the epithelium. The gap junction blocker octanol has been reported to greatly increase inner sulcus cell input membrane resistance as it uncouples the patched cell from the rest of the epithelium (Sirko, Gale and Ashmore, 2019). Alongside this, the cells resting current at -55 mV could also be used as an indication of how coupled the cell is to the rest of the epithelium. A larger inward resting current would suggest a lot of current leak from surrounding cells via the gap junction channels. Additionally, dual patch-clamp experiments would also give an indication of cell-cell coupling in the supporting cells. Stepping the voltage of one patched cell in the epithelium, and measuring the resultant current in another neighbour cell, would also infer the degree of cell-cell coupling by seeing how much of the current induced within the stepped cell was able to leak into neighbour cells.

5.3 Other supporting cell proteins to investigate in the aged cochlea

Following on from the work completed in this thesis, there is a wide range of other supporting cell proteins which could also undergo age-related changes in their expression and function. The combined alterations in P2Y purinergic receptors and gap junction channels, alongside

any other important proteins, could have a cumulative impact on age-related hair cell functional decline. Therefore, it is important to gain insight into any other potential progressive change in support cell proteins to have a more complete understanding of what could be driving age-related hair cell loss.

For instance, an additional function of the supporting cells not discussed in this thesis is their involvement in protection from noise-induced hearing loss (NIHL). As mentioned in Section 1.2.2, NIHL is known to be a risk factor for ARHL development. Therefore, it would be anticipated that any age-related change in the supporting cells affecting the NIHL protective mechanisms would exacerbate the progression of ARHL. One protein involved in this protective mechanism is the glutamate aspartate transporter known as GLAST, which is expressed by the inner phalangeal cells and border cells adjacent to the inner hair cell (IHC) synapse (Furness and Lehre, 1997). This transporter clears glutamate from the IHC synaptic cleft to prevent excitotoxicity which can lead to synaptopathy and hearing loss (Glowatzki *et al.*, 2006; Hakuba *et al.*, 2000). Any age-related change in GLAST expression or function would be expected to influence the efficiency of glutamate recycling from the IHC synapse, and impact how vulnerable the IHCs are to excitotoxicity, synaptopathy and hearing loss. One article examined GLAST expression levels across the apical, middle and basal cochlear turns of patients with ARHL and found the basal turn to have significantly higher GLAST expression (Ahmed *et al.*, 2013). Due to the fact that ARHL is more severe at the base of the cochlea, this upregulation in GLAST might be an attempt to limit further synaptopathy and hearing loss in this area.

Another protein involved in preventing excitotoxicity and NIHL are $P2X_2$ purinergic receptors. Similar to P2Y receptors, they are activated by the extracellular binding of purines such as ATP (Burnstock, 1980) and are expressed by the supporting cells of the cochlea (Järlebark *et al.*, 2002; Xiang, Bo and Burnstock, 1999). However, they are ionotropic receptors, rather than metabotropic like the P2Y subgroup, so exhibit much faster responses. ATP is released from the cochlear partition into the endolymph during damaging levels of noise exposure (Muñoz *et al.*, 2001), which is hypothesised to activate $P2X_2$ non-selective cation channels causing cation influx into supporting cells down the electrical gradient out of the more positive endolymph. Thus, the driving force for hair cell depolarisation will be reduced as the endolymphatic potential has been decreased (Muñoz *et al.*, 1995), and this is thought to delay

glutamate release by the hair cells and limit excitotoxicity (Housley *et al.*, 1999; Housley *et al.*, 2013). Therefore, the cochlea can protect itself from noise-induced damage by modulating the sensitivity of the hair cells to sound. Any age-related changes in the expression or function of $P2X_2$ receptors would therefore be expected to impact the cochlea's response to damaging levels of noise exposure and influence the accumulation of NIHL and ARHL. One article reported that 12-15 month old mice exhibited a much lower upregulation of $P2X_2$ receptor expression, alongside significantly smaller ATP-induced reductions in endocochlear potential, than 3-6 month old mice following damaging levels of noise exposure (Telang *et al.*, 2010). This suggests $P2X_2$ receptors might also undergo age-related changes in their expression and function and this could further influence the build-up of hair cell damage leading to ARHL development.

5.4 Is this ageing of the supporting cells unique to the cochlea?

Across the majority of tissues in the nervous system, sensory cell function requires support from glia-like accessory cells. The most well researched of these being the astrocytes within the brain which assist with the development and functioning of neurons (Benarroch, 2005; Ransom and Ransom, 2012). Astrocytes and cochlear supporting cells share many of the same physiological characteristics and functional roles as they both provide support for a group of specialised sensory cells. For instance, they both express GLAST (glutamate aspartate transporter) and facilitate the uptake and recycling of glutamate to avoid excitotoxicity and neuronal death (Lehre *et al.*, 1995; Chaudhry *et al.*, 1995; Furness and Lehre, 1997; Glowatzki *et al.*, 2006). Furthermore, both groups of cells form a functional syncytium as they are inter-connected by a gap junction channel network (Kikuchi *et al.*, 1995; Dermietzel *et al.*, 1991; Giaume *et al.*, 2021). Therefore it is supposed that, similar to cochlear supporting cells, the astrocytes also facilitate ion and metabolite homeostasis (Wangemann, 2006; Walz, 1989), alongside propagation of intercellular signalling cascades and Ca^{2+} transients (Anselmi *et al.*, 2008; Dani, Chernjavsky and Smith, 1992). Additionally, these Ca^{2+} transients in astrocytes can be induced in a similar way to what we see in cochlear supporting cells: by activation of their P2Y purinergic receptors (Gallagher and Salter, 2003; Agostinho *et al.*, 2020).

Due the conservation of physiological characteristics and functions across the cochlear supporting cells and other glial cells, it might be reasonable to suggest that these cells also undergo similar alterations with age. For instance, astrocytes from 21-month-old mouse brains were reported to have a higher frequency of connexin 43 and connexin 30 gap junction plaques per cell, which were also significantly shorter in length, when compared to 3-month-old mice (Cotrina *et al.*, 2001). Interestingly, they also investigated plaque permeability via FRAP but reported no significant differences in dye redistribution with age. Therefore, it appears that these results produced similar conclusions to those from Chapter 4 of this thesis: as these supporting cells age the gap junction plaques display a fragmentation in their structure which does not appear to elicit any changes in permeability according to dye diffusion experiments. However, it was also reported that astrocytes in human brain slices from older adults (51-72 years old) showed higher cell input resistances and a reduction in gap junction cell-cell coupling compared to younger adult astrocytes (22-50 years-old) (Popov *et al.*, 2023). Therefore, the consequences of age-related changes in the structure of GJC plaques on their permeability needs further investigation in the cochlea and other tissues.

In addition to this, an upregulation of P2Y receptor signalling has been reported in aged astrocytes and associated with neurodegenerative disease. Specifically, astrocyte hyperactivity associated with Alzheimer's disease was linked to an upregulation of $P2Y_1$ receptors and ADP-induced Ca^{2+} transients using mouse models for the disease (Delekate *et al.*, 2014). This is similar to what was observed in Chapter 3 of this thesis as it was reported that more pronounced P2Y receptor upregulation was observed in mice with more severe ARHL (C56BL/6N) than those with good hearing (C3H/HeJ). Therefore, this association between P2Y receptor upregulation and age-related disease is present across multiple tissues. Overall, further comparisons of other glial cells with the cochlear supporting cells might reveal other potential areas to study to better understand how these cells change with age.

5.5 Final conclusions

In conclusion, our sense of hearing relies on the coordinated function of sensory hair cells and glia-like supporting cells. This thesis has revealed that, similar to the hair cells, the supporting

cells also undergo age-related changes in their protein expression and function. Therefore, these changes could potentially influence the ability of the supporting cells to maintain hair cell longevity, and might contribute to the age-related decline in hair cell function driving age-related hearing loss. This work has highlighted the importance of further investigation into how these supporting cells age, as any additional changes in their function could result in new information regarding what drives hair cell loss and ARHL. Furthermore, deciphering whether these age-related changes in supporting cells are protective changes to limit disease progression, or causative changes which contribute to disease progression, could also reveal new targets for potential treatments for ARHL.

Reference List

Abbracchio, M. P., Burnstock, G., Verkhratsky, A. and Zimmermann, H. (2009) 'Purinergic signalling in the nervous system: an overview', *Trends in neurosciences,* 32(1), pp. 19-29.

Agostinho, P., Madeira, D., Dias, L., Simões, A. P., Cunha, R. A. and Canas, P. M. (2020) 'Purinergic signaling orchestrating neuron-glia communication', *Pharmacological research,* 162, pp. 105253.

Agrawal, Y., Platz, E. A. and Niparko, J. K. (2008) 'Prevalence of hearing loss and differences by demographic characteristics among US adults: data from the National Health and Nutrition Examination Survey, 1999-2004', *Archives of internal medicine,* 168(14), pp. 1522-1530.

Ahmad, S., Chen, S., Sun, J. and Lin, X. (2003) 'Connexins 26 and 30 are co-assembled to form gap junctions in the cochlea of mice', *Biochemical and Biophysical Research Communications,* 307(2), pp. 362-368.

Ahmed, S., Vorasubin, N., Lopez, I. A., Hosokawa, S., Ishiyama, G. and Ishiyama, A. (2013) 'The expression of glutamate aspartate transporter (GLAST) within the human cochlea and its distribution in various patient populations', *Brain Res,* 1529, pp. 134-42.

Alaynick, W. A., Way, J. M., Wilson, S. A., Benson, W. G., Pei, L., Downes, M., Yu, R., Jonker, J. W., Holt, J. A. and Rajpal, D. K. (2010) 'ERRγ regulates cardiac, gastric, and renal potassium homeostasis', *Molecular endocrinology,* 24(2), pp. 299-309.

Angelborg, C. and Engström, H. (1972) 'Supporting elements in the organ of Corti I. Fibrillar structures in the supporting cells of the organ of Corti of mammals', *Acta Oto-Laryngologica,* 73(sup301), pp. 49-60.

Anselmi, F., Hernandez, V. H., Crispino, G., Seydel, A., Ortolano, S., Roper, S. D., Kessaris, N., Richardson, W., Rickheit, G. and Filippov, M. A. (2008) 'ATP release through connexin hemichannels and gap junction transfer of second messengers propagate Ca2+ signals

across the inner ear', *Proceedings of the National Academy of Sciences,* 105(48), pp. 18770-18775.

Assad, J. A., Shepherd, G. M. and Corey, D. P. (1991) 'Tip-link integrity and mechanical transduction in vertebrate hair cells', *Neuron,* 7(6), pp. 985-94.

Babola, T. A., Kersbergen, C. J., Wang, H. C. and Bergles, D. E. (2020) 'Purinergic signaling in cochlear supporting cells reduces hair cell excitability by increasing the extracellular space', *Elife,* 9, pp. e52160.

Babola, T. A., Li, S., Gribizis, A., Lee, B. J., Issa, J. B., Wang, H. C., Crair, M. C. and Bergles, D. E. (2018) 'Homeostatic control of spontaneous activity in the developing auditory system', *Neuron,* 99(3), pp. 511-524.

Babola, T. A., Li, S., Wang, Z., Kersbergen, C. J., Elgoyhen, A. B., Coate, T. M. and Bergles, D. E. (2021) 'Purinergic signaling controls spontaneous activity in the auditory system throughout early development', *Journal of Neuroscience,* 41(4), pp. 594-612.

Beardslee, M. A., Laing, J. G., Beyer, E. C. and Saffitz, J. E. (1998) 'Rapid turnover of connexin43 in the adult rat heart', *Circulation research,* 83(6), pp. 629-635.

Beltramello, M., Bicego, M., Piazza, V., Ciubotaru, C. D., Mammano, F. and D'Andrea, P. (2003) 'Permeability and gating properties of human connexins 26 and 30 expressed in HeLa cells', *Biochemical and biophysical research communications,* 305(4), pp. 1024-1033.

Beltramello, M., Piazza, V., Bukauskas, F. F., Pozzan, T. and Mammano, F. (2005) 'Impaired permeability to Ins(1,4,5)P3 in a mutant connexin underlies recessive hereditary deafness', *Nature Cell Biology,* 7(1), pp. 63-69.

Ben-Yosef, T., Belyantseva, I. A., Saunders, T. L., Hughes, E. D., Kawamoto, K., Van Itallie, C. M., Beyer, L. A., Halsey, K., Gardner, D. J., Wilcox, E. R., Rasmussen, J., Anderson, J. M., Dolan, D. F., Forge, A., Raphael, Y., Camper, S. A. and Friedman, T. B. (2003) 'Claudin 14 knockout mice, a model for autosomal recessive deafness DFNB29, are deaf due to cochlear hair cell degeneration', *Hum Mol Genet,* 12(16), pp. 2049-61.

Benarroch, E. E. (2005) 'Neuron-Astrocyte Interactions: Partnership for Normal Function and Disease in the Central Nervous System', *Mayo Clinic Proceedings,* 80(10), pp. 1326-1338.

Bennett, M. V. and Goodenough, D. A. (1978) 'Gap junctions, electrotonic coupling, and intercellular communication', *Neurosci Res Program Bull,* 16(3), pp. 1-486.

Berglund, A. M. and Ryugo, D. K. (1987) 'Hair cell innervation by spiral ganglion neurons in the mouse', *Journal of Comparative Neurology,* 255(4), pp. 560-570.

Berridge, M. J., Bootman, M. D. and Roderick, H. L. (2003) 'Calcium signalling: dynamics, homeostasis and remodelling', *Nature reviews Molecular cell biology,* 4(7), pp. 517-529.

Beurg, M., Fettiplace, R., Nam, J. H. and Ricci, A. J. (2009) 'Localization of inner hair cell mechanotransducer channels using high-speed calcium imaging', *Nat Neurosci,* 12(5), pp. 553-8.

Beutner, D., Voets, T., Neher, E. and Moser, T. (2001) 'Calcium dependence of exocytosis and endocytosis at the cochlear inner hair cell afferent synapse', *Neuron,* 29(3), pp. 681-90.

Beyer, E. C., Paul, D. L. and Goodenough, D. A. (1990) 'Connexin family of gap junction proteins', *J Membr Biol,* 116(3), pp. 187-94.

Bhatt, K. A., Liberman, M. C. and Nadol Jr, J. B. (2001) 'Morphometric analysis of age-related changes in the human basilar membrane', *Annals of Otology, Rhinology & Laryngology,* 110(12), pp. 1147-1153.

Bosher, S. K., Warren, R. L. and Hallpike, C. S. (1997) 'Observations on the electrochemistry of the cochlear endolymph of the rat: a quantitative study of its electrical potential and ionic composition as determined by means of flame spectrophotometry', *Proceedings of the Royal Society of London. Series B. Biological Sciences,* 171(1023), pp. 227-247.

Brant, L. J. and Fozard, J. L. (1990) 'Age changes in pure‐tone hearing thresholds in a longitudinal study of normal human aging', *The Journal of the Acoustical Society of America,* 88(2), pp. 813-820.

Brewster, K. K., Ciarleglio, A., Brown, P. J., Chen, C., Kim, H.-O., Roose, S. P., Golub, J. S. and Rutherford, B. R. (2018) 'Age-related hearing loss and its association with depression in later life', *The American Journal of Geriatric Psychiatry,* 26(7), pp. 788-796.

Brownell, W. E., Bader, C. R., Bertrand, D. and de Ribaupierre, Y. (1985) 'Evoked mechanical responses of isolated cochlear outer hair cells', *Science,* 227(4683), pp. 194-6.

Bruce, I. C., Erfani, Y. and Zilany, M. S. A. (2018) 'A phenomenological model of the synapse between the inner hair cell and auditory nerve: Implications of limited neurotransmitter release sites', *Hearing Research,* 360, pp. 40-54.

Bruzzone, R., White, T. W. and Paul, D. L. (1996) 'Connections with Connexins: the Molecular Basis of Direct Intercellular Signaling', *European Journal of Biochemistry,* 238(1), pp. 1-27.

Bukauskas, F. F., Jordan, K., Bukauskiene, A., Bennett, M. V., Lampe, P. D., Laird, D. W. and Verselis, V. K. (2000) 'Clustering of connexin 43-enhanced green fluorescent protein gap junction channels and functional coupling in living cells', *Proc Natl Acad Sci U S A,* 97(6), pp. 2556-61.

Burnstock, G. (1972) 'Purinergic nerves', *Pharmacological reviews,* 24(3), pp. 509-581.

Burnstock, G. 1978. A basis for distinguishing two types of purinergic receptor Cell Membrane Receptors for Drugs and Hormones: A Multidisciplinary Approach 1978New York. Raven Press.

Burnstock, G. (1980) 'Purinergic nerves and receptors', *Progress in biochemical pharmacology,* 16, pp. 141-154.

Burnstock, G. (2004) 'Introduction: P2 receptors', *Current topics in medicinal chemistry,* 4(8), pp. 793-803.

Burnstock, G. (2008) 'Purinergic signalling and disorders of the central nervous system', *Nature reviews Drug discovery,* 7(7), pp. 575-590.

Burnstock, G. (2018) 'Purine and purinergic receptors', *Brain Neurosci Adv,* 2, pp. 2398212818817494.

Burnstock, G. and Kennedy, C. (1985) 'Is there a basis for distinguishing two types of P2-purinoceptor?', *General Pharmacology: The Vascular System,* 16(5), pp. 433-440.

Casale, J., Kandle, P. F., Murray, I. and Murr, N. (2022) *Physiology, Cochlear Function.* StatPearls Publishing, Treasure Island (FL).

Ceriani, F., Ciubotaru, C. D., Bortolozzi, M. and Mammano, F. (2016) 'Design and Construction of a Cost-Effective Spinning Disk System for Live Imaging of Inner Ear Tissue', *Methods Mol Biol,* 1427, pp. 223-41.

Ceriani, F., Hendry, A., Jeng, J. Y., Johnson, S. L., Stephani, F., Olt, J., Holley, M. C., Mammano, F., Engel, J. and Kros, C. J. (2019a) 'Coordinated calcium signalling in cochlear sensory and non‐sensory cells refines afferent innervation of outer hair cells', *The EMBO journal,* 38(9), pp. e99839.

Ceriani, F., Hendry, A., Jeng, J. Y., Johnson, S. L., Stephani, F., Olt, J., Holley, M. C., Mammano, F., Engel, J., Kros, C. J., Simmons, D. D. and Marcotti, W. (2019b) 'Coordinated calcium signalling in cochlear sensory and non-sensory cells refines afferent innervation of outer hair cells', *Embo j,* 38(9).

Ceriani, F., Pozzan, T. and Mammano, F. (2016) 'Critical role of ATP-induced ATP release for Ca2+ signaling in nonsensory cell networks of the developing cochlea', *Proc Natl Acad Sci U S A,* 113(46), pp. E7194-e7201.

Chan, D. K. and Chang, K. W. (2014) 'GJB2-associated hearing loss: systematic review of worldwide prevalence, genotype, and auditory phenotype', *Laryngoscope,* 124(2), pp. E34-53.

Chan, D. K. and Rouse, S. L. (2016) 'Sound-induced intracellular Ca2+ dynamics in the adult hearing cochlea', *PLoS one,* 11(12), pp. e0167850.

Chang, Q., Tang, W., Ahmad, S., Zhou, B. and Lin, X. (2008) 'Gap junction mediated intercellular metabolite transfer in the cochlea is compromised in connexin30 null mice', *PLoS One,* 3(12), pp. e4088.

Chaudhry, F. A., Lehre, K. P., van Lookeren Campagne, M., Ottersen, O. P., Danbolt, N. C. and Storm-Mathisen, J. (1995) 'Glutamate transporters in glial plasma membranes: highly differentiated localizations revealed by quantitative ultrastructural immunocytochemistry', *Neuron,* 15(3), pp. 711-720.

Chen, J., Chen, P., He, B., Gong, T., Li, Y., Zhang, J., Lv, J., Mammano, F., Hou, S. and Yang, J. (2022) 'Connexin30-Deficiency Causes Mild Hearing Loss With the Reduction of Endocochlear Potential and ATP Release', *Frontiers in Cellular Neuroscience,* 15.

Cieślak, M. and Wojtczak, A. (2018) 'Role of purinergic receptors in the Alzheimer's disease', *Purinergic signalling,* 14(4), pp. 331-344.

Citron, L., Exley, D. and Hallpike, C. S. (1956) 'FORMATION, CIRCULATION AND CHEMICAL PROPERTIES OF THE LABYRINTHINE FLUIDS', *British Medical Bulletin,* 12(2), pp. 101-104.

Clause, A., Kim, G., Sonntag, M., Weisz, C. J. C., Vetter, D. E., Rűbsamen, R. and Kandler, K. (2014) 'The precise temporal pattern of prehearing spontaneous activity is necessary for tonotopic map refinement', *Neuron,* 82(4), pp. 822-835.

Cohen-Salmon, M., Ott, T., Michel, V., Hardelin, J. P., Perfettini, I., Eybalin, M., Wu, T., Marcus, D. C., Wangemann, P., Willecke, K. and Petit, C. (2002) 'Targeted ablation of connexin26 in the inner ear epithelial gap junction network causes hearing impairment and cell death', *Curr Biol,* 12(13), pp. 1106-11.

Cotrina, M. L., Gao, Q., Lin, J. H. C. and Nedergaard, M. (2001) 'Expression and function of astrocytic gap junctions in aging', *Brain Research,* 901(1), pp. 55-61.

Crispino, G., Di Pasquale, G., Scimemi, P., Rodriguez, L., Galindo Ramirez, F., De Siati, R. D., Santarelli, R. M., Arslan, E., Bortolozzi, M., Chiorini, J. A. and Mammano, F. (2011) 'BAAV Mediated GJB2 Gene Transfer Restores Gap Junction Coupling in Cochlear Organotypic Cultures from Deaf Cx26Sox10Cre Mice', *PLOS ONE,* 6(8), pp. e23279.

Crispino, G., Galindo Ramirez, F., Campioni, M., Zorzi, V., Praetorius, M., Di Pasquale, G., Chiorini, J. A. and Mammano, F. (2017) 'In vivo genetic manipulation of inner ear connexin expression by bovine adeno-associated viral vectors', *Scientific Reports,* 7(1), pp. 6567.

Dani, J. W., Chernjavsky, A. and Smith, S. J. (1992) 'Neuronal activity triggers calcium waves in hippocampal astrocyte networks', *Neuron,* 8(3), pp. 429-440.

Defourny, J., Audouard, C., Davy, A. and Thiry, M. (2021) 'Efnb2 haploinsufficiency induces early gap junction plaque disassembly and endocytosis in the cochlea', *Brain Research Bulletin,* 174, pp. 153-160.

Defourny, J., Thelen, N. and Thiry, M. (2019) 'Actin-independent trafficking of cochlear connexin 26 to non-lipid raft gap junction plaques', *Hearing Research,* 374, pp. 69-75.

Defourny, J. and Thiry, M. (2021) 'Tricellular adherens junctions provide a cell surface delivery platform for connexin 26/30 oligomers in the cochlea', *Hearing Research,* 400, pp. 108137.

Defourny, J. and Thiry, M. (2023) 'Recent insights into gap junction biogenesis in the cochlea', *Dev Dyn,* 252(2), pp. 239-246.

del Castillo, F. J. and del Castillo, I. (2017) 'DFNB1 Non-syndromic Hearing Impairment: Diversity of Mutations and Associated Phenotypes', *Frontiers in Molecular Neuroscience,* 10.

Delekate, A., Füchtemeier, M., Schumacher, T., Ulbrich, C., Foddis, M. and Petzold, G. C. (2014) 'Metabotropic P2Y1 receptor signalling mediates astrocytic hyperactivity in vivo in an Alzheimer's disease mouse model', *Nature communications,* 5(1), pp. 5422.

Dermietzel, R., Hertberg, E. L., Kessler, J. A. and Spray, D. C. (1991) 'Gap junctions between cultured astrocytes: immunocytochemical, molecular, and electrophysiological analysis', *Journal of Neuroscience,* 11(5), pp. 1421-1432.

Dolmetsch, R. E., Xu, K. and Lewis, R. S. (1998) 'Calcium oscillations increase the efficiency and specificity of gene expression', *Nature,* 392(6679), pp. 933-936.

Ecke, D., Hanck, T., Tulapurkar, M. E., Schäfer, R., Kassack, M., Stricker, R. and Reiser, G. (2008) 'Hetero-oligomerization of the P2Y11 receptor with the P2Y1 receptor controls the internalization and ligand selectivity of the P2Y11 receptor', *Biochem J,* 409(1), pp. 107-16.

Edelstein, A. D., Tsuchida, M. A., Amodaj, N., Pinkard, H., Vale, R. D. and Stuurman, N. (2014) 'Advanced methods of microscope control using μManager software', *Journal of biological methods,* 1(2).

Erb, L., Cao, C., Ajit, D. and Weisman, G. A. (2015) 'P2Y receptors in Alzheimer's disease', *Biology of the Cell,* 107(1), pp. 1-21.

Fallon, R. F. and Goodenough, D. A. (1981) 'Five-hour half-life of mouse liver gap-junction protein', *The Journal of cell biology,* 90(2), pp. 521-526.

Fernandez, K. A., Jeffers, P. W. C., Lall, K., Liberman, M. C. and Kujawa, S. G. (2015) 'Aging after noise exposure: acceleration of cochlear synaptopathy in "recovered" ears', *Journal of Neuroscience,* 35(19), pp. 7509-7520.

Fetoni, A. R., Zorzi, V., Paciello, F., Ziraldo, G., Peres, C., Raspa, M., Scavizzi, F., Salvatore, A. M., Crispino, G. and Tognola, G. (2018) 'Cx26 partial loss causes accelerated presbycusis by redox imbalance and dysregulation of Nfr2 pathway', *Redox biology,* 19, pp. 301-317.

Fettiplace, R. (2017) 'Hair Cell Transduction, Tuning, and Synaptic Transmission in the Mammalian Cochlea', *Comprehensive Physiology*, pp. 1197-1227.

Forge, A., Becker, D., Casalotti, S., Edwards, J., Marziano, N. and Nevill, G. (2003) 'Gap junctions in the inner ear: comparison of distribution patterns in different vertebrates and assessement of connexin composition in mammals', *J Comp Neurol,* 467(2), pp. 207-31.

Fransen, E., Lemkens, N., Van Laer, L. and Van Camp, G. (2003) 'Age-related hearing impairment (ARHI): environmental risk factors and genetic prospects', *Experimental gerontology,* 38(4), pp. 353-359.

Fredholm, B. B., Abbracchio, M. P., Burnstock, G., Daly, J. W., Harden, K. T., Jacobson, K. A., Leff, P. and Williams, M. (1994) 'VI. Nomenclature and classification of purinoceptors', *Pharmacological reviews,* 46(2), pp. 143.

Furness, D. N. and Lehre, K. P. (1997) 'Immunocytochemical localization of a high‐affinity glutamate‐aspartate transporter, GLAST, in the rat and guinea‐pig cochlea', *European Journal of Neuroscience,* 9(9), pp. 1961-1969.

Gacek, R. R. and Schuknecht, H. F. (1969) 'Pathology of presbycusis', *International Audiology,* 8(2-3), pp. 199-209.

Gaietta, G., Deerinck, T. J., Adams, S. R., Bouwer, J., Tour, O., Laird, D. W., Sosinsky, G. E., Tsien, R. Y. and Ellisman, M. H. (2002) 'Multicolor and electron microscopic imaging of connexin trafficking', *Science,* 296(5567), pp. 503-507.

Gale, J. E., Piazza, V., Ciubotaru, C. D. and Mammano, F. (2004) 'A mechanism for sensing noise damage in the inner ear', *Curr Biol,* 14(6), pp. 526-9.

Gallagher, C. J. and Salter, M. W. (2003) 'Differential properties of astrocyte calcium waves mediated by P2Y1 and P2Y2 receptors', *Journal of Neuroscience,* 23(17), pp. 6728-6739.

Gates, G. A. and Mills, J. H. (2005) 'Presbycusis', *The lancet,* 366(9491), pp. 1111-1120.

Giaume, C., Naus, C. C., Sáez, J. C. and Leybaert, L. (2021) 'Glial connexins and pannexins in the healthy and diseased brain', *Physiological Reviews,* 101(1), pp. 93-145.

Glowatzki, E., Cheng, N., Hiel, H., Yi, E., Tanaka, K., Ellis-Davies, G. C. R., Rothstein, J. D. and Bergles, D. E. (2006) 'The glutamate–aspartate transporter GLAST mediates glutamate uptake at inner hair cell afferent synapses in the mammalian cochlea', *Journal of Neuroscience,* 26(29), pp. 7659-7664.

Glowatzki, E. and Fuchs, P. A. (2002) 'Transmitter release at the hair cell ribbon synapse', *Nat Neurosci,* 5(2), pp. 147-54.

Goman, A. M. and Lin, F. R. (2016) 'Prevalence of hearing loss by severity in the United States', *American journal of public health,* 106(10), pp. 1820-1822.

Gopinath, B., Rochtchina, E., Wang, J. J., Schneider, J., Leeder, S. R. and Mitchell, P. (2009) 'Prevalence of age-related hearing loss in older adults: Blue Mountains Study', *Archives of internal medicine,* 169(4), pp. 415-418.

Grynkiewicz, G., Poenie, M. and Tsien, R. Y. (1985) 'A new generation of Ca2+ indicators with greatly improved fluorescence properties', *Journal of biological chemistry,* 260(6), pp. 3440-3450.

Gu Hur, D., Ho Lee, J., Oh, S.-H., Ho Kim, Y., Hee Lee, J., Hoon Shin, D., Chang, S. O. and Kim, C.-S. (2007) 'KCNQ1/KCNE1 K+ channel and P2Y4 receptor are co-expressed from the time of birth in the apical membrane of rat strial marginal cells', *Acta Oto-Laryngologica,* 127(sup558), pp. 30-35.

Hakuba, N., Koga, K., Gyo, K., Usami, S.-i. and Tanaka, K. (2000) 'Exacerbation of noise-induced hearing loss in mice lacking the glutamate transporter GLAST', *Journal of Neuroscience,* 20(23), pp. 8750-8753.

Hernandez, V. H., Bortolozzi, M., Pertegato, V., Beltramello, M., Giarin, M., Zaccolo, M., Pantano, S. and Mammano, F. (2007) 'Unitary permeability of gap junction channels to second messengers measured by FRET microscopy', *Nature methods,* 4(4), pp. 353-358.

Hervé, J.-C., Derangeon, M., Sarrouilhe, D. and Bourmeyster, N. (2014) 'Influence of the scaffolding protein Zonula Occludens (ZOs) on membrane channels', *Biochimica et Biophysica Acta (BBA)-Biomembranes,* 1838(2), pp. 595-604.

Hibino, H., Nin, F., Tsuzuki, C. and Kurachi, Y. (2010) 'How is the highly positive endocochlear potential formed? The specific architecture of the stria vascularis and the roles of the ion-transport apparatus', *Pflügers Archiv-European Journal of Physiology,* 459, pp. 521-533.

Hinojosa, R. (1977) 'A note on development of Corti's organ', *Acta oto-laryngologica,* 84(1-6), pp. 238-251.

Hool, S. A., Jeng, J.-Y., Jagger, D. J., Marcotti, W. and Ceriani, F. (2023) 'Age-related changes in P2Y receptor signalling in mouse cochlear supporting cells', *The Journal of Physiology,* 601(19), pp. 4375-4395.

Horváth, T., Polony, G., Fekete, Á., Aller, M., Halmos, G., Lendvai, B., Heinrich, A., Sperlágh, B., Vizi, E. S. and Zelles, T. (2016) 'ATP-Evoked Intracellular Ca 2+ Signaling of Different Supporting Cells in the Hearing Mouse Hemicochlea', *Neurochemical research,* 41, pp. 364-375.

Housley, G. D. (2000) 'Physiological effects of extracellular nucleotides in the inner ear', *Clinical and experimental pharmacology & physiology,* 27(8), pp. 575-580.

Housley, G. D., Kanjhan, R., Raybould, N. P., Greenwood, D., Salih, S. G., Järlebark, L., Burton, L. D., Setz, V. C., Cannell, M. B., Soeller, C., Christie, D. L., Usami, S., Matsubara, A., Yoshie, H., Ryan, A. F. and Thorne, P. R. (1999) 'Expression of the P2X(2) receptor subunit of the ATP-gated ion channel in the cochlea: implications for sound transduction and auditory neurotransmission', *J Neurosci,* 19(19), pp. 8377-88.

Housley, G. D., Morton-Jones, R., Vlajkovic, S. M., Telang, R. S., Paramananthasivam, V., Tadros, S. F., Wong, A. C., Froud, K. E., Cederholm, J. M., Sivakumaran, Y., Snguanwongchai, P., Khakh, B. S., Cockayne, D. A., Thorne, P. R. and Ryan, A. F. (2013) 'ATP-gated ion channels mediate adaptation to elevated sound levels', *Proc Natl Acad Sci U S A,* 110(18), pp. 7494-9.

Hu, Q., Deshpande, S., Irani, K. and Ziegelstein, R. C. (1999) '[Ca2+] i oscillation frequency regulates agonist-stimulated NF-κB transcriptional activity', *Journal of Biological Chemistry,* 274(48), pp. 33995-33998.

Huang, L.-C., Thorne, P. R., Vlajkovic, S. M. and Housley, G. D. (2010) 'Differential expression of P2Y receptors in the rat cochlea during development', *Purinergic signalling,* 6(2), pp. 231-248.

Hunter, A. W., Barker, R. J., Zhu, C. and Gourdie, R. G. (2005) 'Zonula occludens-1 alters connexin43 gap junction size and organization by influencing channel accretion', *Molecular biology of the cell,* 16(12), pp. 5686-5698.

Iring, A., Tóth, A., Baranyi, M., Otrokocsi, L., Módis, L. V., Gölöncsér, F., Varga, B., Hortobágyi, T., Bereczki, D. and Dénes, Á. (2022) 'The dualistic role of the purinergic P2Y12-receptor in an in vivo model of Parkinson's disease: signalling pathway and novel therapeutic targets', *Pharmacological Research,* 176, pp. 106045.

Jacobson, K. A., Ivanov, A. A., de Castro, S., Harden, T. K. and Ko, H. (2009) 'Development of selective agonists and antagonists of P2Y receptors', *Purinergic Signalling,* 5(1), pp. 75-89.

Jagger, D. J. and Forge, A. (2006) 'Compartmentalized and signal-selective gap junctional coupling in the hearing cochlea', *Journal of Neuroscience,* 26(4), pp. 1260-1268.

Jagger, D. J. and Forge, A. (2015) 'Connexins and gap junctions in the inner ear--it's not just about K^+ recycling', *Cell Tissue Res,* 360(3), pp. 633-44.

Jagger, D. J., Nickel, R. and Forge, A. (2014) 'Gap junctional coupling is essential for epithelial repair in the avian cochlea', *Journal of Neuroscience,* 34(48), pp. 15851-15860.

Jang, M. W., Lim, J., Park, M. G., Lee, J.-H. and Lee, C. J. (2022) 'Active role of glia-like supporting cells in the organ of Corti: Membrane proteins and their roles in hearing', *Glia,* 70(10), pp. 1799-1825.

Järlebark, L. E., Housley, G. D., Raybould, N. P., Vlajkovic, S. and Thorne, P. R. (2002) 'ATP-gated ion channels assembled from P2X2 receptor subunits in the mouse cochlea', *Neuroreport,* 13(15), pp. 1979-1984.

Jeng, J. Y., Carlton, A. J., Johnson, S. L., Brown, S. D. M., Holley, M. C., Bowl, M. R. and Marcotti, W. (2021) 'Biophysical and morphological changes in inner hair cells and their efferent innervation in the ageing mouse cochlea', *The Journal of physiology,* 599(1), pp. 269-287.

Jeng, J. Y., Ceriani, F., Olt, J., Brown, S. D. M., Holley, M. C., Bowl, M. R., Johnson, S. L. and Marcotti, W. (2020a) 'Pathophysiological changes in inner hair cell ribbon synapses in the ageing mammalian cochlea', *The Journal of physiology,* 598(19), pp. 4339-4355.

Jeng, J. Y., Johnson, S. L., Carlton, A. J., De Tomasi, L., Goodyear, R. J., De Faveri, F., Furness, D. N., Wells, S., Brown, S. D. M., Holley, M. C., Richardson, G. P., Mustapha, M., Bowl, M. R. and Marcotti, W. (2020b) 'Age-related changes in the biophysical and morphological characteristics of mouse cochlear outer hair cells', *J Physiol,* 598(18), pp. 3891-3910.

Johnson, R., Hammer, M., Sheridan, J. and Revel, J.-P. (1974) 'Gap junction formation between reaggregated Novikoff hepatoma cells', *Proceedings of the National Academy of Sciences,* 71(11), pp. 4536-4540.

Johnson, S. L., Ceriani, F., Houston, O., Polishchuk, R., Polishchuk, E., Crispino, G., Zorzi, V., Mammano, F. and Marcotti, W. (2017) 'Connexin-Mediated Signaling in Nonsensory Cells Is

Crucial for the Development of Sensory Inner Hair Cells in the Mouse Cochlea', *J Neurosci,* 37(2), pp. 258-268.

Johnson, S. L., Eckrich, T., Kuhn, S., Zampini, V., Franz, C., Ranatunga, K. M., Roberts, T. P., Masetto, S., Knipper, M. and Kros, C. J. (2011) 'Position-dependent patterning of spontaneous action potentials in immature cochlear inner hair cells', *Nature neuroscience,* 14(6), pp. 711-717.

Johnson, S. L., Forge, A., Knipper, M., Münkner, S. and Marcotti, W. (2008) 'Tonotopic variation in the calcium dependence of neurotransmitter release and vesicle pool replenishment at mammalian auditory ribbon synapses', *Journal of Neuroscience,* 28(30), pp. 7670-7678.

Kamiya, K., Yum, S. W., Kurebayashi, N., Muraki, M., Ogawa, K., Karasawa, K., Miwa, A., Guo, X., Gotoh, S. and Sugitani, Y. (2014) 'Assembly of the cochlear gap junction macromolecular complex requires connexin 26', *The Journal of clinical investigation,* 124(4), pp. 1598-1607.

Kaprielian, R. R., Gunning, M., Dupont, E., Sheppard, M. N., Rothery, S. M., Underwood, R., Pennell, D. J., Fox, K., Pepper, J. and Poole-Wilson, P. A. (1998) 'Downregulation of immunodetectable connexin43 and decreased gap junction size in the pathogenesis of chronic hibernation in the human left ventricle', *Circulation,* 97(7), pp. 651-660.

Kasper, G., Mao, L., Geissler, S., Draycheva, A., Trippens, J., Kühnisch, J., Tschirschmann, M., Kaspar, K., Perka, C. and Duda, G. N. (2009) 'Insights into mesenchymal stem cell aging: involvement of antioxidant defense and actin cytoskeleton', *Stem cells,* 27(6), pp. 1288-1297.

Keithley, E. M. (2020) 'Pathology and mechanisms of cochlear aging', *Journal of Neuroscience Research,* 98(9), pp. 1674-1684.

Kersbergen, C. J. and Bergles, D. E. (2024) 'Priming central sound processing circuits through induction of spontaneous activity in the cochlea before hearing onset', *Trends in Neurosciences,* 47(7), pp. 522-537.

Kikuchi, T., Adams, J. C., Miyabe, Y., So, E. and Kobayashi, T. (2000) 'Potassium ion recycling pathway via gap junction systems in the mammalian cochlea and its interruption in hereditary nonsyndromic deafness', *Med Electron Microsc,* 33(2), pp. 51-6.

Kikuchi, T., Kimura, R. S., Paul, D. L. and Adams, J. C. (1995) 'Gap junctions in the rat cochlea: immunohistochemical and ultrastructural analysis', *Anatomy and Embryology,* 191(2), pp. 101-118.

Klotz-Weigand, L. and Enz, R. (2022) 'Metabotropic Glutamate Receptors at Ribbon Synapses in the Retina and Cochlea', *Cells,* 11(7).

Köles, L., Szepesy, J., Berekméri, E. and Zelles, T. (2019) 'Purinergic Signaling and Cochlear Injury-Targeting the Immune System?', *Int J Mol Sci,* 20(12).

Kros, C. J., Ruppersberg, J. P. and Rüsch, A. (1998) 'Expression of a potassium current in inner hair cells during development of hearing in mice', *Nature,* 394(6690), pp. 281-4.

Kros, C. J., Rusch, A. and Richardson, G. P. (1992) 'Mechano-electrical transducer currents in hair cells of the cultured neonatal mouse cochlea', *Proceedings of the Royal Society of London. Series B: Biological Sciences,* 249(1325), pp. 185-193.

Kudo, T., Kure, S., Ikeda, K., Xia, A.-P., Katori, Y., Suzuki, M., Kojima, K., Ichinohe, A., Suzuki, Y., Aoki, Y., Kobayashi, T. and Matsubara, Y. (2003) 'Transgenic expression of a dominant-negative connexin26 causes degeneration of the organ of Corti and non-syndromic deafness', *Human Molecular Genetics,* 12(9), pp. 995-1004.

Kujawa, S. G. and Liberman, M. C. (2015) 'Synaptopathy in the noise-exposed and aging cochlea: Primary neural degeneration in acquired sensorineural hearing loss', *Hearing research,* 330, pp. 191-199.

Kumar, N. M. and Gilula, N. B. (1996) 'The gap junction communication channel', *Cell,* 84(3), pp. 381-388.

Lahne, M. and Gale, J. E. (2008) 'Damage-induced activation of ERK1/2 in cochlear supporting cells is a hair cell death-promoting signal that depends on extracellular ATP and calcium', *Journal of Neuroscience,* 28(19), pp. 4918-4928.

Lauer, A. M., Fuchs, P. A., Ryugo, D. K. and Francis, H. W. (2012) 'Efferent synapses return to inner hair cells in the aging cochlea', *Neurobiology of Aging,* 33(12), pp. 2892-2902.

Lauf, U., Giepmans, B. N. G., Lopez, P., Braconnot, S., Chen, S.-C. and Falk, M. M. (2002) 'Dynamic trafficking and delivery of connexons to the plasma membrane and accretion to gap junctions in living cells', *Proceedings of the National Academy of Sciences,* 99(16), pp. 10446-10451.

Lautermann, J., ten Cate, W.-J. F., Altenhoff, P., Grümmer, R., Traub, O., Frank, H. G., Jahnke, K. and Winterhager, E. (1998) 'Expression of the gap-junction connexins 26 and 30 in the rat cochlea', *Cell and tissue research,* 294, pp. 415-420.

Lee, Y. J., Galoforo, S. S., Berns, C. M., Chen, J. C., Davis, B. H., Sim, J. E., Corry, P. M. and Spitz, D. R. (1998) 'Glucose deprivation-induced cytotoxicity and alterations in mitogen-activated protein kinase activation are mediated by oxidative stress in multidrug-resistant human breast carcinoma cells', *J Biol Chem,* 273(9), pp. 5294-9.

Lehre, K. P., Levy, L. M., Ottersen, O. P., Storm-Mathisen, J. and Danbolt, N. C. (1995) 'Differential expression of two glial glutamate transporters in the rat brain: quantitative and immunocytochemical observations', *Journal of Neuroscience,* 15(3), pp. 1835-1853.

Lewis, R. S. and Hudspeth, A. J. (1983) 'Voltage- and ion-dependent conductances in solitary vertebrate hair cells', *Nature,* 304(5926), pp. 538-541.

Li, H., Liu, T. F., Lazrak, A., Peracchia, C., Goldberg, G. S., Lampe, P. D. and Johnson, R. G. (1996) 'Properties and regulation of gap junctional hemichannels in the plasma membranes of cultured cells', *J Cell Biol,* 134(4), pp. 1019-30.

Lim, D. J. (1986) 'Functional structure of the organ of Corti: a review', *Hearing Research,* 22(1), pp. 117-146.

Liu, C., Glowatzki, E. and Fuchs, P. A. (2015) 'Unmyelinated type II afferent neurons report cochlear damage', *Proc Natl Acad Sci U S A,* 112(47), pp. 14723-7.

Locke, D., Liu, J. and Harris, A. L. (2005) 'Lipid rafts prepared by different methods contain different connexin channels, but gap junctions are not lipid rafts', *Biochemistry,* 44(39), pp. 13027-13042.

Lopez, P., Balicki, D., Buehler, L. K., Falk, M. M. and Chihchen, S. (2001) 'Distribution and dynamics of gap junction channels revealed in living cells', *Cell communication & adhesion,* 8(4-6), pp. 237-242.

Luke, R. A. and Saffitz, J. E. (1991) 'Remodeling of ventricular conduction pathways in healed canine infarct border zones', *The Journal of clinical investigation,* 87(5), pp. 1594-1602.

Mammano, F. (2013) 'ATP-dependent intercellular Ca2+ signaling in the developing cochlea: Facts, fantasies and perspectives', *Seminars in Cell & Developmental Biology,* 24(1), pp. 31-39.

Manthey, D., Banach, K., Desplantez, T., Lee, C. G., Kozak, C. A., Traub, O., Weingart, R. and Willecke, K. (2001) 'Intracellular domains of mouse connexin26 and -30 affect diffusional and electrical properties of gap junction channels', *J Membr Biol,* 181(2), pp. 137-48.

Marcotti, W., Johnson, S. L., Holley, M. C. and Kros, C. J. (2003a) 'Developmental changes in the expression of potassium currents of embryonic, neonatal and mature mouse inner hair cells', *The Journal of Physiology,* 548(2), pp. 383-400.

Marcotti, W., Johnson, S. L., Rüsch, A. and Kros, C. J. (2003b) 'Sodium and calcium currents shape action potentials in immature mouse inner hair cells', *The Journal of physiology,* 552(3), pp. 743-761.

Maruoka, H., Jayasekara, M. P. S., Barrett, M. O., Franklin, D. A., de Castro, S., Kim, N., Costanzi, S., Harden, T. K. and Jacobson, K. A. (2011) 'Pyrimidine nucleotides with 4-alkyloxyimino and terminal tetraphosphate δ-ester modifications as selective agonists of the P2Y4 receptor', *Journal of medicinal chemistry,* 54(12), pp. 4018-4033.

Marziano, N. K., Casalotti, S. O., Portelli, A. E., Becker, D. L. and Forge, A. (2003) 'Mutations in the gene for connexin 26 (GJB2) that cause hearing loss have a dominant negative effect on connexin 30', *Human Molecular Genetics,* 12(8), pp. 805-812.

Mason, M. J. (2016) 'Structure and function of the mammalian middle ear. II: Inferring function from structure', *Journal of Anatomy,* 228(2), pp. 300-312.

Matsubara, A., Laake, J. H., Davanger, S., Usami, S.-i. and Ottersen, O. P. (1996) 'Organization of AMPA receptor subunits at a glutamate synapse: a quantitative immunogold analysis of hair cell synapses in the rat organ of Corti', *Journal of Neuroscience,* 16(14), pp. 4457-4467.

Mianné, J., Chessum, L., Kumar, S., Aguilar, C., Codner, G., Hutchison, M., Parker, A., Mallon, A.-M., Wells, S. and Simon, M. M. (2016) 'Correction of the auditory phenotype in C57BL/6N mice via CRISPR/Cas9-mediated homology directed repair', *Genome medicine,* 8(1), pp. 1-12.

Mock, B. E., Vijayakumar, S., Pierce, J., Jones, T. A. and Jones, S. M. (2016) 'Differential effects of Cdh23753A on auditory and vestibular functional aging in C57BL/6J mice', *Neurobiology of aging,* 43, pp. 13-22.

Møller, A. R. (2012) *Hearing: anatomy, physiology, and disorders of the auditory system.* Plural Publishing.

Moore, D., Iritani, S., Chambers, J. and Emson, P. (2000) 'Immunohistochemical localization of the P2Y1 purinergic receptor in Alzheimer's disease', *Neuroreport,* 11(17), pp. 3799-3803.

Moshier, J. A., Cornell, T. and Majumdar, A. P. N. (1993) 'Expression of protease genes in the gastric mucosa during aging', *Experimental gerontology,* 28(3), pp. 249-258.

Müller, N. I. C., Sonntag, M., Maraslioglu, A., Hirtz, J. J. and Friauf, E. (2019) 'Topographic map refinement and synaptic strengthening of a sound localization circuit require spontaneous peripheral activity', *The Journal of physiology,* 597(22), pp. 5469-5493.

Muñoz, D. J., Kendrick, I. S., Rassam, M. and Thorne, P. R. (2001) 'Vesicular storage of adenosine triphosphate in the guinea-pig cochlear lateral wall and concentrations of ATP in the endolymph during sound exposure and hypoxia', *Acta Otolaryngol,* 121(1), pp. 10-5.

Muñoz, D. J. B., Thorne, P. R., Housley, G. D., Billett, T. E. and Battersby, J. M. (1995) 'Extracellular adenosine 5′-triphosphate (ATP) in the endolymphatic compartment influences cochlear function', *Hearing research,* 90(1-2), pp. 106-118.

Noben-Trauth, K., Zheng, Q. Y. and Johnson, K. R. (2003) 'Association of cadherin 23 with polygenic inheritance and genetic modification of sensorineural hearing loss', *Nat Genet,* 35(1), pp. 21-3.

Nolan, L. S., Maier, H., Hermans-Borgmeyer, I., Girotto, G., Ecob, R., Pirastu, N., Cadge, B. A., Hübner, C., Gasparini, P. and Strachan, D. P. (2013) 'Estrogen-related receptor gamma and hearing function: evidence of a role in humans and mice', *Neurobiology of aging,* 34(8), pp. 2077-e1.

North, R. A. (2002) 'Molecular Physiology of P2X Receptors', *Physiological Reviews,* 82(4), pp. 1013-1067.

Nouvian, R., Beutner, D., Parsons, T. D. and Moser, T. (2006) 'Structure and function of the hair cell ribbon synapse', *The Journal of membrane biology,* 209, pp. 153-165.

Orrenius, S. (2007) 'Reactive oxygen species in mitochondria-mediated cell death', *Drug metabolism reviews,* 39(2-3), pp. 443-455.

Paciello, F., Zorzi, V., Raspa, M., Scavizzi, F., Grassi, C., Mammano, F. and Fetoni, A. R. (2022) 'Connexin 30 deletion exacerbates cochlear senescence and age-related hearing loss', *Frontiers in Cell and Developmental Biology,* 10, pp. 950837.

Palmer, A. R. and Russell, I. J. (1986) 'Phase-locking in the cochlear nerve of the guinea-pig and its relation to the receptor potential of inner hair-cells', *Hearing research,* 24(1), pp. 1-15.

Piazza, V., Ciubotaru, C. D., Gale, J. E. and Mammano, F. (2007) 'Purinergic signalling and intercellular Ca2+ wave propagation in the organ of Corti', *Cell calcium,* 41(1), pp. 77-86.

Pickles, J. O., Comis, S. D. and Osborne, M. P. (1984) 'Cross-links between stereocilia in the guinea pig organ of Corti, and their possible relation to sensory transduction', *Hearing research,* 15(2), pp. 103-112.

Popov, A., Brazhe, N., Morozova, K., Yashin, K., Bychkov, M., Nosova, O., Sutyagina, O., Brazhe, A., Parshina, E. and Li, L. (2023) 'Mitochondrial malfunction and atrophy of astrocytes in the aged human cerebral cortex', *Nature Communications,* 14(1), pp. 8380.

Rafehi, M., Burbiel, J. C., Attah, I. Y., Abdelrahman, A. and Müller, C. E. (2017) 'Synthesis, characterization, and in vitro evaluation of the selective P2Y 2 receptor antagonist AR-C118925', *Purinergic signalling,* 13, pp. 89-103.

Ransom, B. R. and Ransom, C. B. (2012) 'Astrocytes: multitalented stars of the central nervous system', *Astrocytes: Methods and Protocols*, pp. 3-7.

Ribeiro-Filho, A. C., Buri, M. V., Barros, C. C., Dreyfuss, J. L., Nader, H. B., Justo, G. Z., Craveiro, R. B., Pesquero, J. B., Miranda, A., Ferreira, A. T. and Paredes-Gamero, E. J. (2016) 'Functional and molecular evidence for heteromeric association of P2Y1 receptor with P2Y2 and P2Y4 receptors in mouse granulocytes', *BMC Pharmacol Toxicol,* 17(1), pp. 29.

Salt, A. N., Melichar, I. and Thalmann, R. (1987) 'Mechanisms of endocochlear potential generation by stria vascularis', *Laryngoscope,* 97(8 Pt 1), pp. 984-91.

Santos-Sacchi, J. (1986) 'Dye coupling in the organ of Corti', *Cell Tissue Res,* 245(3), pp. 525-9.

Santos-Sacchi, J. and Dallos, P. (1983) 'Intercellular communication in the supporting cells of the organ of Corti', *Hearing Research,* 9(3), pp. 317-326.

Schuknecht, H. F. (1955) 'Presbycusis', *The Laryngoscope,* 65(6), pp. 402-419.

Sergeyenko, Y., Lall, K., Liberman, M. C. and Kujawa, S. G. (2013) 'Age-related cochlear synaptopathy: an early-onset contributor to auditory functional decline', *Journal of Neuroscience,* 33(34), pp. 13686-13694.

Simmons, D., Duncan, J., de Caprona, D. C. and Fritzsch, B. (2011) 'Development of the inner ear efferent system', *Auditory and vestibular efferents*, pp. 187-216.

Sirko, P., Gale, J. E. and Ashmore, J. F. (2019) 'Intercellular Ca2+ signalling in the adult mouse cochlea', *The Journal of physiology,* 597(1), pp. 303-317.

Smith, C. A., Lowry, O. H. and Wu, M. L. (1954) 'The electrolytes of the labyrinthine fluids', *The Laryngoscope,* 64(3), pp. 141-153.

Smith, C. A. and Sjöstrand, F. S. (1961) 'A synaptic structure in the hair cells of the guinea pig cochlea', *Journal of Ultrastructure Research,* 5(2), pp. 184-192.

Spoendlin, H. (1972) 'Innervation densities of the cochlea', *Acta oto-laryngologica,* 73(2-6), pp. 235-248.

Spongr, V. P., Flood, D. G., Frisina, R. D. and Salvi, R. J. (1997) 'Quantitative measures of hair cell loss in CBA and C57BL/6 mice throughout their life spans', *The Journal of the Acoustical Society of America,* 101(6), pp. 3546-3553.

Sprinzl, G. M. and Riechelmann, H. (2010) 'Current trends in treating hearing loss in elderly people: a review of the technology and treatment options–a mini-review', *Gerontology,* 56(3), pp. 351-358.

Svechtarova, M. I., Buzzacchera, I., Toebes, B. J., Lauko, J., Anton, N. and Wilson, C. J. (2016) 'Sensor devices inspired by the five senses: a review', *Electroanalysis,* 28(6), pp. 1201-1241.

Tajima, S., Danzaki, K., Ikeda, K. and Kamiya, K. (2020) 'Degradation and modification of cochlear gap junction proteins in the early development of age-related hearing loss', *Experimental & Molecular Medicine,* 52(1), pp. 166-175.

Telang, R. S., Paramananthasivam, V., Vlajkovic, S. M., Munoz, D. J. B., Housley, G. D. and Thorne, P. R. (2010) 'Reduced P2x 2 receptor-mediated regulation of endocochlear potential in the ageing mouse cochlea', *Purinergic signalling,* 6, pp. 263-272.

Teubner, B., Michel, V., Pesch, J., Lautermann, J., Cohen-Salmon, M., Söhl, G., Jahnke, K., Winterhager, E., Herberhold, C., Hardelin, J. P., Petit, C. and Willecke, K. (2003) 'Connexin30 (Gjb6)-deficiency causes severe hearing impairment and lack of endocochlear potential', *Hum Mol Genet,* 12(1), pp. 13-21.

Thastrup, O. (1990) 'Role of Ca2(+)-ATPases in regulation of cellular Ca2+ signalling, as studied with the selective microsomal Ca2(+)-ATPase inhibitor, thapsigargin', *Agents Actions,* 29(1-2), pp. 8-15.

Tritsch, N. X. and Bergles, D. E. (2010) 'Developmental regulation of spontaneous activity in the Mammalian cochlea', *Journal of Neuroscience,* 30(4), pp. 1539-1550.

Tritsch, N. X., Yi, E., Gale, J. E., Glowatzki, E. and Bergles, D. E. (2007) 'The origin of spontaneous activity in the developing auditory system', *Nature,* 450(7166), pp. 50-5.

Trune, D. R., Kempton, J. B. and Mitchell, C. (1996) 'Auditory function in the C3H/HeJ and C3H/HeSnJ mouse strains', *Hearing research,* 96(1-2), pp. 41-45.

Tsien, R. Y. (1981) 'A non-disruptive technique for loading calcium buffers and indicators into cells', *Nature,* 290(5806), pp. 527-528.

v. Békésy, G. (1951) 'DC potentials and energy balance of the cochlear partition', *The Journal of the Acoustical Society of America,* 23(5), pp. 576-582.

v. Békésy, G. (1952) 'DC resting potentials inside the cochlear partition', *The Journal of the Acoustical Society of America,* 24(1), pp. 72-76.

Van Eyken, E., Van Camp, G., Fransen, E., Topsakal, V., Hendrickx, J. J., Demeester, K., Van de Heyning, P., Mäki-Torkko, E., Hannula, S. and Sorri, M. (2007) 'Contribution of the N-acetyltransferase 2 polymorphism NAT2* 6A to age-related hearing impairment', *Journal of medical genetics,* 44(9), pp. 570-578.

Van Laer, L., Huyghe, J. R., Hannula, S., Van Eyken, E., Stephan, D. A., Mäki-Torkko, E., Aikio, P., Fransen, E., Lysholm-Bernacchi, A. and Sorri, M. (2010) 'A genome-wide association study for age-related hearing impairment in the Saami', *European Journal of Human Genetics,* 18(6), pp. 685-693.

Veenstra, R. D. (1996) 'Size and selectivity of gap junction channels formed from different connexins', *Journal of bioenergetics and biomembranes,* 28, pp. 327-337.

Viana, L. M., O'Malley, J. T., Burgess, B. J., Jones, D. D., Oliveira, C. A., Santos, F., Merchant, S. N., Liberman, L. D. and Liberman, M. C. (2015) 'Cochlear neuropathy in human presbycusis: Confocal analysis of hidden hearing loss in post-mortem tissue', *Hear Res,* 327, pp. 78-88.

Vincent, P. F. Y., Bouleau, Y., Petit, C. and Dulon, D. (2015) 'A synaptic F-actin network controls otoferlin-dependent exocytosis in auditory inner hair cells', *Elife,* 4, pp. e10988.

Von Békésy, G. (1960) *Experiments in hearing. Experiments in hearing.* Oxford, England: Mcgraw Hill.

von Kügelgen, I. and Hoffmann, K. (2016) 'Pharmacology and structure of P2Y receptors', *Neuropharmacology,* 104, pp. 50-61.

Walz, W. (1989) 'Role of glial cells in the regulation of the brain ion microenvironment', *Progress in Neurobiology,* 33(4), pp. 309-333.

Wan, G., Corfas, G. and Stone, J. S. (2013) 'Inner ear supporting cells: rethinking the silent majority', *Semin Cell Dev Biol,* 24(5), pp. 448-59.

Wang, H. C., Lin, C.-C., Cheung, R., Zhang-Hooks, Y., Agarwal, A., Ellis-Davies, G., Rock, J. and Bergles, D. E. (2015) 'Spontaneous activity of cochlear hair cells triggered by fluid secretion mechanism in adjacent support cells', *Cell,* 163(6), pp. 1348-1359.

Wangemann, P. (2006) 'Supporting sensory transduction: cochlear fluid homeostasis and the endocochlear potential', *J Physiol,* 576(Pt 1), pp. 11-21.

Wangemann, P., Liu, J. and Marcus, D. C. (1995) 'Ion transport mechanisms responsible for K+ secretion and the transepithelial voltage across marginal cells of stria vascularis in vitro', *Hearing research,* 84(1-2), pp. 19-29.

Wells, H. R. R., Newman, T. A. and Williams, F. M. K. (2020) 'Genetics of age-related hearing loss', *J Neurosci Res,* 98(9), pp. 1698-1704.

Wingard, J. C. and Zhao, H.-B. (2015) 'Cellular and deafness mechanisms underlying connexin mutation-induced hearing loss–a common hereditary deafness', *Frontiers in cellular Neuroscience,* 9, pp. 202.

Xiang, Z., Bo, X. and Burnstock, G. (1999) 'P2X receptor immunoreactivity in the rat cochlea, vestibular ganglion and cochlear nucleus', *Hearing research,* 128(1-2), pp. 190-196.

Yum, S. W., Zhang, J., Valiunas, V., Kanaporis, G., Brink, P. R., White, T. W. and Scherer, S. S. (2007) 'Human connexin26 and connexin30 form functional heteromeric and heterotypic channels', *American Journal of Physiology-Cell Physiology,* 293(3), pp. C1032-C1048.

Zetes, D. E., Tolomeo, J. A. and Holley, M. C. (2012) 'Structure and mechanics of supporting cells in the guinea pig organ of Corti', *PLoS One,* 7(11), pp. e49338.

Zhang-Hooks, Y., Agarwal, A., Mishina, M. and Bergles, D. E. (2016) 'NMDA Receptors Enhance Spontaneous Activity and Promote Neuronal Survival in the Developing Cochlea', *Neuron,* 89(2), pp. 337-50.

Zhang, Y., Tang, W., Ahmad, S., Sipp, J. A., Chen, P. and Lin, X. (2005) 'Gap junction-mediated intercellular biochemical coupling in cochlear supporting cells is required for normal cochlear functions', *Proc Natl Acad Sci U S A,* 102(42), pp. 15201-6.

Zhao, H.-B. and Santos-Sacchi, J. (1998) 'Effect of membrane tension on gap junctional conductance of supporting cells in Corti's organ', *The Journal of general physiology,* 112(4), pp. 447-455.

Zhao, H., Kikuchi, T., Ngezahayo, A. and White, T. (2006) 'Gap Junctions and Cochlear Homeostasis', *The Journal of membrane biology,* 209, pp. 177-86.

Zheng, Q. Y., Yan, D., Ouyang, X. M., Du, L. L., Yu, H., Chang, B., Johnson, K. R. and Liu, X. Z. (2005) 'Digenic inheritance of deafness caused by mutations in genes encoding cadherin 23 and protocadherin 15 in mice and humans', *Human molecular genetics,* 14(1), pp. 103-111.

Zhu, Y., Liang, C., Chen, J., Zong, L., Chen, G. D. and Zhao, H. B. (2013) 'Active cochlear amplification is dependent on supporting cell gap junctions', *Nat Commun,* 4, pp. 1786.

Zwislocki, J. J., Slepecky, N. B., Cefaratti, L. K. and Smith, R. L. (1992) 'Ionic coupling among cells in the organ of Corti', *Hearing Research,* 57(2), pp. 175-194.